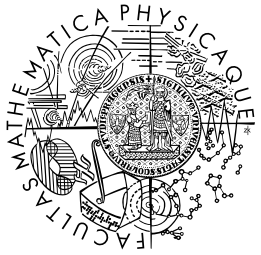

FACULTY
OF MATHEMATICS
AND PHYSICS
Charles University

DOCTORAL THESIS

Petr Vágner

Thermodynamic analysis of solid oxide cells

Mathematical Institute

Supervisor of the doctoral thesis:	Prof. Ing. František Maršík, DrSc.
Advisor of the doctoral thesis:	Prof. Dr. Ing. Karel Bouzek
Advisor of the doctoral thesis:	Dr. Clemens Guhlke
Advisor of the doctoral thesis:	RNDr. Michal Pavelka, Ph.D.
Study programme:	Mathematical and computer modelling
Study branch:	Physics

Prague 2019

I declare that I carried out this doctoral thesis independently, and only with the cited sources, literature and other professional sources.

I understand that my work relates to the rights and obligations under the Act No. 121/2000 Sb., the Copyright Act, as amended, in particular the fact that the Charles University has the right to conclude a license agreement on the use of this work as a school work pursuant to Section 60 subsection 1 of the Copyright Act.

In Prague April 8, 2019 Petr Vágner

Dedicated to my beloved family. Thank you.

My deepest gratitude belongs to my supervisor Prof. Maršík for introducing me to the world of non-equilibrium thermodynamics, for his utmost generosity and support upon which I could rely, for the influential questions he posed and, last but not least, for the inspiringly contagious enthusiasm for the science.

My thanks also belong to my colleagues V. Miloš, Prof. Bouzek, Dr. Kodým and Doc. Paidar from UCT Prague. Our collaboration kept me in touch with the reality of the high temperture solid oxide cells.

I am grateful to my colleagues from the Weierstrass Institute, Prof. Dreyer, Dr. Landstorfer and Dr. Müller for all the challenging dicussions and the good ideas they have enriched me with.

I would like to thank to Dr. Guhlke for his unending patience and openness when he was enduring my questioning of his Ph.D. thesis. These dicussions helped immensely during formulation of the first and also the second chapter.

I thank to Dr. Fuhrmann for the tremendous support and compassion he provided me with at the Weierstrass Institute. I could not have wished for a better superior.

Last, but by no means least, I am genuinely indebted to my friend and colleague Dr. Michal Pavelka. Thank you.

The development of this thesis would hardly have been possible without the support of the below listed projects and institutions.

- European Social Fund, project no. CZ.1.05/2.1.00/03.0088
- Ministry of Education, Youth and Sports of the Czech Republic, project no. LO1402
- Grant Agency of Charles University, project no. 70515
- Czech Science Foundation, project no. 17-15498Y
- German Research Foundation, project no. FU 316/14-1
- Natural Sciences and Engineering Research Council of Canada
- Erasmus+ Programme

The final year of completion of the thesis was supported by the Weierstrass Institute in Berlin, Germany.

Title: Thermodynamic analysis of solid oxide cells

Author: Petr Vágner

Institute: Mathematical Institute

Supervisor: Prof. Ing. František Maršík, DrSc., Institute of Thermomechanics, Czech Academy of Sciences

Abstract: The thesis deals with continuum thermodynamic modeling and analysis of phenomena in solid oxide electrochemical cells. A general description of the evolution of charged mixtures using partial mass densities, momentum density, entropy density, electric induction, magnetic field, polarization, and magnetization based on the GENERIC framework is formulated. The formulation is used to recover the Landau-Lifshitz magnetization relaxation model, the Single Relaxation Time model for dielectrics, and the generalized Poisson-Nernst-Planck model. The latter model is consequently linked to the second part, where a novel double layer model of an yttria-stabilized zirconia interface is formulated within non-equilibrium thermodynamics. The model is solved for numerically in the time domain, and cyclic voltammetry of the system is analyzed. The last part of the thesis demonstrates the limits of Exergy Analysis on a simple solid oxide hydrogen fuel cell model with non-isothermal boundary. It is demonstrated that the minimization of entropy production does not necessarily lead to the maximization of the electric power for certain optimization scenarios.

The thesis consists of a compilation of published and unpublished results of the author.

Keywords: non-equilibrium thermodynamics, GENERIC, electrochemistry, solid oxide cells, numerical simulation

Contents

Introduction

Modeling of electrochemical systems is a broad scientific field encompassing many different theories with aims to describe miscellaneous phenomena on diverse length and times scales. This thesis is mainly focused on the formulation and application of continuum-type non-equilibrium thermodynamic models for solid oxide electrochemical cells (SOEC, SOFC).

The first chapter incorporates a formulation of coupling between the fluid mechanics and electrodynamics using their Hamiltonian structure. On top of this, geometrical methods are used to account for the interaction of the fields of polarization and magnetization with the charged fluid. Eventually, dissipation is introduced and employed to reduce some of the fields recovering constitutive equations on less detailed levels of description. For instance, the generalized Poisson-Nernst-Planck equations or Landau-Lifshitz magnetization models are found again. The main results of this chapter contained in [3]. The results are not limited to the description of electrochemical reactors but may be used also to describe the dynamics of the polarization, e.g., waves stemming from the dipole-dipole interaction.

In the second chapter, a detailed model of a double layer of a solid oxide interface is derived. The derivation is done on the basis of bulk-surface non-equilibrium electrothermodynamics [5]. Models of free energy density, capturing the main features of (crystalline) yttria-stabilized zirconia bulk and surface, are introduced into generalized Poisson-Nernst-Planck system. The resulting system of evolution equations is solved for using the finite volume method and cyclic voltamograms of YSZ—air—metal cell are obtained and discussed in detail. The results of the chapter are content of [4].

The last, third, chapter is a clear-cut demonstration of Exergy Analysis [6] validity. The limits of the theory are demonstrated on an analytically tractable model of solid oxide hydrogen fuel cell. It is shown that the optimization predictions of Exergy Analysis, i.e., the minimization of the entropy production, do not coincide with the power maximization for SOEC with non-isothermal boundary. The underlying principles, on which this chapter is based, are contained in [1], the results itself were published in [2]

The problems in the first chapter are considered on a very abstract level. The model equations employed in the second chapter may be seen as a consequence of the general results of the first chapter. Finally, the device model optimized in the third chapter is, in fact, a non-isothermal electroneutral model from the second section. Hence, the order of the presentation respects the decreasing level of abstractness, although, the chapters were actually created in the exactly opposite order[1].

Let us now focus on the links between the first and second chapter. First, the description of electrodiffusion, see Section 1.4.8, obtained by the Dynamic Maximum Entropy Principle in the first chapter is principally equivalent to the diffusion flux of oxide ions derived in the second chapter, see Section 2.2 (2.36b) and (2.35b), although with a different choice of the diffusion coefficient. Second, the mass action law chemical kinetics, see Appendix 1.4, is equivalent to the con-

[1] As it often happens in real life.

stitutive relation for the chemical reaction (2.63) employed in the second chapter. Third, the novel formulation of adsorption between bulk and surface using mixed bulk-surface dissipation potential, see Appendix 1.5, results in an adsorption flux equivalent to the flux of oxide ions, cf. (2.60). Therefore, the YSZ interface model developed in the second chapter within Classical Irreversible Thermodynamics can be alternatively formulated in the GENERIC framework.

The thermodynamic model of a non-isothermal solid oxide electrochemical cell, worked out in the third chapter, may be regarded as the oxide ion transport formulated in the second chapter considered in electroneutral limit.

At the time of submission of this thesis, the three chapters are either published [1, 2] or submitted to peer-reviewed journals [3, 4]. The publications are alternatively denoted as [P1-P4] in the List of Publications.

1. Multiscale electrodynamics of charged mixtures

Fluid mechanics and electrodynamics are two theories of Hamiltonian nature, which are coupled through the Lorentz force. Besides the fields of electric displacement and magnetic field, there are also the fields of polarization and magnetization, which are interacting with both matter and electromagnetic field. We propose a geometrical construction of reversible evolution equations of all the mentioned fields in mutual coupling. Afterwards, dissipation is imposed to particular fields, which are then reduced to the respective constitutive relations playing a role on less detailed levels of description. In summary, we propose multiscale thermodynamics of mixtures of fluids, electrodynamics, polarization and magnetization in mutual interaction.

1.1 Introduction

Theoretical electrochemistry aims to describe and predict behavior of chemically reacting systems of charged substances. The modeling methods vary according to the characteristic times and lengths of the observed electrochemical systems. This paper aims to develop a hierarchy of continuum models on different levels of description using the framework of the General Equation for Non-Equilibrium Reversible-Irreversible Coupling (GENERIC) [7, 8, 9, 10].

Let us thus briefly recall GENERIC. Consider an isolated system described by state variables $\mathbf{x}$. The state variables can be for instance position and momentum of a particle, field of probability density on phase space, fields of density and momentum density, electromagnetic fields, etc. Evolution of functionals $F(\mathbf{x})$ of the state variables is then expressed as

$$\dot{F} = \{F, E\} + \langle F_{\mathbf{x}}, \Xi_{\mathbf{x}^*}|_{\mathbf{x}^*=S_{\mathbf{x}}} \rangle, \tag{1.1}$$

where the former term on the right hand side stands for a Poisson bracket of the functional and energy while the latter for scalar product of gradient of F and gradient of a dissipation potential. Conjugate variables (derivatives of entropy in the entropic representation) are denoted by $\mathbf{x}^*$. The Poisson bracket is antisymmetric, which leads to automatic energy conservation, and satisfies Jacobi identity, which expresses intrinsic compatibility of the reversible evolution. The irreversible term yields a generalized gradient flow driven by gradient of entropy and ensures the second law of thermodynamics. Many successful models in non-equilibrium thermodynamics have been cast in the GENERIC structure (1.1), and many new thermodynamically consistent models have been obtained by seeking that structure.

Our strategy in this paper will be to couple the Poisson bracket of fluid mechanics and Poisson bracket of electrodynamics in vacuum by semidirect product. In other words, we let the electrodynamics be advected by fluid mechanics as in [10]. To go beyond, we add also the field of polarization density and a canonically coupled momentum of polarization. This is important to express the behavior of dipole moment of molecules in interaction with electromagnetic field and the

overall motion. Moreover, we add magnetization (the famous Landau & Lifschitz model) advected by fluid mechanics. This way we build a hierarchy of levels of description with appropriate Poisson brackets expressing kinematics on the levels.

Subsequently, we introduce dissipation on the most detailed levels of description, which leads to reduction to less detailed (lower) levels, finishing on the level of mechanical equilibrium, where the evolution is governed by the generalized Poisson-Nernst-Planck equations. We believe that such a complete and geometric picture of continuum thermodynamics of matter coupled with electrodynamics (including polarization and magnetization) was missing in the literature.

Remark on $\mathbf{x}^\dagger$ and $\mathbf{x}^*$ notation. Equation (1.1) contains derivatives of energy and entropy with respect to the state variables.

The reversible evolution is generated by derivates of energy in the Poisson bracket. Moreover, the form of Poisson bracket is usually conveniently expressed in the energetic representation, i.e. when entropy density is amongst the state variables. To this end, the energetic representation is employed throughout the first section, where the reversible evolution is developed. The energy-conjugate to variable $\mathbf{x}$, i.e. functional derivative of energy $\frac{\delta E}{\delta \mathbf{x}}$ will be briefly denoted by $\mathbf{x}^\dagger$ or $E_{\mathbf{x}}$.

On the other hand, the irreversible evolution is conveniently expressed in terms of the derivatives of a dissipation potential w.r.t. conjugate variables, which are later on indentified as the derivatives of entropy. Therefore, it is of advantage to express the irreversible using entropic variables, i.e. containing energy density, and in terms of entropy derivatives $\frac{\delta S}{\delta \mathbf{x}}$ will be briefly denoted by $\mathbf{x}^*$ or $S_{\mathbf{x}}$.

1.2 Hamiltonian evolution

Firstly, the Hamiltonian evolution in terms of continuum mechanics will be briefly introduced, see [10, Chapter 3].

Let Ω be an open subset of $\mathbb{R}^d$. Let $I \subset \mathbb{R}$ denote a time interval. Let $\mathbb{X}$ be a set of smooth functions on $(I \times \Omega)^s$. Let $\mathbf{x} \in \mathbb{X}$ be a set of variables, i.e. the assumed level of description. Let $\mathbb{X}^\bigstar$ be space of differentiable functionals on $\mathbb{X}$. Poisson bracket $\{\cdot,\cdot\} : \mathbb{X}^\bigstar \times \mathbb{X}^\bigstar \to \mathbb{X}^\bigstar$ is a map that for all $F, G, H, R \in \mathbb{X}^\bigstar$ and $\alpha, \beta, \gamma, \delta \in \mathbb{R}$ satisfies the following properties:

1. **bilinearity**:

$$\begin{aligned}\{\alpha F + \beta H, \gamma G + \delta R\}(\mathbf{x}) =& \alpha\gamma\{F, G\}(\mathbf{x}) + \alpha\delta\{F, R\}(\mathbf{x}) \\ &+ \beta\gamma\{H, G\}(\mathbf{x}) + \beta\delta\{H, R\}(\mathbf{x}) \ , \end{aligned} \tag{1.2}$$

2. **anticommutativity**:

$$\{F, G\}(\mathbf{x}) = -\{G, F\}(\mathbf{x}) \ , \tag{1.3}$$

3. **the Leibniz rule**:

$$\{FG, H\}(\mathbf{x}) = F(\mathbf{x})\{G, H\}(\mathbf{x}) + \{F, H\}(\mathbf{x})G(\mathbf{x}) \ , \tag{1.4}$$

4. **the Jacobi identity**:

$$\{F,\{G,H\}\}(\mathbf{x})+\{H,\{F,G\}\}(\mathbf{x})+\{G,\{H,F\}\}(\mathbf{x})=0\ . \tag{1.5}$$

The first and second property imply the Poisson bracket being also antisymmetric, i.e. $\{F,F\}=-\{F,F\}=0$.

Let $E\in\mathbb{X}^\star$ be energy of the system. The Hamiltonian evolution of a functional $A\in\mathbb{X}^\star$ is then given as

$$\dot{A}=\frac{\partial}{\partial t}A+\{A,E\}\ . \tag{1.6}$$

Note, that the partial time derivative is zero if A does not depend on time explicitly. This will be tacitly assumed in the remainder of the chapter.

1.3 Hierarchy of Poisson brackets

1.3.1 Fluid mechanics of mixtures

Let us start with fluid mechanics, where state variables are fields of density, momentum density and entropy density, $\mathbf{x}=(\rho,\mathbf{u},s)$. The Poisson bracket expressing kinematics of fluid mechanics has been long known [11, 12, 13, 14, 15]. The Poisson bracket can be easily extended to mixtures with multiple densities, momenta and entropies (i.e. temperatures), see e.g. [16].

Classical fluid mechanics

The Poisson bracket generating one-component compressible fluid mechanics (hydrodynamic Poisson bracket) is

$$\begin{aligned}\{F,G\}^{(FM)}(\rho,\mathbf{u},s)=&\int\mathrm{d}\mathbf{r}\rho\left(\partial_iF_\rho G_{u_i}-\partial_iG_\rho F_{u_i}\right)\\&+\int\mathrm{d}\mathbf{r}u_i\left(\partial_jF_{u_i}G_{u_j}-\partial_jG_{u_i}F_{u_j}\right)\\&+\int\mathrm{d}\mathbf{r}s\left(\partial_iF_sG_{u_i}-\partial_iG_sF_{u_i}\right),\end{aligned} \tag{1.7}$$

where ρ, $\mathbf{u}$ and s are density, momentum density and volume entropy density, respectively, see the references above.

Once energy, usually

$$E=\int\mathrm{d}\mathbf{r}\left(\frac{\mathbf{u}^2}{2\rho}+\varepsilon(\rho,s)\right), \tag{1.8}$$

is provided, reversible evolution of an arbitrary functional F of the state variables reads

$$\begin{aligned}\dot{F}=&\{F,E\}^{(FM)}\\=&\int\mathrm{d}\mathbf{r}F_\rho\left(-\partial_i(\rho E_{u_i})\right)\\&+\int\mathrm{d}\mathbf{r}F_{u_i}\left(-\rho\partial_iE_\rho-u_j\partial_iE_{u_j}-s\partial_iE_s-\partial_j(u_iE_{u_j})\right)\\&+\int\mathrm{d}\mathbf{r}F_s\left(-\partial_i(sE_{u_i})\right),\end{aligned} \tag{1.9}$$

where integration by parts was used several times. Boundary terms disappear as we assume isolated (e.g. periodic) system.

By comparing with the chain rule

$$\dot{F} = \int \mathrm{d}\mathbf{r}\, (F_\rho \partial_t \rho + F_{u_i} \partial_t u_i + F_s \partial_t s) \tag{1.10}$$

we can read the evolution equations for fluid mechanics,

$$\partial_t \rho = -\partial_i (\rho E_{u_i}) \tag{1.11a}$$
$$\partial_t u_i = -\rho \partial_i E_\rho - u_j \partial_i E_{u_j} - s \partial_i E_s - \partial_j (u_i E_{u_j}) \tag{1.11b}$$
$$\partial_t s = -\partial_i (s E_{u_i}), \tag{1.11c}$$

the compressible non-isothermal Euler equations for ideal fluids.

Fluid mechanics of mixtures

Consider now a mixture of n species (denoted by Greek indexes from set Ω), each of which is described by its own density, momentum density and entropy density. The Poisson bracket expressing kinematics of state variables $\mathbf{x} = (\rho_\alpha, \mathbf{u}^\alpha, s_\alpha)$, $\alpha \in \Omega$, is

$$\{F, G\}(\rho_\beta, \mathbf{u}^\beta, s_\beta) = \sum_{\alpha=1}^{n} \{F, G\}^{(\mathrm{FM})_\alpha}(\rho_\alpha, \mathbf{u}^\alpha, s_\alpha) \tag{1.12}$$

This Poisson bracket can be derived for instance by projection from the Liouville equation [16]. It consists of sum of n Poisson brackets (1.7), each expressed in terms of variables of mixture component α.

Poisson bracket (1.12) depends on n momenta and entropies, each for one component of the mixture, which is a rather detailed description allowing for independent motion of the constituents and for different temperatures of them (as in cold plasma, where electrons have different temperature than ions). We are, however, often interested in less detailed description, keeping only densities of the species, the total momentum and total entropy,

$$\mathbf{u} = \sum_{\alpha=1}^{n} \mathbf{u}^\alpha \qquad \text{and} \qquad s = \sum_{\alpha=1}^{n} s_\alpha. \tag{1.13}$$

By letting the arbitrary functional depend only on state variables $\mathbf{x} = (\rho_\alpha, \mathbf{u}, s)$, bracket (1.12) becomes

$$\begin{aligned} \{F, G\}^{(\mathrm{CIT})} = &\sum_{\alpha=1}^{n} \int \mathrm{d}\mathbf{r} \rho_\alpha \left(\partial_i F_{\rho_\alpha} G_{u_i} - \partial_i G_{\rho_\alpha} F_{u_i}\right) \\ &+ \int \mathrm{d}\mathbf{r} u_i \left(\partial_j F_{u_i} G_{u_j} - \partial_j G_{u_i} F_{u_j}\right) \\ &+ \int \mathrm{d}\mathbf{r} s \left(\partial_i F_s G_{u_i} - \partial_i G_s F_{u_i}\right), \end{aligned} \tag{1.14}$$

referred to as the classical mixture hydrodynamic bracket and generating the reversible part of Classical Irreversible Thermodynamics (CIT) [17].

The descriptions of the fluid and fluid mixture dynamic considered in the remainder of the paper will be based mainly on the brackets (1.7) and (1.14), respectively.

1.3.2 Electrodynamics in vacuum

The reversible evolution of electromagnetic fields is generated by the canonical Poisson bracket, see [10],

$$\{F,G\}^{(\mathrm{EM})_{\mathbf{A}}}(\mathbf{A},\mathbf{Y}) = \int \mathrm{d}\mathbf{r}\,(F_{A_i}G_{Y_i} - G_{A_i}F_{Y_i}) = \int \mathrm{d}\mathbf{r}\,(F_{D_i}G_{A_i} - G_{D_i}F_{A_i})\,, \tag{1.15}$$

where $\mathbf{A}$ stands for the vector potential and $\mathbf{Y} = -\mathbf{D}$ denotes negative of electric displacement field (either in variables $(\mathbf{A},\mathbf{Y})$ or $(\mathbf{A},\mathbf{D})$). Let us define the magnetic field as

$$B_i = \varepsilon_{ijk}\partial_j A_k. \tag{1.16}$$

In order to express the bracket (1.15) in terms of magnetic field, the assumed functionals to be dependent only on the curl of $\mathbf{A}$. Bracket (1.15), transformed in terms of $(\mathbf{D},\mathbf{B})$, see [18], reads as

$$\{F,G\}^{(\mathrm{EM})}(\mathbf{D},\mathbf{B}) = \int \mathrm{d}\mathbf{r} F_{D_i}\varepsilon_{ijk}\partial_j G_{B_k} - G_{D_i}\varepsilon_{ijk}\partial_j F_{B_k}. \tag{1.17}$$

This is the Poisson bracket expressing kinematics of electromagnetic fields $\mathbf{D}$ and $\mathbf{B}$.

Let us suppose the following energy of the electromagnetic field in vacuum:

$$E = \int \mathrm{d}\mathbf{r}\frac{1}{2}\left(\frac{\mathbf{D}^2}{\varepsilon_0} + \frac{\mathbf{B}^2}{\mu_0}\right), \tag{1.18}$$

here ε_0 and μ_0 stand for vacuum permittivity and vacuum permeability, respectively. The evolution equations of the electromagnetic field given by (1.17) and (1.16) read

$$\partial_t D_i = \varepsilon_{ijk}\partial_j E_{B_k} \tag{1.19a}$$

$$\partial_t B_i = -\varepsilon_{ijk}\partial_j E_{D_k}, \tag{1.19b}$$

where the conjugate fields are actually electric and magnetic intensities, $E_{\mathbf{D}} = \mathbf{E}$ and $E_{\mathbf{B}} = \mathbf{H}$. Using energy (1.16), the evolution equations can be rewritten as

$$\partial_t E_i = \frac{1}{\varepsilon_0\mu_0}\varepsilon_{ijk}\partial_j B_k \tag{1.20a}$$

$$\partial_t B_i = -\varepsilon_{ijk}\partial_j E_k \tag{1.20b}$$

where $\varepsilon_0\mathbf{E} = \mathbf{D}$ denotes the electric field as well.

Applying divergence to (1.20) gives the following evolution equations:

$$\partial_t \operatorname{div}\mathbf{B} = 0 \qquad \text{and} \qquad \partial_t \operatorname{div}\mathbf{E} = 0 \tag{1.21}$$

Hence, the usual constraints–Gauß's law for electric and magnetic charge [19]– hold true if satisfied by the initial condition, see [20].

1.3.3 Electromagnetic field advected by charged fluids

The purpose of this section is to formulate coupled kinematics of fluids and electromagnetic fields. We employ the theory of semidirect product to find such coupling, and then we perform a transformation unveiling the usual form Lorentz force.

Semidirect product

We have already recalled the Hamiltonian nature of fluid mechanics. There is, however, a finer structure behind, the Lie-Poisson dynamics, where the Poisson bracket is the Lie-Poisson bracket on a Lie algebra dual. Another examples of Lie-Poisson dynamics are rigid body rotation or kinetic theory. In [21] it is explained how to construct new Hamiltonian dynamics by letting one Hamiltonian dynamics be advected by another. Having a Lie algebra dual $\mathfrak{l}^*$ (for instance fluid mechanics), an another Lie algebra dual or cotangent bundle is advected by $\mathfrak{l}^*$ by the construction of semidirect product.

One can even think of mutual action of the two Hamiltonian dynamics, which leads to the structure of matched pairs [18], [22]. Here, however, we restrict the discussion only to one-sided action of one Hamiltonian system to another, i.e. to the semidirect product. A general formula for the Poisson bracket of semidirect product of a Lie algebra dual $\mathfrak{l}^*$ and cotangent bundle $T^*M = V \times V^*$ reads,

$$\begin{aligned}\{F,G\}^{(\mathfrak{l}^*\times T^*M)} &= \{F,G\}^{(\mathfrak{l}^*)} + \{F,G\}^{(T^*M)} \\ &+ \langle F_{\mathbf{A}}, G_{\mathbf{m}} \rhd \mathbf{A}\rangle - \langle G_{\mathbf{A}}, F_{\mathbf{m}} \rhd \mathbf{A}\rangle \\ &+ \langle \mathbf{Y}, F_{\mathbf{m}} \rhd G_{\mathbf{Y}}\rangle - \langle \mathbf{Y}, G_{\mathbf{m}} \rhd F_{\mathbf{Y}}\rangle \end{aligned} \tag{1.22}$$

where $\mathbf{A} \in V$ is a covector field, $\mathbf{A} = A_i dx^i$ and $\mathbf{Y} \in V^*$ is a vector field $\mathbf{Y} = -D^i\partial_i$, $\{F,G\}^{(\mathfrak{l}^*)}$ is the Lie-Poisson bracket on the Lie algebra dual, $\{F,G\}^{(T^*M)}$ is the canonical Poisson bracket on the cotangent bundle, $\langle \bullet, \bullet\rangle$ is a scalar product (usually L^2, i.e. integration over the domain, or duality in distributions $\mathcal{D}'$), $\mathbf{m} \in \mathfrak{l}^*$ is the momentum density (element of the Lie algebra dual) and $\rhd$ is the action of $\mathfrak{l}^*$ on T^*M, minus the Lie derivative $-\mathcal{L}$, see Appendix 1.3.

Instead of single-component fluids, we can take bracket (1.14), and after the transformation from $(\mathbf{A},\mathbf{Y})$ to $(\mathbf{D},\mathbf{B})$, as in Sec. 1.3.2, we obtain Poisson bracket

$$\{F,G\}^{(\mathrm{mEMHD})}(\rho_\alpha,\mathbf{m},s,\mathbf{D},\mathbf{B}) = \{F,G\}^{(\mathrm{CIT})}|_{\mathbf{u}=\mathbf{m}} + \{F,G\}^{(\mathrm{EM})} \tag{1.23}$$

$$\{F,G\}^{(\mathrm{SP})}(\mathbf{D},\mathbf{m}) \left\{ \begin{array}{l} + \int \mathrm{d}\mathbf{r} D_i \left(\partial_j F_{D_i} G_{m_j} - \partial_j G_{D_i} F_{m_j}\right) \\ + \int \mathrm{d}\mathbf{r} \partial_j D_j (F_{m_i} G_{D_i} - G_{m_i} F_{D_i}) \\ + \int \mathrm{d}\mathbf{r} D_j (F_{m_i} \partial_j G_{D_i} - G_{m_i} \partial_j F_{D_i}) \end{array}\right.$$

$$\{F,G\}^{(\mathrm{SP})}(\mathbf{B},\mathbf{m}) \left\{ \begin{array}{l} + \int \mathrm{d}\mathbf{r} B_i \left(\partial_j F_{B_i} G_{m_j} - \partial_j G_{B_i} F_{m_j}\right) \\ + \int \mathrm{d}\mathbf{r} \partial_j B_j (F_{m_i} G_{B_i} - G_{m_i} F_{B_i}) \\ + \int \mathrm{d}\mathbf{r} B_j (F_{m_i} \partial_j G_{B_i} - G_{m_i} \partial_j F_{B_i}), \end{array}\right.$$

where $\mathbf{m}$ denotes total momentum density (of matter and electromagnetic field),

$$\mathbf{m} = \mathbf{u} + \mathbf{D} \times \mathbf{B}\ . \tag{1.24}$$

Note that the notation introduced in (1.23) allows to write briefly

$$\begin{aligned}\{F,G\}^{(\mathrm{mEMHD})}(\rho_\alpha,\mathbf{m},s,\mathbf{D},\mathbf{B}) &= \{F,G\}^{(\mathrm{CIT})}|_{\mathbf{u}=\mathbf{m}} + \{F,G\}^{(\mathrm{EM})} \\ &+ \{F,G\}^{(\mathrm{SP})}(\mathbf{D},\mathbf{m}) + \{F,G\}^{(\mathrm{SP})}(\mathbf{B},\mathbf{m}) \end{aligned} \tag{1.25}$$

Bracket (1.23) expresses kinematics of a CIT mixture and electromagnetic field, with state variables $\mathbf{x} = (\rho_\alpha, \mathbf{m}, s, \mathbf{D}, \mathbf{B})$, and was found (for the single species case) in [23, 24, 25].

Transformation to mass momentum

Let us suppose that each mixture component carries charge $e_0 \frac{z_\alpha}{m_\alpha}$ proportional to mixture density. The free charge density is defined as

$$\rho_{\mathrm{f}} = \sum_{\alpha=1}^{n} \frac{z_\alpha e_0}{m_\alpha} \rho_\alpha. \tag{1.26}$$

Poisson bracket (1.23) can be now transformed by means of relation (1.24) to the mass momentum $\mathbf{u}$ instead of the total momentum $\mathbf{m}$. The calculation was carried out in [18] and [10] and leads to Poisson bracket

$$\begin{aligned}\{F, G\}^{(\mathrm{uEMHD})}(\rho_\alpha, \mathbf{u}, s, \mathbf{D}, \mathbf{B}) = \{F, G\}^{(\mathrm{CIT})} + \{F, G\}^{(\mathrm{EM})} \\ + \int \mathrm{d}\mathbf{r} \sum_{\alpha=1}^{n} e_0 \frac{z_\alpha \rho_\alpha}{m_\alpha} \left(F_{u_i} G_{D_i} - G_{u_i} F_{D_i}\right) \\ + \int \mathrm{d}\mathbf{r} \sum_{\alpha=1}^{n} e_0 \frac{z_\alpha \rho_\alpha}{m_\alpha} B_i \varepsilon_{ijk} F_{u_j} G_{u_k},\end{aligned} \tag{1.27}$$

which is the Poisson bracket expressing evolution of a CIT mixture coupled with electromagnetic field (using the mass momentum $\mathbf{u}$).

The relation between formulation (1.27) and (1.23) can be also viewed in terms of surface balances of the electric induction flux and magnetic induction flux for static and co-moving surfaces as it is shown in [26]

For a mixture described by means of not only multiple densities, but also multiple momentum and entropy densities, see bracket (1.12), the Poisson bracket coupling it with electromagnetic field is

$$\begin{aligned}\{F, G\}^{(\mathrm{EMHD})}(\rho_\beta, \mathbf{u}^\beta, s_\beta, \mathbf{D}, \mathbf{B}) = \sum_{\alpha=1}^{n} \{F, G\}^{(FM)_\alpha} + \{F, G\}^{(EM)} \\ + \int \mathrm{d}\mathbf{r} \sum_{\alpha=1}^{n} e_0 \frac{z_\alpha \rho_\alpha}{m_\alpha} \left(F_{u_{\alpha,i}} G_{D_i} - G_{u_{\alpha,i}} F_{D_i}\right) \\ + \int \mathrm{d}\mathbf{r} \sum_{\alpha=1}^{n} e_0 \frac{z_\alpha \rho_\alpha}{m_\alpha} B_i \varepsilon_{ijk} F_{u_{\alpha,j}} G_{u_{\alpha,k}}.\end{aligned} \tag{1.28}$$

This bracket indeed leads back to Poisson bracket (1.27) by projection (1.13), but can be also derived by projection from the Liouville equation [10], which constitutes an alternative way of the derivation.

Gauß's law for electric and magnetic charges

Equations (1.20) represent the Gauß's law for the electric and magnetic charges in vacuum. Let us now consider the dynamics of coupled matter and electromagnetic field generated by brackets (1.27) and (1.23). The evolution equation of magnetic field for bracket (1.27) reads as

$$\partial_t B_i = -\varepsilon_{ijk} \partial_j D_k^\dagger \tag{1.29}$$

and for (1.23) as

$$\partial_t B_i = -\varepsilon_{ijk}\partial_j D_k^\dagger - \partial_j \left(B_i m_j^\dagger - B_j m_i^\dagger \right) - m_i^\dagger \partial_j B_j. \tag{1.30}$$

As for vacuum, if the initial condition $\operatorname{div} \mathbf{B}(\mathbf{r}, t = 0) = 0$ is satisfied then neither (1.29) nor (1.30) can violate the Gauß's for magnetic charge for further times.

The discussion for the electric charge is more subtle. The evolution equations of $\mathbf{D}$ for brackets (1.27) and (1.23) are

$$\partial_t D_i = \varepsilon_{ijk}\partial_j B_k^\dagger - \sum_{\alpha=1}^{n} e_0 \frac{z_\alpha \rho_\alpha}{m_\alpha} u_i^\dagger \ , \tag{1.31}$$

$$\partial_t D_i = \varepsilon_{ijk}\partial_j B_k^\dagger - \partial_j \left(D_i m_j^\dagger - D_j m_i^\dagger \right) - m_i^\dagger \partial_j D_j \ , \tag{1.32}$$

respectively. The divergent part of the first two equations is equal to the charge-weighted sum of the evolution equations of the partial mass densities generated by the respective brackets. Therefore, if

$$\operatorname{div} \mathbf{D} = \rho_\mathrm{f} \tag{1.33}$$

is satisfied as an initial condition then again neither (1.31) nor (1.32) can violate it.

Casting divergence on equation (1.32) gives

$$\partial_t \partial_i D_i = -\partial_i \left(m_i^\dagger \partial_j D_j \right) \ . \tag{1.34}$$

Clearly, the form of equation (1.34) is the same as for a conserved continuum-advected density (quantity). Therefore, analogously to the previous, if (1.33) is satisfied as an initial condition it will be satisfied during the evolution.

From the geometric point of view the Gauß's laws can be seen as gauge invariance of the respective Lie algebraic structures [20].

We have shown that the dynamics of charged continuum generated by brackets (1.27) and (1.23) structurally preserves the Gauß's laws for electric and magnetic charge.

1.3.4 Polarization

The reversible evolution of a charged mixture in electromagnetic field is described by one of the Poisson brackets in the previous section and a choice of energy. But such description does not, in general, capture the intrinsic dipole moments of the molecules, i.e. *polarization*. An additional *bound* charge is present due to internal dipole density of the matter on top of the modeled free charge.

Description of the polarization charge depends profoundly on the chosen variables, the time/space scales and the internal structure of the assumed matter. The classical treatment on the macroscopic level, see e.g. [27], resorts to the definition of polarization vector $\mathbf{P}$. The divergence part of $\mathbf{P}$ is set equal to the density of polarization charge. The time derivative of $\mathbf{P}$ represents current, therefore it is added to the left-hand side of the Ampère's law.

Russakoff in [28] acquired the polarization as a consequence of averaging of microscopic Maxwell's equations with point charges and subsequent expansion

with respect to spatially correlated charges. This approach leads, compared to the Purcell's, to a definition of the polarization related magnetization $\mathbf{M}$ which is proportional to the averaged relative velocities of the correlated charges. Neither Russakoff nor Purcell discussed the dynamics of the point charges nor the correlated collections of charges, i.e. molecules and ions.

Disturbances of the electric field propagate with the speed of light. The polarization depends on the internal dynamics of atoms and molecules, therefore, the speed of disturbance propagation should be small compared to the speed of light.

Intrinsic dynamics of polarization

Density of polarization $\mathbf{P}$ represents a vector field just as the displacement field $\mathbf{D}$. Advection of the vector field by the fluid mechanics is then expressed by a semidirect product as in Sec. 1.3.3. Similarly as in that Section, we can add (besides $\mathbf{P}$) the conjugate momentum variable (to be denoted by $\boldsymbol{\mu}$). The Poisson bracket expressing advection of the pair $(\boldsymbol{\mu}, -\mathbf{P})$ by fluid mechanics is shown in the following section.

The canonical Poisson bracket of state variables $\boldsymbol{\mu}$ and $\mathbf{P}$ reads

$$\{F, G\}^{\mathbf{P}\mu}(\mathbf{P}, \mu) = \int \mathrm{d}\mathbf{r} \left(F_{P_i} G_{\mu_i} - G_{P_i} F_{\mu_i}\right) \ , \tag{1.35}$$

which is analogical to (1.15). Bracket (1.35) can represent a continuum of elementary dipoles with fixed centres of mass, but changing length and orientation. Indeed, covector field μ can be interpreted as proportional to the relative momentum of a dipole particles, c.f. variable $\mathbf{t}$ in (1.151) and (1.152). The divergence part of $\mathbf{P}$ represents the bound charge density,

$$\rho_b = -\operatorname{div} \mathbf{P}. \tag{1.36}$$

Advected cotangent bundle $(\boldsymbol{\mu}, -\mathbf{P})$

When the dipoles are not fixed in space, but advected by a fluid, the interaction is captured by coupling of bracket (1.35) and fluid dynamics bracket (1.14) by semidirect product,

$$\begin{aligned}
\{F, G\}^{\mathrm{FMP}\mu}(\rho_\alpha, {}^{\mu}\mathbf{u}, s, \mathbf{P}, \boldsymbol{\mu}) = \{F, G\}^{(\mathrm{CIT})}(\rho_\alpha, {}^{\mu}\mathbf{u}, s) + \{F, G\}^{\mathbf{P}\boldsymbol{\mu}}(\mathbf{P}, \boldsymbol{\mu}) \\
+ \int \mathrm{d}\mathbf{r} P_i \left(\partial_j F_{P_i} G_{{}^{\mu}u_j} - \partial_j G_{P_i} F_{{}^{\mu}u_j}\right) \\
+ \int \mathrm{d}\mathbf{r} \partial_j P_j (F_{{}^{\mu}u_i} G_{P_i} - G_{{}^{\mu}u_i} F_{P_i}) \\
+ \int \mathrm{d}\mathbf{r} P_j (F_{{}^{\mu}u_i} \partial_j G_{P_i} - G_{{}^{\mu}u_i} \partial_j F_{P_i}) \\
\{F, G\}^{(\mathrm{SP})_{\mathbf{A}}}(\boldsymbol{\mu}, {}^{\mu}\mathbf{u}) \begin{cases} - \int \mathrm{d}\mathbf{r} \partial_j \mu_i \left(F_{\mu_i} G_{{}^{\mu}u_j} - G_{\mu_i} F_{{}^{\mu}u_j}\right) \\ - \int \mathrm{d}\mathbf{r} \mu_i \left(F_{\mu_j} \partial_j G_{{}^{\mu}u_i} - G_{\mu_j} \partial_j F_{{}^{\mu}u_i}\right), \end{cases}
\end{aligned} \tag{1.37}$$

which is analogical to bracket (1.157). Note that the total momentum of the coupled system is denoted as ${}^{\mu}\mathbf{u}$. This Poisson bracket expresses kinematics of

fluid mechanics advecting the polarization density with its conjugate momentum (relative momentum of the intrinsic dipole charges).

Note that bracket (1.37) may be briefly expressed as

$$\{F,G\}^{\mathrm{FMP}\mu}(\rho_\alpha, {}^{\mu}\mathbf{u}, s, \mathbf{P}, \boldsymbol{\mu}) = \{F,G\}^{(\mathrm{CIT})}(\rho_\alpha, {}^{\mu}\mathbf{u}, s) + \{F,G\}^{\mathbf{P}\mu}(\mathbf{P}, \boldsymbol{\mu}) + \{F,G\}^{(\mathrm{SP})}(\mathbf{P}, {}^{\mu}\mathbf{u}) + \{F,G\}^{(\mathrm{SP})_{\mathbf{A}}}(\boldsymbol{\mu}, {}^{\mu}\mathbf{u}) \,, \tag{1.38}$$

using the definition of $\{F,G\}^{(\mathrm{SP})}$ from (1.23) and $\{F,G\}^{(\mathrm{SP})_{\mathbf{A}}}$ from (1.37).

The evolution equations given by (1.37) are as follows,

$$(\partial_t \rho_\alpha)_{\mathrm{rev}} = -\partial_j(\rho_\alpha \, {}^{\mu}u_j{}^{\dagger}) \tag{1.39a}$$

$$(\partial_t s)_{\mathrm{rev}} = -\partial_j(s \, {}^{\mu}u_j{}^{\dagger}) \tag{1.39b}$$

$$(\partial_t \, {}^{\mu}u_i)_{\mathrm{rev}} = -\sum_{\alpha=1}^{n} \rho_\alpha \partial_i \rho_\alpha^{\dagger} - s\partial_i s^{\dagger} - {}^{\mu}u_j \partial_i \, {}^{\mu}u_j{}^{\dagger} - P_j \partial_i P_j^{\dagger} + \mu_j^{\dagger} \partial_i \mu_j + \partial_j \left(P_i^{\dagger} P_j - \mu_i \mu_j^{\dagger} - {}^{\mu}u_i \, {}^{\mu}u_j{}^{\dagger} \right) \,, \tag{1.39c}$$

$$(\partial_t P_i)_{\mathrm{rev}} = \mu_i^{\dagger} - \partial_j \left(P_i \, {}^{\mu}u_j{}^{\dagger} - P_j \, {}^{\mu}u_i{}^{\dagger} \right) - {}^{\mu}u_i{}^{\dagger} \partial_j P_j \tag{1.39d}$$

$$(\partial_t \mu_i)_{\mathrm{rev}} = -P_i^{\dagger} - {}^{\mu}u_j{}^{\dagger} \partial_j \mu_i - \mu_j \partial_i \, {}^{\mu}u_i{}^{\dagger}, \tag{1.39e}$$

where $\mathbf{x}^{\dagger}$ denotes derivative of energy with respect to $\mathbf{x}$ (as everywhere in this paper). Later they will be equipped with dissipation of $\boldsymbol{\mu}$ triggering subsequent relaxation of polarization.

Reduced variable $\mathcal{M}$

Instead of the conjugate polarization momentum $\boldsymbol{\mu}$, we can choose to work with curl of it,

$$\mathcal{M} = \operatorname{curl} \mu. \tag{1.40}$$

Similarly to the relation of vector potential and magnetic field, considering functionals depending only on $\mathcal{M}$ instead of μ turns Poisson bracket (1.39) to

$$\{F,G\}^{\mathbf{P}}(\mathbf{P}, \mathcal{M}) = \int \mathrm{d}\mathbf{r} \, (F_{P_i} \varepsilon_{ijk} \partial_j G_{\mathcal{M}_k} - G_{P_i} \varepsilon_{ijk} \partial_j F_{\mathcal{M}_k}) \,. \tag{1.41}$$

Bracket (1.41) has identical form as electromagnetic bracket (1.17), and gives evolution equation structurally similar to (1.136) due to the presence of curl $\mathcal{M}^{\dagger}$.

Coupling of (1.41) and (1.7) given by the semidirect product reads as

$$\{F,G\}^{\mathrm{FMP}}(\rho_\alpha, {}^{\mathcal{M}}\mathbf{u}, s, \mathbf{P}, \mathcal{M}) = \{F,G\}^{\mathrm{FM}}(\rho_\alpha, {}^{\mathcal{M}}\mathbf{u}, s) + \{F,G\}^{\mathbf{P}}(\mathbf{P}, \mathcal{M}) + \{F,G\}^{\mathrm{SP}}({}^{\mathcal{M}}\mathbf{u}, \mathbf{P}) + \{F,G\}^{\mathrm{SP}}({}^{\mathcal{M}}\mathbf{u}, \mathcal{M}) \,. \tag{1.42}$$

The form of $\{F,G\}^{\mathrm{SP}}$, defined in (1.23), is the same as for coupling of $\{F,G\}^{(\mathrm{EM})}$ and the fluid mixture due to the form of (1.41). In this case, the relation of the total momentum, denoted ${}^{\mathcal{M}}\mathbf{u}$, and the mass momentum is related to the total momentum as

$${}^{\mathcal{M}}\mathbf{u} = \mathbf{u} + \mathbf{P} \times \mathcal{M}. \tag{1.43}$$

The evolution equations given by (1.42) are as follows,

$$(\partial_t \rho_\alpha)_{\text{rev}} = -\partial_j(\rho_\alpha \, {}^{\mathcal{M}}u_j^\dagger) \tag{1.44a}$$

$$(\partial_t s)_{\text{rev}} = -\partial_j(s \, {}^{\mathcal{M}}u_j^\dagger) \tag{1.44b}$$

$$\begin{aligned}(\partial_t \, {}^{\mathcal{M}}u_i)_{\text{rev}} = &-\sum_{\alpha=1}^{n} \rho_\alpha \partial_i \rho_\alpha^\dagger - s\partial_i s^\dagger - {}^{\mathcal{M}}u_j \partial_i \, {}^{\mathcal{M}}u_j^\dagger - P_j \partial_i P_j^\dagger - \mathcal{M}_j \partial_i \mathcal{M}_j^\dagger \\ &+ \partial_j \left(P_i^\dagger P_j + \mathcal{M}_i^\dagger \mathcal{M}_j - {}^{\mathcal{M}}u_i \, {}^{\mathcal{M}}u_j^\dagger \right) ,\end{aligned} \tag{1.44c}$$

$$(\partial_t P_i)_{\text{rev}} = \varepsilon_{ijk}\partial_j \mathcal{M}_k^\dagger - \partial_j \left(P_i \, {}^{\mathcal{M}}u_j^\dagger - P_j \, {}^{\mathcal{M}}u_i^\dagger \right) - {}^{\mathcal{M}}u_i^\dagger \partial_j P_j \tag{1.44d}$$

$$(\partial_t \mathcal{M}_i)_{\text{rev}} = -\varepsilon_{ijk}\partial_j P_k^\dagger - \partial_j(\mathcal{M}_i \, {}^{\mathcal{M}}u_j^\dagger - \mathcal{M}_j \, {}^{\mathcal{M}}u_i^\dagger) - {}^{\mathcal{M}}u_i^\dagger \partial_j \mathcal{M}_j. \tag{1.44e}$$

The reason to carry out the projection from $\boldsymbol{\mu}$ to $\mathcal{M}$ was to bring the equations closer to comparable results in literature, e.g. [5]. Contrary to the construction used in (1.136), $\mathcal{M}$ plays role of an independent variable beforehand and its reversible evolution does not depend on the employed entropy principle (nor dissipation) as it is the case in [5]. Moreover, $\mathcal{M}$ itself does not appear in the evolution equation for $\mathbf{P}$, the conjugate $\mathcal{M}^\dagger$ does due to (1.41). Therefore, $\mathbf{M} = \mathcal{M}^\dagger$ in the context of (1.136) and (1.142).

Coupling to the electromagnetic field

Having coupled fluid mechanics with polarization density and its conjugate momentum, let us make the final step - coupling electromagnetic field. Both pairs $(\boldsymbol{\mu}, \mathbf{P})$ and $(\mathbf{D}, \mathbf{B})$ were coupled to fluid mechanics by semidirect product. Advection of both pairs by fluid mechanics can be thus expressed (using (1.17), (1.23), (1.37)) by Poisson bracket

$$\begin{aligned}\{F,G\}^{\text{EFP}\mu}(\rho_\alpha, {}^{\mu}\mathbf{m}, s, \mathbf{D}, \mathbf{B}, \mathbf{P}, \mu) = &\{F,G\}^{(\text{CIT})}(\rho_\alpha, {}^{\mu}\mathbf{m}, s) \\ &+ \{F,G\}^{(\text{EM})}(\mathbf{D}, \mathbf{B}) + \{F,G\}^{(\text{SP})}({}^{\mu}\mathbf{m}, \mathbf{D}) + \{F,G\}^{(\text{SP})}({}^{\mu}\mathbf{m}, \mathbf{B}) \\ &+ \{F,G\}^{\mathbf{P}\boldsymbol{\mu}}(\mathbf{P}, \boldsymbol{\mu}) + \{F,G\}^{(\text{SP})}({}^{\mu}\mathbf{m}, \mathbf{P}) + \{F,G\}^{(\text{SP})_{\mathbf{A}}}({}^{\mu}\mathbf{m}, \boldsymbol{\mu})\end{aligned} \tag{1.45}$$

The evolution equations implied by (1.45) are

$$(\partial_t \rho_\alpha)_{\text{rev}} = -\partial_j(\rho_\alpha \, {}^{\mu}m_j^\dagger) \tag{1.46a}$$

$$(\partial_t s)_{\text{rev}} = -\partial_j(s \, {}^{\mu}m_j^\dagger) \tag{1.46b}$$

$$\begin{aligned}(\partial_t \, {}^{\mu}m_i)_{\text{rev}} = &-\sum_{\alpha=1}^{n} \rho_\alpha \partial_i \rho_\alpha^\dagger - s\partial_i s^\dagger - {}^{\mu}m_j \partial_i \, {}^{\mu}m_j^\dagger \\ &- D_j \partial_i D_j^\dagger - B_j \partial_i B_j^\dagger - P_j \partial_i P_j^\dagger + \mu_j^\dagger \partial_i \mu_j \\ &+ \partial_j \left(D_i^\dagger D_j + B_i^\dagger B_j + P_i^\dagger P_j - \mu_i \mu_j^\dagger - {}^{\mu}m_i \, {}^{\mu}m_j^\dagger \right) ,\end{aligned} \tag{1.46c}$$

$$(\partial_t D_i)_{\text{rev}} = \varepsilon_{ijk}\partial_j B_k^\dagger - \partial_j \left(D_i \, {}^{\mu}m_j^\dagger - D_j \, {}^{\mu}m_i^\dagger \right) - {}^{\mu}m_i^\dagger \partial_j D_j \tag{1.46d}$$

$$(\partial_t B_i)_{\text{rev}} = -\varepsilon_{ijk}\partial_j D_k^\dagger - \partial_j \left(B_i \, {}^{\mu}m_j^\dagger - B_j \, {}^{\mu}m_i^\dagger \right) - {}^{\mu}m_i^\dagger \partial_j B_j \tag{1.46e}$$

$$(\partial_t P_i)_{\text{rev}} = \mu_i^\dagger - \partial_j \left(P_i \, {}^{\mu}m_j^\dagger - P_j \, {}^{\mu}m_i^\dagger \right) - {}^{\mu}m_i^\dagger \partial_j P_j \tag{1.46f}$$

$$(\partial_t \mu_i)_{\text{rev}} = -P_i^\dagger - {}^{\mu}m_j^\dagger \partial_j \mu_i - \mu_j \partial_i \, {}^{\mu}m_i{}^\dagger. \tag{1.46g}$$

Bracket (1.45) can be further projected, using (1.42) and thus replacing $\boldsymbol{\mu}$ with $\mathcal{M}$, as follows,

$$\begin{aligned}\{F,G\}^{\mathrm{EFP}}(\rho_\alpha,\, {}^{\mathcal{M}}\mathbf{m}, s, \mathbf{D}, \mathbf{B}, \mathbf{P}, \mathcal{M}) &= \{F,G\}^{\mathrm{CIT}}(\rho_\alpha,\, {}^{\mathcal{M}}\mathbf{m}, s) \\ &+ \{F,G\}^{(\mathrm{EM})}(\mathbf{D},\mathbf{B}) + \{F,G\}^{\mathrm{SP}}({}^{\mathcal{M}}\mathbf{m},\mathbf{D}) + \{F,G\}^{\mathrm{SP}}({}^{\mathcal{M}}\mathbf{m},\mathbf{B}) \\ &+ \{F,G\}^{\mathbf{P}}(\mathbf{P},\mathcal{M}) + \{F,G\}^{\mathrm{SP}}({}^{\mathcal{M}}\mathbf{m},\mathbf{P}) + \{F,G\}^{\mathrm{SP}}({}^{\mathcal{M}}\mathbf{m},\mathcal{M})\end{aligned} \tag{1.47}$$

This bracket leads to the following system of equations:

$$(\partial_t \rho_\alpha)_{\mathrm{rev}} = -\partial_j(\rho_\alpha\, {}^{\mathcal{M}}m_j^\dagger) \tag{1.48a}$$

$$(\partial_t s)_{\mathrm{rev}} = -\partial_j(s\, {}^{\mathcal{M}}m_j^\dagger) \tag{1.48b}$$

$$\begin{aligned}(\partial_t\, {}^{\mathcal{M}}m_i)_{\mathrm{rev}} = &-\sum_{\alpha=1}^{n}\rho_\alpha\partial_i\rho_\alpha^\dagger - s\partial_i s^\dagger - {}^{\mathcal{M}}m_j\partial_i\, {}^{\mathcal{M}}m_j^\dagger \\ &- D_j\partial_i D_j^\dagger - B_j\partial_i B_j^\dagger - P_j\partial_i P_j^\dagger - \mathcal{M}_j^\dagger\partial_i\mathcal{M}_j \\ &+ \partial_j\left(D_i^\dagger D_j + B_i^\dagger B_j + P_i^\dagger P_j + \mathcal{M}_i\mathcal{M}_j^\dagger - {}^{\mathcal{M}}m_i\, {}^{\mathcal{M}}m_j^\dagger\right)\,,\end{aligned} \tag{1.48c}$$

$$(\partial_t D_i)_{\mathrm{rev}} = \varepsilon_{ijk}\partial_j B_k^\dagger - \partial_j\left(D_i\, {}^{\mathcal{M}}m_j^\dagger - D_j\, {}^{\mathcal{M}}m_i^\dagger\right) - {}^{\mathcal{M}}m_i^\dagger\partial_j D_j \tag{1.48d}$$

$$(\partial_t B_i)_{\mathrm{rev}} = -\varepsilon_{ijk}\partial_j D_k^\dagger - \partial_j\left(B_i\, {}^{\mathcal{M}}m_j^\dagger - B_j\, {}^{\mathcal{M}}m_i^\dagger\right) - {}^{\mathcal{M}}m_i^\dagger\partial_j B_j \tag{1.48e}$$

$$(\partial_t P_i)_{\mathrm{rev}} = \varepsilon_{ijk}\partial_j \mathcal{M}_k^\dagger - \partial_j\left(P_i\, {}^{\mathcal{M}}m_j^\dagger - P_j\, {}^{\mathcal{M}}m_i^\dagger\right) - {}^{\mathcal{M}}m_i^\dagger\partial_j P_j \tag{1.48f}$$

$$(\partial_t \mathcal{M}_i)_{\mathrm{rev}} = -\varepsilon_{ijk}\partial_j P_k^\dagger - \partial_j\left(\mathcal{M}_i\, {}^{\mathcal{M}}m_j^\dagger - \mathcal{M}_j\, {}^{\mathcal{M}}m_i^\dagger\right) - {}^{\mathcal{M}}m_i^\dagger\partial_j\mathcal{M}_j. \tag{1.48g}$$

Brackets (1.45) and (1.47) can be also seen as coupling of (1.35) and (1.40) to (1.23), respectively, using the Lie derivative technique. The total momenta are

$${}^{\mu}\mathbf{m} = {}^{\mu}\mathbf{u} + \mathbf{D}\times\mathbf{B}\,, \tag{1.49}$$

$${}^{\mathcal{M}}\mathbf{m} = {}^{\mathcal{M}}\mathbf{u} + \mathbf{D}\times\mathbf{B}\,. \tag{1.50}$$

Total charge

Maxwell equation (1.33) was derived by taking divergence of the evolution equation for $\mathbf{D}$. However, the usual form of the equation also contains the bound charge explicitly. Let us thus define the field of electric induction $\mathcal{D}$ as

$$\mathcal{D} = \mathbf{D} - \mathbf{P}. \tag{1.51}$$

For a functional $\widetilde{F}(\mathbf{D},\mathbf{P}) = F(\mathcal{D},\mathbf{P})$ then holds that

$$\left(\frac{\delta\widetilde{F}}{\delta\mathbf{P}}\right)_{\mathbf{D}} = \left(\frac{\delta F}{\delta\mathbf{P}}\right)_{\mathcal{D}} - \left(\frac{\delta F}{\delta\mathcal{D}}\right)_{\mathbf{P}} \tag{1.52}$$

or

$$\mathbf{P}^\dagger \to \mathbf{P}^\dagger - \mathcal{D}^\dagger \quad \text{and} \quad \mathbf{D}^\dagger \to \mathcal{D}^\dagger. \tag{1.53}$$

For the quadratic energy of the electromagnetic field $\mathcal{D}^2/(2\varepsilon_0)$, Eq. (1.51) can be rewritten as

$$\varepsilon_0\mathbf{E} + \mathbf{P} = \mathbf{D}\,, \tag{1.54}$$

which is the usual relation between electric displacement $\mathcal{D}$, electric field $\mathbf{E} = \mathcal{D}^\dagger$ and polarization. Since $\operatorname{div}\mathbf{D}$ is equal to the free charge density, it also holds that

$$\varepsilon_0 \operatorname{div}\mathbf{E} + \operatorname{div}\mathbf{P} = \rho_\mathrm{f} \ , \tag{1.55}$$

which is the usual form of the Maxwell equation for $\operatorname{div}\mathcal{D}$.

Transformation (1.51) has of course implications on the form of Poisson brackets (1.37) and (1.42). Let us assume the functionals in (1.45) and (1.47) depend on $\mathcal{D}$ instead of $\mathbf{D}$. The former then reads

$$\begin{aligned}\{F,G\}^{\mathcal{D}\mu}(\rho_\alpha,\, {}^\mu\mathbf{m}, s, \mathcal{D}, \mathbf{B}, \mathbf{P}, \mu) = \\ \{F,G\}^{\mathrm{EFP}\mu}(\rho_\alpha,\, {}^\mu\mathbf{m}, s, \mathcal{D}, \mathbf{B}, \mathbf{P}, \mu) - \{F,G\}^{\mathbf{P}\boldsymbol{\mu}}(\mathcal{D}, \boldsymbol{\mu})\end{aligned} \tag{1.56}$$

Bracket (1.56) can be further projected, using (1.42) and thus replacing $\boldsymbol{\mu}$ with $\mathcal{M}$, as follows,

$$\begin{aligned}\{F,G\}^{\mathcal{D}}(\rho_\alpha,\, {}^\mathcal{M}\mathbf{m}, s, \mathcal{D}, \mathbf{B}, \mathbf{P}, \mathcal{M}) = \\ \{F,G\}^{\mathrm{EFP}}(\rho_\alpha,\, {}^\mathcal{M}\mathbf{m}, s, \mathcal{D}, \mathbf{B}, \mathbf{P}, \mathcal{M}) - \{F,G\}^{\mathbf{P}}(\mathcal{D}, \mathcal{M})\end{aligned} \tag{1.57}$$

The form of (1.56) and (1.57) makes it clear that the transformation (1.51) just slightly alters the evolution equations given in (1.45) and (1.48), respectively. Obviously, only the evolution of $\mathcal{D}$ and the covector variable to $\mathbf{P}$, either $\boldsymbol{\mu}$ or $\mathcal{M}$, are changed.

The altered evolution equations – in the respective cases – of the electric induction and the covector quantity then become, cf. (1.46),

$$\partial_t \mathcal{D}_i = \varepsilon_{ijk}\partial_j B^\dagger_k - \mu^\dagger_i - \partial_j\left(\mathcal{D}_i\, {}^\mu m^\dagger_j - \mathcal{D}_j\, {}^\mu m^\dagger_i\right) - {}^\mu m^\dagger_i \partial_j \mathcal{D}_j \ , \tag{1.58}$$

$$\partial_t \mu_i = \ - P^\dagger_i + \mathcal{D}^\dagger_i - \partial_j \mu_i\, {}^\mu m^\dagger_j - \mu_j \partial_i\, {}^\mu m^\dagger_j \ , \tag{1.59}$$

and, cf. (1.48),

$$\partial_t \mathcal{D}_i = \varepsilon_{ijk}\partial_j\left(B^\dagger_k - \mathcal{M}^\dagger_i\right) - \partial_j\left(\mathcal{D}_i\, {}^\mathcal{M} m^\dagger_j - \mathcal{D}_j\, {}^\mathcal{M} m^\dagger_i\right) - {}^\mathcal{M} m^\dagger_i \partial_j \mathcal{D}_j \ , \tag{1.60}$$

$$\partial_t \mathcal{M}_i = \ - \varepsilon_{ijk}\partial_j\left(P^\dagger_k - \mathcal{D}^\dagger_i\right) - \partial_j\left(\mathcal{M}_i\, {}^\mathcal{M} m^\dagger_j - \mathcal{M}_j\, {}^\mathcal{M} m^\dagger_i\right) - {}^\mathcal{M} m^\dagger_i \partial_j \mathcal{M}_j \ , \tag{1.61}$$

respectively.

The formulation with $\mathcal{D}$ and $\mathcal{M}$ are comparable with similar equations known from literature, see [5, Section 3].

The divergent part of (1.58) evolves as a convected density although the polarization charge density is not conserved due to $\operatorname{div}\boldsymbol{\mu}^\dagger$. After the conjugate polarization momentum $\boldsymbol{\mu}$ has relaxed to zero, bound charge becomes a conserved quantity. In other words, by transformation (1.51) one recovers the usual from of the Maxwell equation (1.54). Apparently, the divergent part of (1.60) evolves as a conserved mass-related density.

In summary, reversible evolution equations for a mixture coupled with electromagnetic fields, polarization and its conjugate momentum were constructed in a geometric way (semidirect products). By further transformation from $\mathbf{D}$ to $\mathcal{D}$ the usual form of the Gauß law including bound charge is recovered.

Polarization waves and stress

Let us begin with the canonical polarization bracket (1.35). Let us assume that the energy contains a contribution corresponding to dipole-dipole interaction proportional to the square of polarization gradient. Hence, we have

$$E^{\mathrm{Pw}} = \int \mathrm{d}\mathbf{r} \frac{1}{2} \left(\beta \partial_j P_i \partial_j P_i + \alpha \mu^2 \right) \ , \tag{1.62}$$

where α and β are assumed to be positive constant parameters. The Hamiltonian evolution of $\mathbf{P}$ and $\boldsymbol{\mu}$ due to bracket (1.35) with energy (1.62) reads

$$\partial_t P_i = \alpha \mu_i \tag{1.63a}$$

$$\partial_t \mu_i = \beta \partial_j \partial_j P_i \tag{1.63b}$$

Let us calculate

$$\partial_{tt} P_i = \partial_t (\alpha \mu_i) = \alpha \beta \partial_j \partial_j P_i \ , \tag{1.64}$$

which is a polarization wave equation. The speed of polarization sound is given by $\sqrt{\alpha\beta}$.

Let us now consider $(\rho_\alpha, s, {}^{\mu}\mathbf{m}, \mathcal{D}, \mathbf{B}, \mathbf{P}, \boldsymbol{\mu})$ level of description equipped with bracket (1.45) where (1.62) contributes to the energy. The evolution equation for total momentum ${}^{\mu}\mathbf{m}$ (1.46c), without specifying the other energy contributions, reads

$$\begin{aligned} (\partial_t \, {}^{\mu}m_i)_{\mathrm{rev}} = & - \sum_{\alpha=1}^{n} \rho_\alpha \partial_i \rho_\alpha^\dagger - s \partial_i s^\dagger - {}^{\mu}m_j \partial_i \, {}^{\mu}m_j^\dagger \\ & - D_j \partial_i D_j^\dagger - B_j \partial_i B_j^\dagger + P_j \partial_i \partial_k \left(\beta \partial_k P_j \right) + \alpha \mu_j \partial_i \mu_j \\ & + \partial_j \left(D_i^\dagger D_j + B_i^\dagger B_j - \partial_k (\beta \partial_k P_i) P_j - \mu_i \alpha \mu_j - {}^{\mu}m_i \, {}^{\mu}m_j^\dagger \right) \ . \end{aligned} \tag{1.65}$$

The terms with $\mathbf{P}$ and $\boldsymbol{\mu}$ in the right hand side of (1.65) may be written in a divergence form as

$$\partial_j \left(\beta P_l \partial_i (\partial_j P_l) - \delta_{ij} \frac{\beta}{2} \partial_k P_l \partial_k P_l - \beta \partial_k (\partial_k P_i) P_j - \alpha \mu_i \mu_j + \frac{\alpha}{2} \delta_{ij} \mu_k \mu_k \right) \ , \tag{1.66}$$

which is the stress contribution due to the polarization. The third term in (1.66) is not symmetric w.r.t. i and j, therefore, the conservation of the angular momentum is not granted. It is sufficient to show that the cross product of the discussed term and position $\mathbf{r}$ can be written in a divergence form. We have, omitting β,

$$\begin{aligned} \varepsilon_{sri} r_r \partial_j \left(P_j \partial_k (\partial_k P_i) \right) &= \varepsilon_{sri} \partial_j \left(r_r P_j \partial_k (\partial_k P_i) \right) - \varepsilon_{sri} P_j \partial_k (\partial_k P_i) \delta_{rj} \\ &= \varepsilon_{sri} \partial_j \left(r_r P_j \partial_k (\partial_k P_i) \right) - \varepsilon_{sji} \partial_k (P_j \partial_k P_i) + \varepsilon_{sji} \partial_k P_j \partial_k P_i \ , \end{aligned} \tag{1.67}$$

where the second terms is simultaneously symmetric and antisymmetric in i and j, hence it is zero.

1.3.5 Magnetization

The magnetization of matter, see e.g. [27, Sec. 11], is due to the orientation of spins. Perhaps due to the resemblance with dynamics of rigid body rotation, the pioneering model of magnetization by Landau & Lifshitz [29] was based on that dynamics. In the following text we first recall the Hamiltonian formulation of rigid body dynamics and then we let the rigid body dynamics be advected by the fluid (using again the semidirect product theory).

Intrinsic dynamics of magnetization

The configuration manifold of rigid body rotations is the Lie group $SO(3)$. The standard machinery of differential geometry, e.g. [11, 30] or [10, Eq. 3.69], concludes that the Lie algebra dual, where angular momentum $\mathbf{M}$ seen from the body reference frame plays the role of state variable, is equipped with Poisson bracket

$$\{F,G\}^{\mathrm{SO(3)}}(\mathbf{M}) = -\gamma \int \mathrm{d}\mathbf{r} M_i \varepsilon_{ijk} F_{M_j} G_{M_k} \ , \tag{1.68}$$

where γ is the gyromagnetic ratio. Bracket (1.68) is also called the spin bracket, see e.g. [31]. The evolution equation implied by this bracket is (by the same procedure as in Sec. 1.3.1)

$$\dot{\mathbf{M}} = \mathbf{M} \times E_{\mathbf{M}}, \tag{1.69}$$

E being energy of the rotation. Derivative of energy with respect to $\mathbf{M}$ is the angular velocity $\boldsymbol{\omega}$.

Advection by fluid mechanics

Similarly as in the case of electromagnetic field or polarization, we will now construct the Poisson bracket expressing advection of magnetization and its dynamics by fluid mechanics (using again semidirect product). Now, however, the advected structure is not a cotangent bundle, but a Lie algebra dual. The general formula for semidirect product of two Lie algebra duals, see [18, Eq. 40], then gives Poisson bracket

$$\begin{aligned}\{F,G\}^{\mathrm{SO(3)}\times(\mathrm{mEHMD})}(\rho_\alpha, {}^{\mathbf{M}}\mathbf{m}, s, \mathbf{D}, \mathbf{B}, \mathbf{M}) = \{F,G\}^{\mathrm{mEHMD}} + \{F,G\}^{\mathrm{SO(3)}} \\ + \gamma \left\langle \mathbf{M}, F_{\mathfrak{M}_{\mathbf{m}}} \triangleright G_{\mathbf{M}} \right\rangle - \gamma \left\langle \mathbf{M}, G_{\mathfrak{M}_{\mathbf{m}}} \triangleright F_{\mathbf{M}} \right\rangle \ ,\end{aligned} \tag{1.70}$$

where ${}^{\mathbf{M}}\mathbf{m}$ is the new total momentum of the coupled system and $\mathbf{M}$ denotes the magnetization. Note that the advected electrodynamics are kept in the bracket for completeness. The right action of velocity field $F_{\mathbf{m}}$ on the vector field $G_{\mathbf{m}}$ is defined as negative of Lie derivative as usually,

$$(F_{\mathfrak{M}_{\mathbf{m}}} \triangleright G_{\mathbf{M}})_i = -\left(F_{\mathfrak{M}_{m_j}} \partial_j G_{M_i} - G_{M_j} \partial_j F_{\mathfrak{M}_{m_i}} \right) \ . \tag{1.71}$$

Using (1.71), bracket (1.70) becomes

$$\begin{aligned}\{F,G\}^{\mathrm{SO(3)}\times(\mathrm{mEHMD})}(\rho_\alpha, {}^{\mathbf{M}}\mathbf{m}, s, \mathbf{D}, \mathbf{B}, \mathbf{M}) = \{F,G\}^{\mathrm{mEHMD}} + \{F,G\}^{\mathrm{SO(3)}} \\ \{F,G\}^{\mathrm{SP}\mathfrak{M}}({}^{\mathbf{M}}\mathbf{m}, \mathbf{M}) := \begin{cases} \quad + \gamma \int \mathrm{d}\mathbf{r} M_i \left(\partial_j F_{\mathfrak{M}_{m_i}} G_{M_j} - \partial_j G_{\mathfrak{M}_{m_i}} F_{M_j} \right) \\ \quad + \gamma \int \mathrm{d}\mathbf{r} M_i \left(\partial_j F_{M_i} G_{\mathfrak{M}_{m_j}} - \partial_j G_{M_i} F_{\mathfrak{M}_{m_j}} \right), \end{cases}\end{aligned} \tag{1.72}$$

which is the explicit form of Poisson bracket expressing kinematics of magnetization advected by fluid mechanics.

The evolution equation equations implied by (1.72) are

$$\begin{aligned}(\partial_t {}^{\mathbf{M}}m_i)_{\mathrm{rev}} = -\sum_{\alpha=1}^{n} \rho_\alpha \partial_i \rho_\alpha^\dagger - s\partial_i s^\dagger - {}^{\mathbf{M}}m_j \partial_i {}^{\mathbf{M}}m_j^\dagger - D_j \partial_i D_j^\dagger - B_j \partial_i B_j^\dagger - \gamma M_j \partial_i M_j^\dagger \\ + \partial_j \left(D_i^\dagger D_j + B_i^\dagger B_j - \gamma M_i M_j^\dagger - {}^{\mathbf{M}}m_i \, {}^{\mathbf{M}}m_j^\dagger \right) \ ,\end{aligned} \tag{1.73a}$$

$$(\partial_t M_i)_{\mathrm{rev}} = \gamma \varepsilon_{ijk} M_j M_k^\dagger - \gamma M_j \partial_i {}^{\mathbf{M}}m_j^\dagger - \partial_j \left(\gamma M_i \, {}^{\mathbf{M}}m_j^\dagger \right) \ . \tag{1.73b}$$

These evolution equations show how magnetization is advected by fluid mechanics, and how such advection affects the fluid motion itself. Moreover, magnetization keeps its intrinsic rigid-body-like dynamics. Finally, note that there is no explicit coupling to the electromagnetic field just as in the original [29] paper. The coupling is achieved implicitly later by letting energy depend on both $\mathbf{M}$ and $\mathbf{B}$.

Spin-spin interaction stress

The spin-spin interaction contribution to the energy can, on the continuum level, be modeled by the gradient of magnetization as in [29]. Let us assume

$$E^{\mathrm{Ms}} = \int \mathrm{d}\mathbf{r} \frac{\alpha}{2} \partial_k M_i \partial_j M_i \ , \tag{1.74}$$

where α is a constant positive parameter. The Hamiltonian evolution of the magnetization field due to bracket (1.68) reads

$$\dot{M}_i = -\gamma\alpha\varepsilon_{ijk} M_j \partial_l \partial_l M_k \tag{1.75}$$

Let now $(\rho_\alpha, {}^{\mathbf{M}}\mathbf{m}, s, \mathbf{D}, \mathbf{B}, \mathbf{M})$ be the considered level of description governed by (1.70). The evolution of the total momentum, see (1.73a), reads

$$\begin{aligned}(\partial_t {}^{\mathbf{M}}m_i)_{\mathrm{rev}} = &- \sum_{\alpha=1}^{n} \rho_\alpha \partial_i \rho_\alpha^\dagger - s\partial_i s^\dagger - {}^{\mathbf{M}}m_j \partial_i {}^{\mathbf{M}}m_j^\dagger - D_j \partial_i D_j^\dagger - B_j \partial_i B_j^\dagger \\ &+ \gamma\alpha M_j \partial_i \partial_k \partial_k M_j + \partial_j \left(D_i^\dagger D_j + B_i^\dagger B_j + \gamma\alpha M_i \partial_k \partial_k M_j - {}^{\mathbf{M}}m_i \, {}^{\mathbf{M}}m_j^\dagger \right),\end{aligned} \tag{1.76}$$

where only the derivatives of energy w.r.t. $\mathbf{M}$ are expressed. Thus, the magnetization terms in (1.76) specify the stress due to the spin-spin interaction. The terms can be, similarly to the dipole-dipole interaction (1.66), written in the divergence form as

$$\gamma\alpha\partial_j \left(M_l \partial_i \partial_j M_l - \frac{\delta_{ij}}{2} \partial_k M_l \partial_k M_l + M_i \partial_k \partial_k M_j \right) \ . \tag{1.77}$$

The non-symmetric term in (1.77) is equivalent to the one already discussed in the polarization case (1.67), therefore, it also does not violate the conservation of the angular momentum.

1.3.6 General level $(\rho_\alpha, \widehat{\mathbf{m}}, s, \mathcal{D}, \mathbf{B}, \mathbf{P}, \boldsymbol{\mu}, \mathbf{M})$

The hierarchy of the brackets built in the preceding paragraphs will be completed on the level of description containing all the discussed variables. The General bracket reads

$$\begin{aligned}\{F,G\}^{\mathrm{GEMHD}}(\rho_\alpha, \widehat{\mathbf{m}}, s, \mathcal{D}, \mathbf{B}, \mathbf{P}, \boldsymbol{\mu}, \mathbf{M}) = &\{F,G\}^{\mathrm{CIT}}(\rho_\alpha, \widehat{\mathbf{m}}, s) \\ &+ \{F,G\}^{(\mathrm{EM})}(\mathcal{D}, \mathbf{B}) + \{F,G\}^{(\mathrm{SP})}(\widehat{\mathbf{m}}, \mathcal{D}) + \{F,G\}^{(\mathrm{SP})}(\widehat{\mathbf{m}}, \mathbf{B}) \\ &+ \{F,G\}^{\mathbf{P}\boldsymbol{\mu}}(\mathbf{P}, \boldsymbol{\mu}) \quad + \{F,G\}^{(\mathrm{SP})}(\widehat{\mathbf{m}}, \mathbf{P}) + \{F,G\}^{(\mathrm{SP})_{\mathbf{A}}}(\widehat{\mathbf{m}}, \boldsymbol{\mu}) \\ &+ \{F,G\}^{\mathrm{SO}(3)}(\mathbf{M}) \quad + \{F,G\}^{(\mathrm{SP})_{\mathbf{M}}}(\widehat{\mathbf{m}}, \mathbf{M}) \ .\end{aligned} \tag{1.78}$$

The first line is due to the dynamics of the CIT-mixture. The second line of (1.78) accounts for the electromagnetism and its coupling to continuum. The third line contains the polarization bracket and its coupling to continuum. The fourth line of (1.78) is due to the magnetization dynamics and its coupling to continuum. Brackets $\{\cdot,\cdot\}^{(\mathrm{SP})}$, $\{\cdot,\cdot\}^{(\mathrm{SP})_{\mathbf{A}}}$ and $\{\cdot,\cdot\}^{(\mathrm{SP})_{\mathbf{M}}}$ were found due to the semidirect product theory.

The evolution equations implied by the General bracket are

$$(\partial_t \rho_\alpha)_{\mathrm{rev}} = -\partial_j(\rho_\alpha \widehat{m}_j^\dagger) \tag{1.79a}$$

$$(\partial_t s)_{\mathrm{rev}} = -\partial_j(s\widehat{m}_j^\dagger) \tag{1.79b}$$

$$\begin{aligned}(\partial_t \widehat{m}_i)_{\mathrm{rev}} = &-\sum_{\alpha=1}^{n} \rho_\alpha \partial_i \rho_\alpha^\dagger - s\partial_i s^\dagger - \widehat{m}_j \partial_i \widehat{m}_j^\dagger \\ &- \mathcal{D}_j \partial_i \mathcal{D}_j^\dagger - B_j \partial_i B_j^\dagger - P_j \partial_i P_j^\dagger + \mu_j^\dagger \partial_i \mu_j - \gamma M_j \partial_i M_j^\dagger \\ &+ \partial_j \left(\mathcal{D}_i^\dagger \mathcal{D}_j + B_i^\dagger B_j + P_i^\dagger P_j - \mu_i \mu_j^\dagger - \gamma M_i M_j^\dagger - \widehat{m}_i \widehat{m}_j^\dagger \right) \ ,\end{aligned} \tag{1.79c}$$

$$(\partial_t \mathcal{D}_i)_{\mathrm{rev}} = \varepsilon_{ijk}\partial_j B_k^\dagger - \mu_i^\dagger - \partial_j \left(\mathcal{D}_i \widehat{m}_j^\dagger - \mathcal{D}_j \widehat{m}_i^\dagger \right) - \widehat{m}_i^\dagger \partial_j \mathcal{D}_j \ , \tag{1.79d}$$

$$(\partial_t B_i)_{\mathrm{rev}} = -\varepsilon_{ijk}\partial_j \mathcal{D}_k^\dagger - \partial_j \left(B_i \widehat{m}_j^\dagger - B_j \widehat{m}_i^\dagger \right) - \widehat{m}_i^\dagger \partial_j B_j \tag{1.79e}$$

$$(\partial_t P_i)_{\mathrm{rev}} = \mu_i^\dagger - \partial_j \left(P_i \widehat{m}_j^\dagger - P_j \widehat{m}_i^\dagger \right) - \widehat{m}_i^\dagger \partial_j P_j \tag{1.79f}$$

$$(\partial_t \mu_i)_{\mathrm{rev}} - P_i^\dagger + \mathcal{D}_i^\dagger - \partial_j \mu_i \widehat{m}_j^\dagger - \mu_j \partial_i \widehat{m}_j^\dagger \tag{1.79g}$$

$$(\partial_t M_i)_{\mathrm{rev}} = \gamma \varepsilon_{ijk} M_j M_k^\dagger - \gamma M_j \partial_i \widehat{m}_j^\dagger - \partial_j \left(\gamma M_i \widehat{m}_j^\dagger \right) \ . \tag{1.79h}$$

This is the most detailed set of reversible evolution equations expressing evolution of a mixture coupled with electromagnetic field, polarization and its conjugate momentum and magnetization.

The bracket (1.78) can be projected to the levels of description upon which it was built. One can simply evaluate the bracket (1.78) on a set of functionals independent of a certain variables, see [16]. For instance the projection from $\boldsymbol{\mu}$ to $\mathcal{M}$ can be seen as evaluation on functionals independent of $\operatorname{div}\boldsymbol{\mu}$. In the rest of this paper we enrich the reversible equations for irreversible terms in order to reduce this rather detailed description to the common continuum models coupling matter and electromagnetic field.

1.4 Continuum thermodynamics and reductions

After having constructed a hierarchy of Poisson brackets for fluid mechanics of mixtures advecting electrodynamics, polarization and its conjugate momentum and magnetization, let us now enrich that detailed reversible dynamics by dissipative irreversible terms. This allows to see relaxation of fast mesoscopic variables and the effects on dynamics of less detailed variables. For instance we let the conjugate polarization momentum $\boldsymbol{\mu}$ relax to recover the standard Single Relaxation Time (SRT) model, which is widely used for comparison with experiments. We also let the magnetization $\mathbf{M}$ relax to recover the full Landau & Lifshitz model not only evolving in the laboratory frame, but being advected by the fluid. Finally, we approach the level of mechanical equilibrium, where evolution is governed

by generalized Nernst-Planck-Poisson equations. In summary, a comprehensive multiscale thermodynamic construction of fluid mixtures equipped with electrodynamics, polarization and magnetization is provided.

1.4.1 Gradient dynamics

But before adding dissipative terms to the actual evolution equations, let us recall the general framework of gradient dynamics, where irreversible evolution is generated by derivatives of a dissipation potential [32]. Sound statistical arguments for gradient dynamics based on the large deviations principle was found in [33, 34, 35]. This paragraph closely follows [10, Sec. 4.5, 4.6].

Dissipation potential

Consider a set of state variables $\mathbf{x}$, and let energy, entropy and mass of the system be denoted by $E(\mathbf{x})$, $S(\mathbf{x})$ and $M(\mathbf{x})$, respectively. A dissipation potential $\widetilde{\Xi} : \mathbf{x}^* \to \mathbb{R}$ is a family of functionals of conjugate variables $\mathbf{x}^*$ parametrized by $\mathbf{x}$. We require every parametrization $\Xi[\mathbf{x}^*] = \widetilde{\Xi}(\mathbf{x})[\mathbf{x}^*]$ to satisfy:

1. Positiveness: $\Xi[\mathbf{x}^*] \geq 0$ and $\Xi[\mathbf{x}^* = 0] = 0$.
2. Monotonicity of derivative: $\left\langle \frac{\delta \Xi}{\delta \mathbf{x}^*}, \mathbf{x}^* \right\rangle \geq 0 \quad \forall \mathbf{x}^*$.
3. Convexity near $\mathbf{x}^* = 0$.
4. Degeneracy with respect to mass $\left\langle \frac{\delta \Xi}{\delta \mathbf{x}^*}, \frac{\delta M(\mathbf{x})}{\delta \mathbf{x}} \right\rangle = 0$.
5. Degeneracy with respect to energy $\left\langle \frac{\delta \Xi}{\delta \mathbf{x}^*}, \frac{\delta E(\mathbf{x})}{\delta \mathbf{x}} \right\rangle = 0$.
6. $\Xi[\mathbf{x}^*]$ be even with respect to time-reversal transformation.

The irreversible evolution of a functional $F(\mathbf{x})$ is then given as

$$\left(\dot{F}(\mathbf{x})\right)_{irr} = \left\langle \left. \frac{\delta \Xi}{\delta \mathbf{x}^*} \right|_{\mathbf{x}^* = \frac{\delta S(\mathbf{x})}{\delta \mathbf{x}}}, \frac{\delta F(\mathbf{x})}{\delta \mathbf{x}} \right\rangle. \tag{1.80}$$

Gradient dynamics automatically satisfies the second law of thermodynamics (growth of entropy in isolated systems). This is guaranteed for instance for convex dissipation potentials, but also non-convexity far from the origin (equilibrium) can be taken into account [36]. Moreover, it is in close relation to the method of entropy production maximization [37]. Gradient dynamics plays a key role when formulating dissipation in the GENERIC framework.

Energetic representation of gradient dynamics

The reversible evolution, treated in the preceding sections, has two building blocks, a Poisson bracket and energy. Energy then enters the evolution equations via the conjugate variables to the energy,

$$\mathbf{x}^\dagger = \frac{\delta E}{\delta \mathbf{x}}, \tag{1.81}$$

while entropy being one of the state variables. This is the energetic representation [38]. In contrast, the irreversible evolution is expressed with respect to conjugates to the entropy (1.80) to keep the gradient structure, i.e. in the entropic representation. Let us now recall the conversion rules between the two representations.

Entropy in the entropic representation and energy in the energetic representation are expressed as

$$S(e,\xi) = \int \mathrm{d}\mathbf{r}\; s\left((e,\xi)(\mathbf{r})\right) \quad \text{and} \quad E(s,\xi) = \int \mathrm{d}\mathbf{r}\; e\left((s,\xi)(\mathbf{r})\right), \tag{1.82}$$

where ξ_i are the state variables other than s and e. Assuming that $s(e,\xi)$ and $e(s,\xi)$ are locally algebraic (i.e. not involving any gradients), the transformation rules can be also resolved locally. It holds that

$$\frac{\delta E}{\delta s}(\mathbf{r}) = \frac{\partial e}{\partial s}((s,\xi)(\mathbf{r})). \tag{1.83}$$

Hence, the known transformation rules [10] can be applied. Eventually, we have

$$s^\dagger(\mathbf{r}) = \frac{1}{e^*}(\mathbf{r}), \quad \xi_i^\dagger(\mathbf{r}) = -\frac{\xi_i^*}{e^*}(\mathbf{r})\ . \tag{1.84}$$

Pointwise application of the transformation rules (1.84) yields

$$\frac{\partial \xi_i^\dagger}{\partial \xi_j^*} = -\frac{\delta_{ij}}{e^*} = -s^\dagger \delta_{ij}, \qquad \frac{\partial \xi_i^\dagger}{\partial e^*} = \frac{\xi_i^*}{\left(e^*\right)^2} = \xi_i \left(s^\dagger\right)^2, \tag{1.85}$$

$$\frac{\partial s^\dagger}{\partial \xi_j^*} = 0, \qquad \frac{\partial s^\dagger}{\partial e^*} = -\frac{1}{\left(e^*\right)^2} = -\left(s^\dagger\right)^2, \tag{1.86}$$

Suppose that $\widehat{\Xi}(e^*,\xi^*) = \Xi(s^\dagger,\xi^\dagger)$. Then the functional derivatives with respect to the entropic variables can be locally transformed into derivatives with respect to the energetic variables as follows,

$$\frac{\delta \widehat{\Xi}}{\delta \xi_i^*}(\mathbf{r}) = -s^\dagger \frac{\delta \Xi}{\delta \xi_i^\dagger}(\mathbf{r}) \tag{1.87a}$$

$$\frac{\delta \widehat{\Xi}}{\delta e^*}(\mathbf{r}) = -s^\dagger \left(s^\dagger \frac{\delta \Xi}{\delta s^\dagger} + \xi_i^\dagger \frac{\delta \Xi}{\delta \xi_i^\dagger} \right)(\mathbf{r}) \tag{1.87b}$$

Conservation of energy requires that $\frac{\delta \Xi}{\delta e^*}|_{e^*=S_e} = 0$ (recalling the assumption of algebraic dependencies). Therefore,

$$\left(s^\dagger \frac{\delta \Xi}{\delta s^\dagger} + \xi_i^\dagger \frac{\delta \Xi}{\delta \xi_i^\dagger} \right)(\mathbf{r}) = 0 \tag{1.88}$$

has to be satisfied. This is for instance satisfied for zero-homogeneous functions of $\frac{\xi_i^\dagger}{s^\dagger}$.

Gradient dynamics of state variable ξ_i at point $\mathbf{r}$ is then

$$\left(\partial_t \xi_i\right)_{\mathrm{irr}}(\mathbf{r}) = \frac{\delta \widehat{\Xi}}{\delta \xi_i^*}|_{\mathbf{x}^*=S_\xi} = -s^\dagger \frac{\delta \Xi}{\delta \xi_i^\dagger}(\mathbf{r})\ , \tag{1.89}$$

and irreversible evolution of entropy at point $\mathbf{r}$, $s(\mathbf{r}) = \langle S, \delta_{\mathbf{r}} \rangle$ becomes, according to (1.80),

$$(\partial_t s(\mathbf{r}))_{irr} = \left\langle \frac{\delta \widehat{\Xi}}{\delta \mathbf{x}^*}\bigg|_{\mathbf{x}^* = \frac{\delta S(\mathbf{x})}{\delta \mathbf{x}}}, \delta_{\mathbf{r}} \frac{\delta S(\mathbf{x})}{\delta \mathbf{x}} \right\rangle \tag{1.90}$$

$$= \left(\frac{\delta \widehat{\Xi}}{\delta e^*} e^* + \frac{\delta \widehat{\Xi}}{\delta \xi_i^*} \xi_i^* \right)(\mathbf{r}) \tag{1.91}$$

$$= \xi_i^\dagger \frac{\delta \Xi}{\delta \xi_i^\dagger}(\mathbf{r}) \geq 0 \ . \tag{1.92}$$

A simple notorious example of the dissipation potential is

$$\widehat{\Xi}^{\mathrm{q}} = \int \mathrm{d}\mathbf{r} \frac{1}{2\tau} \left(\frac{\xi^\dagger}{s^\dagger} \right)^2 \quad \text{and} \quad \frac{\delta \Xi^{\mathrm{q}}}{\delta \xi^\dagger} = \frac{1}{\tau} \frac{\xi^\dagger}{(s^\dagger)^2} \ . \tag{1.93}$$

This is a prototype of dissipation potential, since any general dissipation potential can be approximated by a quadratic one due to the convexity near equilibrium and flatness at equilibrium.

1.4.2 Dynamic maximum entropy principle

The principle of maximum entropy (MaxEnt), where unknown value of a variable is determined by finding the maximum value of entropy subject to constraints given by declared knowledge, has been successfully applied in many fields (information theory, thermodynamics, etc.) [39]. However, in non-equilibrium thermodynamics the problem is not only to find value of a fast variable that has relaxed, but also to find the vector field along which the fast variable evolves, its evolution equation, when only less detailed variables are among the state variables (observables). To this end we recall the method of Dynamic MaxEnt (DynMaxEnt) [40, 10].

Let us demonstrate the principle on perhaps the simplest possible example – an isothermal damped particle in potential field. State variables are position and momentum of the particle (q, p). Reversible evolution is given by Hamilton canonical equations (canonical Poisson bracket on the cotangent bundle and energy). Let the irreversible evolution be given by friction velocity $v = p^\dagger$, i.e. using a quadratic dissipation potential. The overall evolution equations are then

$$\dot{q} = p^\dagger \tag{1.94a}$$

$$\dot{p} = -q^\dagger - \zeta p^\dagger, \tag{1.94b}$$

taking energy as

$$E = \frac{p^2}{2m} + V(q). \tag{1.95}$$

These are the equations for a particle in potential field $V(q)$ moving with friction coefficient $\zeta > 0$.

Let us now treat the state and conjugate variables as independent quantities. Motivation for this is provided by contact-geometric formulation of non-equilibrium thermodynamics [41] and [10]. The minimum of energy subject to

the knowledge of q is at $p = 0$, which is the value approached by evolution of p. At this relaxed value the evolution equation for momentum becomes

$$0 = -q^\dagger - \zeta p^\dagger. \tag{1.96}$$

To satisfy this equation, we have solve it, which actually provides a constitutive relation for the conjugate variable $p^\dagger$. Plugging this constitutive relation back into the equation for q, we obtain

$$\dot{q} = -\frac{1}{\zeta} q^\dagger = -\frac{1}{\zeta} V_q. \tag{1.97}$$

This evolution drives position q towards minima of potential $V(q)$.

In summary, by relaxing the fast variable p, the originally reversible equation for q becomes irreversible while p being enslaved by q. This procedure can be carried out analogically in the case of continuum thermodynamics as we shall demonstrate below.

1.4.3 Relaxation of conjugate polarization momentum $\boldsymbol{\mu}$

In subsection 1.3.4 polarization was equipped with conjugate momentum $\boldsymbol{\mu}$. Inspired by the relaxation of the damped particle in subsection 1.4.2, we shall let the conjugate momentum relax to recover dissipative evolution of polarization.

Polarization relaxation via μ

For convenience we suppose that the energy of the considered system does depend on the magnetic field and magnetization. Therefore, all derivatives of energy w.r.t the aforementioned fields vanish.

Let us moreover assume a dissipation potential quadratic in $\boldsymbol{\mu}$, see (1.93),

$$\Xi^{(\boldsymbol{\mu})} = \int \mathrm{d}\mathbf{r} \frac{1}{2} \frac{1}{\tau_\mu} (\boldsymbol{\mu}^*)^2 = \int \mathrm{d}\mathbf{r} \frac{1}{2} \frac{1}{\tau_\mu} \left(\frac{\boldsymbol{\mu}^\dagger}{s^\dagger} \right)^2. \tag{1.98}$$

Assuming also energy quadratic in $\boldsymbol{\mu}$, the MaxEnt value of $\boldsymbol{\mu}$ is zero. Using (1.79f), the DynMaxEnt relaxation of $\boldsymbol{\mu}$ can be formulated as

$$0 = \partial_t \mu_i = \mathcal{D}_i^\dagger - P_i^\dagger - \frac{1}{\tau_\mu} \frac{\mu^\dagger}{s^\dagger}, \tag{1.99}$$

which is the constitutive relation to be plugged into the remaining evolution equations. In particular, equation for polarization becomes

$$\partial_t P_i = s^\dagger \tau_\mu (\mathcal{D}_i^\dagger - P_i^\dagger) - \partial_j \left(P_i m_j^\dagger - P_j m_i^\dagger \right) - m_i^\dagger \partial_j P_j \ . \tag{1.100}$$

Note that the new terms appearing in the right hand side of equation (1.100) can be seen as generated by dissipation potential $\Xi^{(\boldsymbol{\mu})}$ evaluated at constitutive relation (1.99),

$$\Xi^{(\mathbf{P})} = \Xi^{(\boldsymbol{\mu})}|_{\boldsymbol{\mu}^\dagger = \tau_\mu s^\dagger (\mathcal{D}^\dagger - \mathbf{P}^\dagger)} = \int \mathrm{d}\mathbf{r} \frac{\tau_\mu}{2} \left(\mathbf{P}^\dagger - \mathcal{D}^\dagger \right)^2. \tag{1.101}$$

Similar ideas were presented in [42]. This is the dissipation potential generating irreversible evolution of $\mathbf{P}$.

We may also pursue further relaxation of the polarization. Assuming energy quadratic in $\mathbf{P}$,

$$E^{\mathbf{P}} = \int \mathrm{d}\mathbf{r} \frac{1}{2\chi\varepsilon_0}\mathbf{P}^2 \implies \mathbf{P}^\dagger = \frac{1}{\chi\varepsilon_0}\mathbf{P} \,, \tag{1.102}$$

implies the MaxEnt value of $\mathbf{P}$ being zero. Equation (1.100) consequently gives

$$P_i^\dagger = \mathcal{D}_i^\dagger \,. \tag{1.103}$$

as the Dynamic MaxEnt value of $\mathbf{P}^\dagger$. Moreover, if the energy is quadratic in $\mathcal{D}$, then, using (1.55), we can write:

$$\operatorname{div}\mathcal{D} = \operatorname{div}\varepsilon_0\mathbf{E} = -\operatorname{div}\varepsilon_0\chi\mathbf{E} + \rho_\mathrm{f} \implies \varepsilon_0 \operatorname{div}((1+\chi)\mathbf{E}) = \rho_\mathrm{f} \,. \tag{1.104}$$

Hence, we have recovered the usual form of Coulomb's law for a linear isotropic dielectric material.

Single Relaxation Time model

Consider again equation (1.100) with a further assumption of mechanical equilibrium, i.e. $\mathbf{m}^\dagger = 0$. Then, for quadratic energy

$$E = \int \mathrm{d}\mathbf{r} \frac{1}{2\varepsilon_0}\left(\mathcal{D}^2 + \frac{\mathbf{P}^2}{\chi}\right) \tag{1.105}$$

the evolution of polarization (1.100) becomes

$$\partial_t P_i = \frac{s^\dagger\tau_\mu}{\varepsilon_0}\left(\mathcal{D}_i - \frac{1}{\chi}P_i\right), \tag{1.106}$$

which represents a dissipative evolution of polarization subjected to electric field.

Let us first analyze the evolution equation by applying harmonic electric field $\frac{\mathcal{D}}{\varepsilon_0} = E_0\exp(i\omega t)$. Equation (1.106) then gives the Single Relaxation Time (SRT) model of polarization, see e.g. [43],

$$P_0 = \frac{\chi E_0}{1 + \varepsilon_0\frac{i\omega\chi}{\tau_\mu s^\dagger}}, \tag{1.107}$$

provided that $P = P_0\exp(i\omega t)$.

In summary, by letting the conjugate polarization momentum $\boldsymbol{\mu}$ relax, a dissipative evolution of polarization is obtained (1.100). If the mechanical equilibrium is further assumed, this dissipative evolution is compatible with the SRT model widely used for comparison to experiments. Finally, the equilibrium of the dissipative evolution is the linear relation between polarization and electric intensity known from electrostatics.

1.4.4 Polarization relaxation via $\mathcal{M}$

The conjugate momentum to polarization $\boldsymbol{\mu}$ can be replaced by its curl, $\mathcal{M}$, as above in Eq. (1.40), which brings the equations closer to results in literature (see Sec. 1.5). Suppose that energy of the considered system is independent of the magnetic field and magnetization, so that derivatives of energy w.r.t the aforementioned fields vanish. Quadratic dissipation in $\varepsilon_{ijk}\partial_j M_k^\dagger$ reads

$$\Xi = \int \mathrm{d}\mathbf{r} \frac{1}{2\tau_{\mathcal{M}}} \left(\nabla \times \mathcal{M}^*\right)^2 \implies \frac{\delta \Xi}{\delta \mathcal{M}_i^*} = \frac{1}{\tau_{\mathcal{M}}} \varepsilon_{ija}\varepsilon_{als}\partial_j\partial_l \mathcal{M}_s^*. \tag{1.108}$$

Assuming also energy quadratic in $\mathcal{M}$, the MaxEnt value of $\mathcal{M}$ is zero. Relaxation of $\mathcal{M}$ can be then expressed as, using (1.61) and (1.84),

$$0 = \partial_t \mathcal{M}_i = \varepsilon_{ijk}\partial_j \left(\mathcal{D}_k^\dagger - P_k^\dagger - \frac{1}{\tau_{\mathcal{M}}} \varepsilon_{kls}\partial_l \frac{\mathcal{M}_s^\dagger}{s^\dagger} \right). \tag{1.109}$$

In the isothermal case ($s^\dagger = \text{const.}$) it follows from (1.48) that

$$\varepsilon_{ijk}\partial_j\partial_t P_i = s^\dagger \tau_M \varepsilon_{ijk}\partial_j \left(\mathcal{D}_k^\dagger - P_k^\dagger - \partial_l \left(P_k m_l^\dagger - P_l m_k^\dagger \right) - m_k^\dagger \partial_l P_l \right), \tag{1.110}$$

which represents relaxation only of the curl part of the polarization field, keeping the bound charge intact.

The Dynamic MaxEnt allows to obtain the value of $\mathbf{M}^\dagger$ consistent with a given dissipation potential. The impact of such reduction on the polarization will be always introduced through $\operatorname{curl} \mathcal{M}^\dagger$. Clearly, the divergence part of $\mathbf{P}$ cannot be by this affected. Therefore, Dynamic MaxEnt of $\mathcal{M}$ cannot, in principle, lead to relation (1.103).

1.4.5 Relaxation of magnetization

Let us now discuss relaxation of magnetization $\mathbf{M}$ inspired by the Landau & Lifshitz model [29]. Consider the following dissipation potential analogical to (1.108),

$$\Xi^{\mathbf{M}} = \int \mathrm{d}\mathbf{r} \frac{1}{2\tau_{\mathbf{M}}} \left(\frac{\mathbf{M} \times \mathbf{M}^\dagger}{s^\dagger} \right)^2 . \tag{1.111}$$

The derivative of (1.111) w.r.t $\mathbf{M}^\dagger$ is

$$\frac{\delta \Xi^{\mathbf{M}}}{\delta M_i^\dagger} = \frac{1}{{s^\dagger}^2 \tau_{\mathbf{M}}} \varepsilon_{smi} M_m \varepsilon_{sjk} M_j M_k^\dagger = -\frac{1}{{s^\dagger}^2 \tau_{\mathbf{M}}} \left(\mathbf{M} \times (\mathbf{M} \times \mathbf{M}^\dagger) \right)_i . \tag{1.112}$$

Hence, the irreversible evolution of $\mathbf{M}$ due to (1.111) reads

$$\begin{aligned} \left(\partial_t M_i\right)_{irr} &= -s^\dagger \frac{\delta \Xi^{\mathbf{M}}}{\delta M_i^\dagger} = \frac{1}{s^\dagger \tau_{\mathbf{M}}} \varepsilon_{ims} M_m \varepsilon_{sjk} M_j M_k^\dagger \\ &= \frac{1}{s^\dagger \tau_{\mathbf{M}}} \left((\mathbf{M} \cdot \mathbf{M}^\dagger)\mathbf{M} - (\mathbf{M} \cdot \mathbf{M})\mathbf{M}^\dagger \right), \end{aligned} \tag{1.113}$$

which is compatible with the Landau & Lifshitz model of magnetization once suitable energy is provided, [44, Sec. 3.7].

Having recovered the Landau & Lifshitz model, let us also formulate its generalization version advected by fluid mechanics and interacting with magnetic field. We take quadratic energy

$$E = \frac{(\mathbf{B} - \mu_0 \mathbf{M})^2}{2\mu_0}, \tag{1.114}$$

derivatives of which energy are

$$E_{\mathbf{M}} = \mu_0 \mathbf{M} - \mathbf{B} \quad \text{and} \quad E_{\mathbf{B}} = \frac{\mathbf{B}}{\mu_0} - \mathbf{M} \ . \tag{1.115}$$

This permits us to define the field of *magnetic intensity*

$$\mathbf{H} \stackrel{\text{def}}{=} E_{\mathbf{B}} = \frac{\mathbf{B}}{\mu_0} - \mathbf{M}, \tag{1.116}$$

which is the usual relation between $\mathbf{H}$, $\mathbf{B}$ and $\mathbf{M}$. This is our motivation of the choice of energy (1.115).

For energy (1.114) it holds, moreover, that

$$\mu_0 \mathbf{B}^\dagger = -\mathbf{M}^\dagger. \tag{1.117}$$

Combining (1.73b) and (1.113) then leads to the evolution of the magnetization, using also (1.114), (1.115) and 1.117,

$$\partial_t M_i = -\gamma \varepsilon_{ijk} M_j B_k - \gamma M_j \partial_i^{\mathbf{M}} m_j^\dagger - \gamma \partial_j \left(M_i {}^{\mathbf{M}} m_j^\dagger \right) - \frac{1}{s^\dagger \tau_{\mathbf{M}}} \varepsilon_{ims} M_m \varepsilon_{sjk} M_j B_k \ . \tag{1.118}$$

Equation (1.118), supplied with the rest of Eqs. (1.79f), is the generalized Landau-Lishitz magnetization relaxation model, where magnetization relaxes, interact with electromagnetic field and where it is advected by the fluid.

1.4.6 Electro-diffusion – dissipation of $\mathcal{D}$ and ρ_α

Poisson bracket (1.78) for mixtures may be endowed with a weakly non-local electro-diffusion dissipation potential describing an irreversible evolution of the partial densities (friction between components of the mixture and the zero-th species, e.g. solvent),

$$\Xi^{\mathrm{D}}(\rho_\alpha^*, \mathcal{D}^*) = \int \mathrm{d}\mathbf{r} \sum_{\alpha,\beta \neq 0}^{n} \left[\left(\partial_i \left(\rho_\alpha^* - \rho_0^* \right) - e_0 \left(\frac{z_\alpha}{m_\alpha} - \frac{z_0}{m_0} \right) \mathcal{D}_i^* \right) \frac{M_{\alpha\beta}}{2} \left(\partial_i \left(\rho_\beta^* - \rho_0^* \right) - e_0 \left(\frac{z_\beta}{m_\beta} - \frac{z_0}{m_0} \right) \mathcal{D}_i^* \right) \right], \tag{1.119}$$

where $M_{\alpha\beta}$ is a symmetric, positive definite matrix of binary diffusion coefficients. The dissipation potential conserves both mass and energy.

The irreversible part of the evolution equations can be expressed in energy-conjugate variables, using (1.84), as

$$(\partial_t \rho_\alpha)_{\text{irr}} = \sum_{\beta\neq 0}^{n} \partial_i \left(M_{\alpha\beta} \left(\partial_i \frac{\rho_\beta^\dagger - \rho_0^\dagger}{s^\dagger} - e_0 \left(\frac{z_\beta}{m_\beta} - \frac{z_0}{m_0} \right) \frac{\mathcal{D}_i^\dagger}{s^\dagger} \right) \right) \tag{1.120a}$$

$$(\partial_t \rho_0)_{\text{irr}} = -\sum_{\alpha,\beta\neq 0}^{n} \partial_i \left(M_{\alpha\beta} \left(\partial_i \frac{\rho_\beta^\dagger - \rho_0^\dagger}{s^\dagger} - e_0 \left(\frac{z_\beta}{m_\beta} - \frac{z_0}{m_0} \right) \frac{\mathcal{D}_i^\dagger}{s^\dagger} \right) \right) \tag{1.120b}$$

$$(\partial_t \mathcal{D}_i)_{\text{irr}} = \sum_{\alpha,\beta\neq 0}^{n} e_0 \left(\frac{z_\alpha}{m_\alpha} - \frac{z_0}{m_0} \right) M_{\alpha\beta} \left(\partial_i \frac{\rho_\beta^\dagger - \rho_0^\dagger}{s^\dagger} - e_0 \left(\frac{z_\beta}{m_\beta} - \frac{z_0}{m_0} \right) \frac{\mathcal{D}_i^\dagger}{s^\dagger} \right) \tag{1.120c}$$

Note that the divergent part of (1.120c) is identical to the sum of (1.120b) and (1.120a) weighted by the charge per mass of the respective species. Therefore, the irreversible evolution given by (1.119) is compatible with Gauß's law given by (1.33). In other words

$$\partial_i \left((\partial_t \mathcal{D}_i)_{\text{irr}} \right) = \sum_{\alpha=0}^{n} e_0 \frac{z_\alpha}{m_\alpha} (\partial_t \rho_\alpha)_{\text{irr}} \tag{1.121}$$

Equations (1.120) express irreversible evolution of densities of the constituents and electric displacement under mutual interaction. The right hand sides of the equations for densities can be regarded as gradients of respective electrochemical potentials. Evolution for the $\mathcal{D}$ field leads to relaxation of the field consistent with the Gauß law and with the Poisson equation. Equations (1.120a) and (1.120b) represent generalized Nernst-Planck fluxes with evolution equation for $\mathcal{D}$, see also Sec. 1.4.7.

Note that a dissipation potential introducing dissipation of the partial mass densities (i.e. containing ρ_α^*) is required to contain corresponding terms with $\mathcal{D}^*$ so that an irreversible evolution compatible with the Gauß law, c.f. (1.121), is introduced via $\Xi_{\mathcal{D}^*}$ into the evolution equation for $\mathcal{D}$ and vice-versa. Therefore, if the validity of Gauß's law for the free charge is required then the form of dissipation potential involving $\mathcal{D}^\dagger$ is thus restricted. For example, the irreversible evolution given by

$$\Xi = \int \mathrm{d}\mathbf{r} \frac{1}{2\tau} \left(\mathcal{D}^* \right)^2 \quad \text{or} \quad \Xi = \int \mathrm{d}\mathbf{r} \sum_{\alpha,\beta\neq 0} \frac{1}{2} \partial_i \left(\rho_\alpha^* - \rho_0^* \right) \widetilde{M}_{\alpha\beta} \, \partial_i \left(\rho_\beta^* - \rho_0^* \right), \tag{1.122}$$

would not preserve the structure of Gauß's law. This is our motivation for suggesting dissipation potential (1.119).

1.4.7 Generalized Poisson-Nernst-Planck-Stokes

The electro-diffusion due to (1.119) introduces a dissipative fluxes identical to those of the generalized Planck-Nernst-Poisson systems (gPNP) presented in [5], although, on more detailed level of description. In this paragraph, we would like to discuss the reduction of the description of the mass momenta for the gPNP systems. Let us consider a level of description where $\mu, \mathbf{M}, \mathbf{P}$ are already relaxed, i.e. (1.23). Moreover, on short enough distances magnetic field effects are usually

negligible compared with effects of the electric field, in contrast to long distances, where electric field usually does not play any relevant role due to screening. Let us analyze the former case, paving the way towards electrochemical problems.

Assuming that no magnetic field is present and that its evolution equation (1.29) be satisfied, it follows that

$$\mathbf{E} = E_{\mathcal{D}} = -\nabla\varphi \ , \tag{1.123}$$

where φ plays the role of electric potential. Following (1.104), energy

$$E^{(\mathrm{EM})} = \int \mathrm{d}\mathbf{r} \frac{\mathcal{D}^2}{2\varepsilon} \quad \text{implies} \quad \mathcal{D} = -\varepsilon\nabla\varphi \tag{1.124}$$

where $\varepsilon = \varepsilon_0(1+\chi)$. Moreover, negligible magnetic field also implies $\mathbf{m} = \mathbf{u}$.

The considered level of description consists of $(\rho_\alpha, \mathbf{u}, s, \varphi)$. Further relaxation of momentum may lead to certain difficulties. Suppose for a moment that energy does not depend on the momentum and so the unknowns are $(\rho_\alpha, s, \varphi)$. The momentum equation then reads

$$0 \asymp -\sum_{\alpha=1}^{n} \rho_\alpha \partial_i \rho_\alpha^\dagger - s\partial_i s^\dagger - n^{\mathrm{F}} \partial_i \varphi \ . \tag{1.125}$$

Clearly, the first two terms of equation (1.125) form the gradient of the fluid pressure, so that curl of the equation would be:

$$0 \asymp \varepsilon_{ijk}\partial_j \left(\sum_{\alpha=1}^{n} e_0 \frac{z_\alpha}{m_\alpha} \rho_\alpha \partial_k \varphi \right) \ . \tag{1.126}$$

Thus φ would have to satisfy an additional equation, so that the unknowns (ρ_α, φ) would be overdetermined if considered in more than one spatial dimension, see [45, Eq. 16a] or [5, Eq. 132].

To avoid this, a dissipation of mass momentum might be introduced. Again, the energy is quadratic in $\mathbf{u}$, see (1.8), hence, its MaxEnt value is zero, leaving the remainder of the momentum equation as an constitutive equation for the velocity field. For the dissipation potential generating the irreversible part of the Navier-Stokes equations, see e.g. [10, Eqns. 4.74, 4.76]. The viscous dissipative terms are then added to the reversible balance of mass momentum (1.23), with neglected magnetic field. The whole gPNP-Stokes systems eventually reads:

$$\partial_t \rho_\alpha = \partial_i \left(\rho_\alpha v_i + \sum_{\beta\neq 0}^{n} M_{\alpha\beta} \left(\partial_i \frac{\rho_\beta^\dagger - \rho_0^\dagger}{s^\dagger} - e_0 \left(\frac{z_\beta}{m_\beta} - \frac{z_0}{m_0} \right) \frac{\mathcal{D}_i^\dagger}{s^\dagger} \right) \right) \tag{1.127}$$

$$\partial_t \rho_0 = \partial_i \left(\rho_0 v_i - \sum_{\alpha,\beta\neq 0}^{n} M_{\alpha\beta} \left(\partial_i \frac{\rho_\beta^\dagger - \rho_0^\dagger}{s^\dagger} - e_0 \left(\frac{z_\beta}{m_\beta} - \frac{z_0}{m_0} \right) \frac{\mathcal{D}_i^\dagger}{s^\dagger} \right) \right) \tag{1.128}$$

$$\begin{aligned} 0 = &-\sum_{\alpha=0}^{n} \rho_\alpha \partial_i \rho_\alpha^\dagger - s\partial_i s^\dagger - \varepsilon \partial_j\varphi\partial_i\partial_j\varphi \\ &+ \partial_j \left(\frac{\widehat{\mu}}{2} \left(\partial_j v_i + \partial_i v_j \right) + \varepsilon \partial_i\varphi\partial_j\varphi \right) + \lambda \partial_i\partial_j v_j \end{aligned} \tag{1.129}$$

$$0 = -\partial_i \left(e_0(1+\chi)\partial_i\varphi \right) + \sum_{\alpha=0}^{n} e_0 \frac{z_\alpha}{m_\alpha} \rho_a. \tag{1.130}$$

The reversible part of partial mass densities evolution are equipped with the generalized Nernst-Planck flux (1.120a) and (1.120b). The unknowns of the system the are $(\rho_\alpha, s, \varphi, \mathbf{v})$.

In summary, the reduction of momentum in $(\rho_\alpha, \mathbf{u}, s, \varphi)$ should either consider dissipation in $\mathbf{u}$ or give no further relevance to the momentum equation.

1.4.8 Maxwell-Stefan Poisson-Nernst-Planck

Mutual dissipation of the momenta can be introduced on, $(\rho_\alpha, \mathbf{u}_\alpha, s_\alpha, \mathbf{D}, \mathbf{B})$-level of description, see (1.28), as follows,

$$\Xi^{\mathrm{f}} = \int_\Omega \mathrm{d}\mathbf{r} \sum_{\alpha=1}^{n} \frac{M_\alpha}{2} \left(\mathbf{u}_\alpha^* - \mathbf{u}_0^*\right)^2 \ . \tag{1.131}$$

Dissipation potential (1.131) is similar to the Maxwell-Stefan diffusion relations and represents a friction proportional to the differences of velocities with respect to 0th-species. The MaxEnt values of the partial momenta gives, using

$$0 = M_\alpha(\mathbf{u}_\alpha^* - \mathbf{u}_0^*)_i - \left(\rho_\alpha \partial_i \rho_\alpha^\dagger - \frac{e_0 z_\alpha}{m_\alpha} \rho_\alpha D_i^\dagger\right) \qquad \alpha = \{1, \dots, n\} \ , \tag{1.132}$$

where isothermal conditions, i.e., relaxation of the partial entropies, and relaxation of magnetic field are assumed. The formulas for the partial velocities can be directly introduced into the partial mass balances. Depending on the considered problem, the zero-th species can be selected as the crystalline lattice or the solvent. Its velocity might be regarded as unaffected by the process, therefore, spatially constant. The partial mass balances read as

$$\partial_t \rho = \partial_i \left(\frac{\rho_\alpha s^\dagger}{M_\alpha} \left(\partial_i \rho_\alpha^\dagger + \frac{e_0 z_\alpha}{m_\alpha} \partial_i \varphi \right) \right) \qquad \alpha = \{1, \dots, n\} \ . \tag{1.133}$$

Equation (1.132) may introduced into Ξ^{f} so that the dissipation potential on the reduced level is found,

$$\Xi^{\mathrm{f}}|_{(1.132)} = \Xi^{\mathrm{MSP}} = \int_\Omega \mathrm{d}\mathbf{r} \sum_{\alpha=1}^{n} \frac{1}{2M_\alpha} \left(s^\dagger \rho_\alpha \left(\partial_i \rho_\alpha^* - \frac{e_0 z_\alpha}{m_\alpha} D_i^* \right) \right)^2 \ . \tag{1.134}$$

1.5 Comparison to the Dreyer et al. approach

C. Guhlke, W. Dreyer et al. in [46] published a comprehensive analysis of fluid mixtures coupled with electromagnetic fields, including polarization and magnetization. Their treatment of surfaces as independent thermodynamic systems interacting with the bulk, being beyond the scope of the presented work, have elucidated many electrochemical problems using non-equilibrium thermodynamics, for instance unified theory of the Helmholtz and Stern layers, a derivation of Butler-Volmer equations, or useful asymptotic techniques, see [47, 48, 5, 49].

Since our goal is in close relation to that works, let us compare the two approaches in detail. Dreyer et al. assumed that the total charge density can be described as a continuum-advected density giving, formally, the divergent part of $\mathcal{D}$. Additionally, they assumed the free charge density as (1.26), therefore, they

concluded that the polarized charge density is also a continuum-advected density,

$$-\operatorname{div}\mathbf{P}=\rho_{\mathrm{b}}\ . \tag{1.135}$$

They formally defined the evolution of the polarization as

$$\partial_t P_i=-\varepsilon_{ijk}\partial_j\widehat{M}_k+v_i\partial_j P_j+J_i^{\mathrm{P}}, \tag{1.136}$$

where $\widehat{\mathbf{M}}$ is magnetization and J_i^{P} is the dissipative polarization flux and $\mathbf{v}$ is the barycentric velocity. The divergent part of (1.136) is

$$\partial_t(-\partial_i P_i)=-\partial_i\left(v_i\partial_j P_j+J_i^{\mathrm{P}}\right)\ . \tag{1.137}$$

They assume that the total momentum, i.e. the momentum of the electromagnetic field and the mass, and the total energy are conserved. The coupling between the charged fluid and the electromagnetic field is then given by the choice of Lorentz force [5, Eqn. 36a]:

$$k_i=\left(\sum_{\alpha=1}^{n}e_0\frac{z_\alpha}{m_\alpha}\rho_\alpha+\rho_{\mathrm{b}}\right)\left(E_i+\varepsilon_{ijk}v_jB_k\right), \tag{1.138}$$

as a source term in the mass momentum balance and choice of Joule heating:

$$\pi=(J_i^{\mathrm{F}}+J_i^{\mathrm{P}})E_i \tag{1.139}$$

as a source term in the internal energy balance. Symbol J^{F} denotes the dissipative free charge flux equivalent to (1.120c). $\mathbf{E}$ and $\mathbf{B}$ stand for the electric and magnetic field, respectively. Eventually, the system of equations is closed with making use of an entropy principle. First, this leads to a reformulation of the polarization evolution equation. Second, an additional evolution equation for the magnetization is found. They read

$$\partial_t P_i=\ -v_j\partial_j P_i+\frac{1}{2}P_j\left(\partial_j v_i-\partial_i v_j\right)+\frac{1}{\tau^{\mathrm{P}}}\left(\frac{\partial\rho\psi}{\partial P_i}+E_i+\frac{1}{T}\varepsilon_{ijk}v_jB_k\right)\ , \tag{1.140}$$

$$\partial_t\widehat{M}_i=\ -v_j\partial_j\widehat{M}_i+\frac{1}{2}\widehat{M}_j\left(\partial_j v_i-\partial_i v_j\right)+\frac{1}{\tau^{\mathrm{M}}}\left(\frac{\partial\rho\psi}{\partial\widehat{M}_i}+\frac{1}{T}B_i\right)\ , \tag{1.141}$$

where $\rho\psi$ denotes the free energy density.

The divergence part of the reversible part of (1.140); i.e. neglecting the dissipative term, e.g. assuming τ_{P} be large, yields

$$\partial_t\partial_i P_i=\partial_i\left(-v_j\partial_j P_i+\frac{1}{2}P_j\left(\partial_j v_i-\partial_i v_j\right)\right)\ . \tag{1.142}$$

Clearly, the closure-supplied additional terms to the evolution of the polarization do not respect the continuum-advected density structure of (1.135) compared to (1.136) which was used for the construction of the balance equations. In other words, the reversible evolution suggested by Dreyer et al. does not conserve the polarization charge density.

In summary, the main difference between the treatment of the polarization charge presented by Dreyer et al. and those introduced in subsection 1.3.4 is the

recognition of the co-vector quantities structures $(\mathbf{P}, \boldsymbol{\mu})$ and $(\mathbf{P}, \mathcal{M})$, respectively. This results to a different coupling to the continuum.

Also the Lorentz force acting on the total charge is different for the two treatments. The total momentum [5, Eqn. 35a], cf. (1.138), reads

$$\mathbf{m}^{Dreyer} = \mathbf{u} + \mathcal{D} \times \mathbf{B} \ . \tag{1.143}$$

Hence, the magnetic field acts upon the polarization charge as it would be a free charge density. This we find controversial as the form should stem, in our opinion, from a reduction of more detailed level of description of a charged mixture. On the other hand, this is certainly a shortcoming of the presented treatment as a certain form of interaction between the magnetic field and moving polarization charge should be present. Although, once the magnetic field is relaxed, this coupling does not alter the form of equations.

1.6 Summary and Conclusions

In the first section a hierarchy of Poisson brackets describing the reversible dynamics of a charged, polarized and magnetized continua coupled with electromagnetic field has been developed by means of differential geometry. The semidirect product of the fluid mechanics Lie Algebra dual $(\rho, \mathbf{u}, s)$ and electromagnetism cotangent bundle $(\mathbf{A}, -\mathbf{D})$ results in a reversible electro-magneto-hydrodynamics was already known [20, 25, 18]. Newly, cotangent bundle $(\boldsymbol{\mu}, -\mathbf{P})$ describing dynamics of polarization charge is also coupled using the same technique. Finally, the spin dynamics represented by the Lie algebra of SO(3) is coupled to the Lie algebra dual of fluid mechanics giving rise to the reversible dynamics of spin fluid.

The second section is dedicated to the introduction of the irreversible dynamics and reduction of the before-built levels of description using the dissipation potential to formulate the irreversible evolution and the Dynamic Maximization of Entropy (DynMaxEnt) technique to find passage from finer to rougher levels of description. In this manner, the conjugate momentum to the polarization, $\boldsymbol{\mu}$, is relaxed giving rise to dissipation of the polarization itself. The further exploitation of the induced dissipation of $\mathbf{P}$ leads to recovering of $\mathbf{P} = \varepsilon_0 \chi \mathbf{E}$ formula and the Single Relaxation Time model for dielectrics. The dissipation potential for the magnetic moment $\mathbf{M}$ was found so that the Landau-Lifshitz model of spin relaxation was recreated. Finally, the electro-diffusion dissipation potential was introduced, leading to a generalized Nernst-Planck-Poisson-Stokes model.

In summary, we present a geometric construction of a hierarchy of Poisson brackets expressing kinematics of fluid mixtures, electrodynamics, polarization and its conjugate momentum and magnetization. Afterwards, dissipation is introduced on detailed levels of description, which are then reduced to less detailed and more common levels.

Appendix

The quantities used troughout the section are listed below.

Quantity	Symbol	SI units
magnetic field	$\mathbf{B}$	$\mathrm{kg/s^2/A}$
magnetic field intensity	$\mathbf{B}^\dagger, \mathbf{H}$	$\mathrm{A\,m^{-1}}$
displacement field	$\mathbf{D}$	$\mathrm{C/m^2}$
electric induction field	$\mathcal{D}$	$\mathrm{C/m^2}$
electric field	$\mathbf{E}, \mathbf{D}^\dagger, \mathcal{D}^\dagger$	$\mathrm{V\,m^{-1}}$
polarization density	$\mathbf{P}$	$\mathrm{C/m^2}$
polarization momentum	$\boldsymbol{\mu}$	$\mathrm{V\,s\,m^{-1}}$
polarization momentum	$\mathcal{M}$	$\mathrm{A\,m^{-1}}$
magnetization density	$\mathbf{M}$	$\mathrm{A\,m^{-1}}$
partial mass density	ρ_α	$\mathrm{kg/m^3}$
mass momentum density	$\mathbf{u}$	$\mathrm{kg/m^2/s}$

List of momenta densities and the corresponding levels of description.

momentum density	level of description
$\mathbf{u}$	$(\rho_\alpha, s, \mathbf{u})$
$\mathbf{m}$	$(\rho_\alpha, s, \mathbf{u}, \mathbf{D}, \mathbf{B})$
${}^{\mathbf{M}}\mathbf{u}$	$(\rho_\alpha, s, \mathbf{u}, \mathbf{P}, \mathcal{M})$
${}^{\mu}\mathbf{u}$	$(\rho_\alpha, s, \mathbf{u}, \mathbf{P}, \boldsymbol{\mu})$
${}^{\mu}\mathbf{m}$	$(\rho_\alpha, s, \mathbf{u}, \mathbf{P}, \boldsymbol{\mu}, \mathbf{D}, \mathbf{B})$
${}^{\mu}\mathbf{m}$	$(\rho_\alpha, s, \mathbf{u}, \mathbf{P}, \boldsymbol{\mu}, \mathcal{D}, \mathbf{B})$
${}^{\mathbf{M}}\mathbf{m}$	$(\rho_\alpha, s, \mathbf{u}, \mathbf{P}, \mathcal{M}, \mathcal{D}, \mathbf{B})$
$\widehat{\mathbf{m}}$	$(\rho_\alpha, s, \mathbf{u}, \mathbf{P}, \boldsymbol{\mu}, \mathcal{D}, \mathbf{B}, \mathbf{M})$

1.1 Total momentum transformation

We presented two Poisson brackets describing the dynamics of charged mixture. The first, $\{F, G\}^{(\mathrm{mEMHD})}(\rho_\alpha, \mathbf{m}, s, \mathbf{D}, \mathbf{B})$ is expressed with the total momentum $\mathbf{m}$ in (1.23). The second, $\{\widetilde{F}, \widetilde{G}\}^{(\mathrm{uEMHD})}(\rho_\alpha, \mathbf{u}, s, \mathbf{D}, \mathbf{B})$ is expressed with the mass momentum $\mathbf{u}$ in (1.27). A sketch of the transformation of the latter to the former is presented below.

Let us assume that $\widetilde{F}$ is a functional depending on $(\rho_\alpha, \mathbf{u}, s, \mathbf{D}, \mathbf{B})$. We define $F(\rho_\alpha, \mathbf{m}, s, \mathbf{D}, \mathbf{B}) = \widetilde{F}(\rho_\alpha, \mathbf{u}, s, \mathbf{D}, \mathbf{B})$ provided

$$\mathbf{m} = \mathbf{u} + \mathbf{D} \times \mathbf{B} \,. \tag{1.144}$$

Hence, the derivative of the functionals may by transformed to each other em-

ploying chain rule which yields

$$\widetilde{F}_{\rho_\alpha} = F_{\rho_\alpha} \ , \tag{1.145a}$$
$$\widetilde{F}_{u_i} = F_{m_i} \ , \tag{1.145b}$$
$$\widetilde{F}_{s} = F_{s} \ , \tag{1.145c}$$
$$\widetilde{F}_{D_i} = F_{D_i} - \varepsilon_{ijk} F_{m_j} B_k \ , \tag{1.145d}$$
$$\widetilde{F}_{B_i} = F_{B_i} + \varepsilon_{ijk} F_{m_j} D_k \ . \tag{1.145e}$$

We define G analogously to F. Hence, introducing (1.144) and (1.145) into (1.27) gives

$$\begin{aligned}
\{\widetilde{F},\widetilde{G}\}^{(\mathrm{uEMHD})}(\rho_\alpha,\mathbf{u},s,\mathbf{D},\mathbf{B}) = & \int \mathrm{d}\mathbf{r} \sum_{\alpha=1}^{n} \rho_\alpha \left(\partial_i F_{\rho_\alpha} G_{m_i} - \dots\right) \\
& + \int \mathrm{d}\mathbf{r} s \left(\partial_i F_s G_{m_i} - \dots\right) \\
& + \int \mathrm{d}\mathbf{r} \left(m_i - \varepsilon_{ijk} D_j B_k\right) \left(\partial_l F_{m_i} G_{m_l} - \dots\right) \\
& + \int \mathrm{d}\mathbf{r} \left[\left(F_{D_i} - \varepsilon_{ipq} F_{m_p} B_q\right) \varepsilon_{ijk} \partial_j \left(G_{B_k} + \varepsilon_{krs} G_{m_r} D_s\right) - \dots\right] \\
& + \int \mathrm{d}\mathbf{r} \sum_{\alpha=1}^{n} e_0 \frac{z_\alpha \rho_\alpha}{m_\alpha} \left(F_{m_i}(G_{D_i} - \varepsilon_{ijk} G_{m_j} B_k) - \dots\right) \\
& + \int \mathrm{d}\mathbf{r} \sum_{\alpha=1}^{n} e_0 \frac{z_\alpha \rho_\alpha}{m_\alpha} B_i \varepsilon_{ijk} F_{m_j} G_{m_k} \ ,
\end{aligned} \tag{1.146}$$

where the dots are in place of the antisymmetric terms, i.e. terms with F and G swapped. We collect the terms forming $\{F,G\}^{(\mathrm{CIT})}|_{\mathbf{m}}$ and $\{F,G\}^{(\mathrm{EM})}$, see (1.14) and (1.17), respectively, and replace the charge density with the divergence of $\mathbf{D}$, cf. (1.33). We obtain

$$\{\widetilde{F},\widetilde{G}\}^{(\mathrm{uEMHD})}(\rho_\alpha,\mathbf{u},s,\mathbf{D},\mathbf{B}) = \{F,G\}^{(\mathrm{CIT})}|_{\mathbf{m}} + \{F,G\}^{(\mathrm{EM})} \tag{1.147}$$

$$\text{elmag.-mom. } A = \begin{cases}
- \int \mathrm{d}\mathbf{r} \left[\varepsilon_{ijk}\varepsilon_{ipq} F_{m_p} B_q \partial_j G_{B_k} - \dots\right] \\
+ \int \mathrm{d}\mathbf{r} \left[\varepsilon_{ijk}\varepsilon_{krs} F_{D_i} \partial_j \left(G_{m_r} D_s\right) - \dots\right] \\
+ \int \mathrm{d}\mathbf{r} \partial_l D_l \left(F_{m_i} G_{D_i} - \dots\right)
\end{cases}$$

$$\text{mom.-mom. } R = \begin{cases}
- \int \mathrm{d}\mathbf{r} \varepsilon_{ijk} D_j B_k \left(\partial_l F_{m_i} G_{m_l} - \dots\right) \\
- \int \mathrm{d}\mathbf{r} \left[\varepsilon_{ijk}\varepsilon_{ipq}\varepsilon_{krs} F_{m_p} B_q \partial_j \left(G_{m_r} D_s\right) - \dots\right] \\
- \int \mathrm{d}\mathbf{r} \partial_l D_l \left(\varepsilon_{ijk} F_{m_i} G_{m_j} B_k - \dots\right) \\
+ \int \mathrm{d}\mathbf{r} \partial_l D_l B_i \varepsilon_{ijk} F_{m_j} G_{m_k}
\end{cases}$$

The first line contains the bracket of Classical Irreversible Thermodynamics with $\mathbf{m}$ instead of $\mathbf{u}$ and the electromagnetic bracket. The remaining terms can be sorted out into two categories. The terms on the second, third and fourth line of (1.147) are the electromagnetic field-momentum coupling . The remainder of the terms are the momentum-momentum coupling, i.e. containing $F_{\mathbf{m}} G_{\mathbf{m}}$.

With making use of by-parts integration and the properties of Levi-Civita's symbol[1] the terms of (1.147) labeled with A read

$$A = \{F, G\}^{(\mathrm{SP})}(\mathbf{D}, \mathbf{m}) + \{F, G\}^{(\mathrm{SP})}(\mathbf{B}, \mathbf{m}) \ . \tag{1.148}$$

thus we can rewrite (1.147) as

$$\begin{aligned}\{\widetilde{F}, \widetilde{G}\}^{(\mathrm{uEMHD})}(\rho_\alpha, \mathbf{u}, s, \mathbf{D}, \mathbf{B}) = &\{F, G\}^{(\mathrm{CIT})}|_{\mathbf{m}} + \{F, G\}^{(\mathrm{EM})} \\ &+ \{F, G\}^{(\mathrm{SP})}(\mathbf{D}, \mathbf{m}) + \{F, G\}^{(\mathrm{SP})}(\mathbf{B}, \mathbf{m}) \\ &+ R \ .\end{aligned} \tag{1.149}$$

Therefore, we have recovered the bracket $\{F, G\}^{(\mathrm{mEMHD})}$ in (1.149). The cumbersome proof that $R = 0$ is contained in [10, Eqns (3.251)-(3.257)].

1.2 Elementary dipole

Two classical charged mass points are described by their positions, $\mathbf{r}^1$ and $\mathbf{r}^2$, momenta $\mathbf{p}^1$ and $\mathbf{p}^2$, carrying charge q_1 and q_2, respectively. The dynamics of the particles is governed by the canonical Poisson bracket:

$$\{F, G\}^{\mathrm{mp}}(\mathbf{r}^\beta, \mathbf{p}^\beta) = \sum_{\beta=1}^{2} (F_{r_i^\beta} G_{p_i^\beta} - G_{r_i^\beta} F_{p_i^\beta}) \ . \tag{1.150}$$

Assume that $q = q_1 = -q_2$ and consider the following transformation of the variables:

$$\mathbf{R} = \frac{m_1 \mathbf{r}^1 + m_2 \mathbf{r}^2}{m_1 + m_2}, \quad \mathcal{P} = q(\mathbf{r}^1 - \mathbf{r}^2), \tag{1.151}$$

$$\Pi = \mathbf{p}^1 + \mathbf{p}^2, \quad \mathbf{t} = \frac{m_2 \mathbf{p}^1 - m_1 \mathbf{p}^2}{q(m_1 + m_2)}, \tag{1.152}$$

Bracket (1.150) then transforms into:

$$\begin{aligned}\{F, G\}^{\mathrm{mp}}(\mathbf{R}, \Pi, \mathcal{P}, \mathbf{t}) = &(F_{R_i} G_{\Pi_i} - G_{R_i} F_{\Pi_i}) \\ &+ (F_{\mathcal{P}_i} G_{t_i} - G_{\mathcal{P}_i} F_{t_i}) \ .\end{aligned} \tag{1.153}$$

1.3 Semi-direct product

This Section closely follows [18] and [10, Sec. 3]. Hamiltonian formulation of electromagnetism is given by the co-tangent bundle $T^*M = V \times V^*$, and canonical Poisson bracket for $\mathbf{A} \in V$ and $\mathbf{Y} \in V^*$, interpreting $\mathbf{Y}$ as $-\mathbf{D}$.

Hamiltonian fluid mechanics is the Lie Algebra dual $\mathfrak{l}^* = (\mathfrak{X} \ltimes (\mathcal{F} \times \mathcal{F}))^*$ with the Poisson bracket $\{F, G\}^{\mathrm{FM}}(\rho, \mathbf{u}, s)$. Where $\mathbf{u}(\mathbf{r}) \in \mathfrak{X}$ and $\rho(\mathbf{r}), s(\mathbf{r}) \in \mathcal{F}$.

[1] i.e. $\varepsilon_{kij}\varepsilon_{klm} = \delta_{il}\delta_{jm} - \delta_{im}\delta_{jl}$

The semidirect product of the latter and former is, see [18, Eq. 64] given as

$$\begin{aligned}\{F,G\}^{\mathfrak{l}^*\ltimes T^*M}(\rho,\mathbf{m},s,\mathbf{Y},\mathbf{A}) &= \{F,G\}^{\mathrm{FM}} + \int \mathrm{d}\mathbf{r}(F_{A_i}G_{Y_i} - G_{A_i}F_{Y_i}) \\ &+ \langle F_{\mathbf{A}}, G_{\mathbf{m}} \rhd \mathbf{A}\rangle - \langle G_{\mathbf{A}}, F_{\mathbf{m}} \rhd \mathbf{A}\rangle \\ &+ \langle \mathbf{Y}, F_{\mathbf{m}} \rhd G_{\mathbf{Y}}\rangle - \langle \mathbf{Y}, G_{\mathbf{m}} \rhd F_{\mathbf{Y}}\rangle \end{aligned} \tag{1.155}$$

where $\mathbf{m}$ denotes the total momentum of the joined dynamics. The right action of $\mathfrak{l}$ on T^*M is defined as

$$F_{\mathbf{m}} \rhd \mathbf{a} = -\mathcal{L}_{\mathbf{F_m}}\mathbf{a} = -\left(F_{m_j}\partial_j a_i + a_j\partial_i F_{m_j}\right)\mathrm{d}r^i \ . \tag{1.156}$$

for the co-vector field $\mathbf{a}$. Introducing (1.156) for $\mathbf{A}$ and $\mathbf{Y} = -\mathbf{D}$ into (1.155) yields

$$\begin{aligned}\{F,G\}^{\mathrm{mEMHD}_{\mathbf{A}}}(\rho,\mathbf{m},s,\mathbf{D},\mathbf{A}) &= \{F,G\}^{\mathrm{FM}}|_{\mathbf{u}=\mathbf{m}} + \{F,G\}^{\mathrm{EM}_{\mathbf{A}}} \\ &+ \int \mathrm{d}\mathbf{r} D_i\left(\partial_j F_{D_i}G_{m_j} - \partial_j G_{D_i}F_{m_j}\right) \\ &+ \int \mathrm{d}\mathbf{r}\partial_j D_j(F_{m_i}G_{D_i} - G_{m_i}F_{D_i}) \\ &+ \int \mathrm{d}\mathbf{r} D_j(F_{m_i}\partial_j G_{D_i} - G_{m_i}\partial_j F_{D_i}) \\ &- \int \mathrm{d}\mathbf{r}\partial_j A_i\left(F_{A_i}G_{m_j} - G_{A_i}F_{m_j}\right) \\ &- \int \mathrm{d}\mathbf{r} A_i\left(F_{A_j}\partial_j G_{m_i} - G_{A_j}\partial_j F_{m_i}\right) \ , \end{aligned} \tag{1.157}$$

after some algebra. This bracket can be further projected to the functional dependent on $\mathbf{B}$, see (1.16), then

$$\widetilde{F}_{A_i} = \varepsilon_{imn}\partial_m F_{B_n}. \tag{1.158}$$

Bracket $\{F,G\}^{(\mathrm{EM})_{\mathbf{A}}}$ transforms to electromagnetic bracket (1.17). The remainder of the terms of (1.157) affected by (1.158) can be written as

$$\begin{aligned} &- \int \mathrm{d}\mathbf{r}\partial_j A_i\varepsilon_{imn}\left(\partial_m F_{B_n}G_{m_j} - \dots\right) - \int \mathrm{d}\mathbf{r} A_i\varepsilon_{jmn}\left(\partial_m F_{B_n}G_{m_i} - \dots\right) \\ &= \int \mathrm{d}\mathbf{r}(\partial_i A_j - \partial_i A_j)\varepsilon_{imn}\left(\partial_m F_{B_n}G_{m_j} - \dots\right) \\ &= \int \mathrm{d}\mathbf{r}\varepsilon_{ijk}B_k\varepsilon_{imn}\left(\partial_m F_{B_n}G_{m_j} - \dots\right) \\ &= \int \mathrm{d}\mathbf{r} B_k\left(\partial_j F_{B_k}G_{m_j} - \dots\right) - \int \mathrm{d}\mathbf{r} B_k\left(\partial_k F_{B_j}G_{m_j} - \dots\right) \end{aligned} \tag{1.159}$$

The term with second derivatives stemming from by-parts integration cast of the second term on the first line of (1.157) contains $\varepsilon_{imn}\partial_i\partial_m F_{B_n}$ and is, therefore, identically zero. Finally, introducing (1.159) into (1.157) gives the sought bracket (1.23) for one-species continuum.

1.4 Chemical reactions

Let us denote species by A_α. Consider M chemical reactions written as

$$\sum_{\alpha=1}^{n} \mathrm{a}_\alpha^r \mathrm{A}_\alpha \rightleftharpoons \sum_{\alpha=1}^{n} \mathrm{b}_\alpha^r \mathrm{A}_\alpha \qquad \text{for } r = 1,\dots,M \ . \tag{1.160}$$

The stoichiometric coefficient γ is given by $\gamma_\alpha^r := \mathrm{b}_\alpha^r - \mathrm{a}_\alpha^r$ for species A_α and r-th chemical reaction. Let us define the dissipation potential

$$\Xi^{(\mathrm{chk})}(\rho_\alpha, \rho_\alpha^*) = \int \mathrm{d}\mathbf{r} \sum_{r=1}^{M} R_r(\rho_\alpha) \Big(\frac{1}{\beta_r(1-\beta_r)} \tag{1.161}$$

$$+ \frac{1}{1-\beta_r} \exp\Big((1-\beta_r)\mathbf{X}_r(\rho_\alpha^*)\Big) + \frac{1}{\beta_r} \exp\Big(-\beta_r \mathbf{X}_r(\rho_\alpha^*)\Big)\Big) \,, \tag{1.162}$$

where $\beta_r \in [0,1]$, $R_r(\rho_\alpha) \geq 0$ and

$$\mathbf{X}_r(\rho_\alpha^*) = \frac{1}{k_\mathrm{B}} \sum_{l=1}^{M} \gamma_\alpha^r \rho_\alpha^* \qquad\qquad \text{for } r = 1, \ldots, M \,, \tag{1.163}$$

are symmetry factors, reaction rates and chemical affinities, respectively.

Then $\Xi^{(\mathrm{chk})}$ gives, using (1.80), the irreversible evolution of ρ_α due to chemical reactions (1.160) for a given entropy. That is

$$\begin{aligned}(\partial_t \rho_\alpha)_{\mathrm{irr}} =& \left\langle \frac{\delta \Xi^{(\mathrm{chk})}}{\delta \rho_\alpha^*}\bigg|_{\rho_\alpha^* = S_{\rho_\alpha}}, \frac{\delta \rho_\alpha}{\delta \rho_\alpha} \right\rangle \\ =& R_r(\rho_\alpha)\Big(\exp\Big((1-\beta_r)\mathbf{X}_r(\rho_\alpha^*)\Big) - \exp\Big(-\beta_r \mathbf{X}_r(\rho_\alpha^*)\Big)\Big) \,. \end{aligned} \tag{1.164}$$

The presented formulation of chemical kinetics as a dissipative evolution was given in [50, 10, 1].

1.5 Boundary terms for MSPNP

The specification of the boundary conditions in continuum non-equilibrium thermodynamics, see e.g. [51] or [5], is based on global balance equations for surfaces with discontinuities. The fluxes of quantities across the boundary stemming from the balances are later on specified with making use of an entropy principle for surface quantities. Öttinger [52] introduced the notion of boundary conditions for GENERIC formulation of Navier-Stokes equations formulated in terms of Poisson bracket and dissipation brackets. The two approaches give, for the description of single momentum continuum, fairly similar results.

Let us restrict ourselves to the irreversible evolution to demonstrate a possible way of obtaining similar, although less general, results for the case of weakly non-local dissipation. Consider the following linear functional,

$$m_\alpha^\gamma = \int_\Omega \mathrm{d}\mathbf{r} \rho_\alpha \gamma \,, \tag{1.165}$$

where γ is a sufficiently smooth function with, in general, non-zero trace on $\partial\Omega$. The flux of ρ_α across $\partial\Omega$ due to weakly non-local dissipation potential (1.134) is obtained by evaluating the irreversible evolution of m_α^γ as

$$\begin{aligned}(\partial_t m_\alpha^\gamma)_{\mathrm{irr}} = \left\langle \frac{\delta \Xi^{\mathrm{MSP}}}{\delta \rho_\alpha^*}, \frac{\delta m_\alpha^\gamma}{\delta \rho_\alpha} \right\rangle_S =& \int_{\partial\Omega} \mathrm{d}\mathbf{r} \frac{1}{M_\alpha} \left(-(s^\dagger \rho_\alpha)^2 \left(\partial_i \rho_\alpha^\dagger + \frac{e_0 z_\alpha}{m_\alpha} \partial_i \varphi \right) \right) \nu_i \gamma \\ &- \int_\Omega \mathrm{d}\mathbf{r} \partial_i \left[\frac{1}{M_\alpha} \left(-(s^\dagger \rho_\alpha)^2 \left(\partial_i \rho_\alpha^\dagger + \frac{e_0 z_\alpha}{m_\alpha} \partial_i \varphi \right) \right) \right] \gamma \,. \end{aligned} \tag{1.166}$$

The surface integral, here not neglected/omitted, contains the flux of ρ_α across Ω. For $\gamma = 1$ in $\overline{\Omega}$ is (1.166) equivalent to a global balance equation of ρ_α in volume Ω without convection (which was already relaxed for (1.134)).

Adsorption

Let $\Omega \subset \mathbb{R}^d$ be simply connected with smooth boundary. Let us further assume that a distinct thermodynamic system is carried by $\partial\Omega$ described by surface mass densities $\underset{\mathrm{s}}{\rho}_\alpha$ and surface entropy density $\underset{\mathrm{s}}{s}$. Let us also assume that the values of the bulk quantities may be defined on $\partial\Omega$, e.g. in sense of traces as in (1.166). Let us define the following dissipation potential,

$$\underset{\mathrm{s}}{\Xi}^{\mathrm{A}}(\underset{\mathrm{s}}{\rho}{}^*_\alpha, \rho^*_\alpha|_\Gamma) = \int_{\partial\Omega} \mathrm{d}S \frac{1}{2\tau_{\mathrm{A}}} \left(\underset{\mathrm{s}}{\rho}{}^*_\alpha - \rho^*_\alpha\right)^2 \ , \tag{1.167}$$

where the trace of bulk partial mass density ρ_α on $\partial\Omega$ appears. We propose to evaluate the irreversible evolution of $\underset{\mathrm{s}}{\rho}_\alpha$ due to $\underset{\mathrm{s}}{\Xi}^{\mathrm{A}}$ analogously as in (1.80), that is,

$$(\partial_t \underset{\mathrm{s}}{\rho}_\alpha)_{\mathrm{irr}} = \left\langle \frac{\delta \underset{\mathrm{s}}{\Xi}^{\mathrm{A}}}{\delta \underset{\mathrm{s}}{\rho}_\alpha}, \frac{\delta \underset{\mathrm{s}}{\rho}_\alpha}{\delta \underset{\mathrm{s}}{\rho}_\alpha} \right\rangle_{\partial\Omega} = \frac{1}{\tau_{\mathrm{A}}} \left(\underset{\mathrm{s}}{\rho}{}^*_\alpha - \rho^*_\alpha|_{\partial\Omega}\right) \ . \tag{1.168}$$

The flux of $\rho_\alpha|_{\partial\Omega}$ due to Ξ^{MSP} and $\underset{\mathrm{s}}{\Xi}^{\mathrm{A}}$ may be interpreted, similarly to (1.166), using m^γ_α, see (1.165), as

$$(\partial_t m^\gamma_\alpha)_{\mathrm{irr}} = \left\langle \frac{\delta \Xi^{\mathrm{MSP}}}{\delta \rho^*_\alpha}, \frac{\delta m^\gamma_\alpha}{\delta \rho_\alpha} \right\rangle_\Omega + \left\langle \frac{\delta \Xi^{\mathrm{A}}}{\delta \rho^*_\alpha}, \frac{\delta m^\gamma_\alpha}{\delta \rho_\alpha} \right\rangle_{\partial\Omega} \ , \tag{1.169}$$

where the first term on the right hand side is (1.166). The function γ can be localized to the boundary, so that the volume integrals vanish. Therefore, one can compare the surface terms , using (1.166), and conclude for isothermal conditions that

$$\frac{(s^\dagger \rho_\alpha)^2}{M_\alpha} \left(\partial_i \rho^\dagger_\alpha + \frac{e_0 z_\alpha}{m_\alpha} \partial_i \varphi\right)\Big|_{\partial\Omega} \nu_i = -\frac{1}{\tau_{\mathrm{A}}} \left(\underset{\mathrm{s}}{\rho}{}^*_\alpha - \rho^*_\alpha|_{\partial\Omega}\right) \quad \text{on } \partial\Omega \ , \tag{1.170}$$

thus obtaining the interpretation of the irreversble flux of $\rho_\alpha|_{\partial\Omega}$. Because the reversible evolution is already relaxed, the formula (1.170) specifies the boundary condition for the flux of ρ_α.

1.5.1 Application to yttria-stabilized zirconia interface

This section demonstrates a particular connection between the first and second chapter. The bulk diffusion equation (2.35b) and the surface balance (2.66) for the mobile oxide ions will be derived below using the results of the first chapter. The free energy models for bulk (2.9) and surface (2.44) YSZ and, consequently, the bulk (2.31) and surface (2.52) chemical potentials are shared by the both formulations.

Bulk diffusion of oxide ions

Let us assume the isothermal setting of the second chapter, where Zr^{4+}, Y^{3+} and immobile O^{2-} form the crystalline lattice with vanishing velocity, see Sec. 2.2. The flux of mobile oxide ions w.r.t. the crystalline lattice in the bulk is given by (1.133). The flux, using the standard notation for the chemical potential and temperature $\rho_\alpha^\dagger = \mu_\alpha$ and $s^\dagger = T$, respectively, reads

$$\partial_t \rho_{\mathrm{Om}} = \partial_i \left(\frac{\rho_{\mathrm{Om}} T}{M_{\mathrm{Om}}} \left(\partial_i \mu_{\mathrm{Om}} + \frac{e_0 z_{\mathrm{Om}}}{m_{\mathrm{Om}}} \partial_i \varphi \right) \right) \ , \tag{1.171}$$

where subscript Om denotes the mobile oxide ions. Let us employ the gradient of the chemical potential of mobile oxide, see (2.31a), that reads

$$\partial_i \mu_{\mathrm{Om}} = \frac{k_{\mathrm{B}} T}{m} \frac{1}{y(1-y)} \partial_i y \ . \tag{1.172}$$

The choice

$$\frac{1}{M_{\mathrm{Om}}} = \frac{1}{k_{\mathrm{B}} T^2 \left(1 + \frac{m_{\mathrm{Om}}(1-\nu^\#)m}{m^\#} \right)^2} \ , \tag{1.173}$$

renders (1.171) equivalent to (2.35b) with (2.36b) which is derived differently within the second chapter. in (1.173) and (1.172), the notation of the second chapter is used .

The surface balance of oxide ions

Let us further apply (1.168) to the surface of YSZ, see Sec. 2.4. Again, the usual notation for the symbols in (1.168) is

$$\rho_\alpha^* = -\frac{\mu_\alpha}{T} \quad \text{and} \quad \underset{\mathrm{s}}{\rho}{}_\alpha^* = -\frac{\underset{\mathrm{s}}{\mu}{}_\alpha}{\underset{\mathrm{s}}{T}} \ . \tag{1.174}$$

Hence, the evolution equation (1.168) for mobile oxide ions reads

$$(\partial_t \underset{\mathrm{s}}{\rho}{}_{\mathrm{Om}}) = \frac{1}{\tau_{\mathrm{A}}} \left(-\frac{\underset{\mathrm{s}}{\mu}{}_{\mathrm{Om}}}{T} + \frac{\mu_{\mathrm{Om}}}{T}|_{\partial\Omega} \right) \ . \tag{1.175}$$

and is, in an isothermal setting, for suitable choice of τ_{A} and vanishing lattice velocity, equivalent to the adsorption flux of mobile oxide ions (2.60).

It remains to derive the production of oxide ions due to the chemical reaction. The chemical kinetics in Appendix 1.4 can be straightforwardly reformulated for the surface species, due to the absence of spatial derivatives. It is sufficient to use surface densities in place of the volume densities, that is, to equip the quantities with the subscript s, i.e., to write $\underset{\mathrm{s}}{\rho}{}_\alpha$ and $\underset{\mathrm{s}}{s}$ instead of ρ_α and s, respectively.

The constitutive equations for the mass production (1.164), assuming the surface densities, is identical to those employed in the second section (2.63), see notation (1.174). Therefore, the same production term (2.64a) for electron-transfer reaction $(2.69)_{\mathrm{right}}$,i.e., the production of the surface mobile oxide ions, follows from (1.164). This, combined with (1.175), renders the evolution for mobile oxide ions identical to (2.66) derived in the second chapter.

2. Charged double layer of high temperature solid oxide interface

2.1 Introduction

Detailed continuum models of high temperature solid oxide electrochemical cells (SOEC)[1]describe the underlying chemistry with spatially distinguished phases (oxide ion conductor, electric conductor, gas) of the triple phase boundary [53, 54, 55, 56]. Surface physics processes such as tangential diffusion and surface chemical reactions of the surface species are employed. In particular, the electron-transfer reaction at the triple phase boundary is usually modelled with Butler-Volmer-type kinetics containing overpotential, the difference of the electric potential between the metal and the bulk of the YSZ, as the driving force. The ionically or electrically conductive parts of a solid oxide cell are electroneutral in the respective bulks. The overpotential, appearing at the phase interface is caused by formation of a charged double layer of oxide ions in YSZ and electrons in the electrode. Although the overpotential correlates with the excess concentration of oxide ions available for the electron-transfer reaction in steady-state scenarios, it cannot capture the dynamics of the double layer. Therefore, if such a model is compared to the results of a dynamic current-voltage measurement, e.g., electrochemical impedance spectroscopy or linear-sweep voltammetry, the dynamics of the double layer is underrepresented.

To determine the structure and dynamics of the space-charge layer of oxide ions in the YSZ, at the continuum level, the Poisson-Nernst-Planck (PNP) system, generalized in order to account for the effect of the finite density of available lattice sites for oxide ions, can employed.

Such an approach was already used to capture the formation and behavior of the electrochemical double layers at electrode-electrolyte interfaces [57, 58]. The PNP system was successfully applied to the solid-state electrochemical systems, e.g., lithium batteries [59, 60, 61].In [62], the PNP equations were already applied for proton ceramic fuel cells, however, the thermodynamics of the crystalline lattice and of the surface were not taken into account.

In this work, a modeling approach for charged bulk-surface interfaces based on first principles of nonequilibrium thermodynamics resulting in a generalized Poisson-Nernst-Planck system [5] (based on [17]) is used to formulate the model of dynamics of the space-charged layer at the YSZ-metal-air triple interface. The main advantage of this approach is its consistency between the free energy (equilibrium) and fluxes (dynamics).

The paper is organized as follows. The free energy model of the bulk YSZ, capturing the crystalline structure, immobile oxide ions and elastic deformation, is developed in section 2.2. The resulting chemical potentials are introduced into the gPNP model [5] after its modification for the description of the lattice velocity. Section 2.3 is dedicated to the treatment of the bulk metal and gas. Both phases are assumed to be in a diffusional equilibrium. The free energy of the surface and the surface dynamics are described and developed in the Section

[1]Either fuel cells, or electrolysis cells.

2.4. The modeling approach results in a coupled system of evolution equation describing the transport of oxide ions in the bulk of electrolyte, adsorption of oxide ions from bulk to the surface and electron-transfer reaction alongside with the Poisson equation.

Using a finite volume based discretization, double layer capacitance and linear-sweep voltammetry simulations are performed in Section 2.5. The performed simulations study the effects of the newly introduced concept immobile oxide ions, the free energy parameters and the kinetic rates on the current response.

The novelty of the approach lies in the synthesis of the crystalline lattice bulk-surface free energy description and the coupled bulk-surface dynamics in non-equilibrium thermodynamics framework. Owing to this, it is possible to simulate the equilibrium behavior, e.g., the double layer capacitance, and dynamic behavior, e.g., the cyclic voltammetry, using a single model. Notable contribution to the state of the art models of YSZ is the thermodynamic treatment of the surface dynamics.

2.2 Bulk YSZ

We consider the charge transport exclusively in the isothermal electrostatic setting, therefore the temperature T is assumed to be constant and the electric field is given as $\boldsymbol{E} = -\nabla\varphi$. Moreover, a simple material model for polarization based on a constant susceptibility χ is chosen.

2.2.1 General mixture and crystalline structure

Mixture quantities. We model YSZ as mixture of four constituents: zirconium and yttrium cations denoted by Zr and Y, respectively, and oxide anions. We assume that only a part of the oxide anions is freely mobile and refer to these as Om, whereas the remaining immobile oxide anions Oi are fixed to the underlying crystal structure. For referencing the different constituents of the mixture we use the index set $\mathcal{I}_{\mathrm{YSZ}} = \{\mathrm{Zr}, \mathrm{Y}, \mathrm{Oi}, \mathrm{Om}\}$. Each constituent is characterized by the atomic mass m_α and its atomic charges $z_\alpha e_0$, where $\alpha \in \mathcal{I}_{\mathrm{YSZ}}$. The constant e_0 is the elementary charge and z_α is the charge number of the constituent. Multiplication of the number densities n_α by m_α gives the partial mass densities,

$$\rho_\alpha = m_\alpha n_\alpha \ . \tag{2.1}$$

The (total) mass density ρ and the free charge density n^{F} of YSZ are defined as follows,

$$\rho = \sum_{\alpha\in\mathcal{I}_{\mathrm{YSZ}}} m_\alpha n_\alpha \ , \qquad\qquad n^{\mathrm{F}} = e_0 \sum_{\alpha\in\mathcal{I}_{\mathrm{YSZ}}} z_\alpha n_\alpha \ . \tag{2.2}$$

While each species is transported by its partial velocity $\boldsymbol{v}_\alpha$, we introduce for the mixture the barycentric velocity

$$\boldsymbol{v} = \frac{1}{\rho} \sum_{\alpha\in\mathcal{I}_{\mathrm{YSZ}}} \rho_\alpha \boldsymbol{v}_\alpha \ . \tag{2.3}$$

The diffusion fluxes of the constituents are determined by the transport relative to the barycentric velocity, viz.,

$$\boldsymbol{J}_\alpha = \rho_\alpha(\boldsymbol{v}_\alpha - \boldsymbol{v}) \qquad \text{implying the constraint} \quad \sum_{\alpha\in\mathcal{I}_{\mathrm{YSZ}}} \boldsymbol{J}_\alpha = 0 \ . \tag{2.4}$$

Crystalline structure. The crystalline structure of pure ZrO_2 is well known, see e.g. [63] and might be described conveniently in terms of unit crystal cells. Unit crystal cells of yttria-doped zirconia are, due to the yttria doping, difficult to be described systematically [64]. To overcome this, we introduce cation and anion spatial lattices, so that they coincide with the respective lattices in pure cubic ZrO_2, i.e., locations of Zr^{4+} or O^{2-}. Contrary to the pure ZrO_2, the cation lattice of YSZ is occupied also by Y^{3+} and some of the anion lattice sites may be empty. The cation lattice unit cell is assumed to be face-centered cubic and contains 8 cations in its vertices and 4 in the centers of the faces. Each vertex site is shared by seven other unit cells and each face-center site by one additional unit cell. Hence, there are $M_{\mathrm{C}}^{\#} = 4$ cation lattice sites belonging to one unit cell. There are $M_{\mathrm{A}}^{\#} = 8$ anion lattice sites contained in the cation lattice unit cell, these are located inside the unit cell and not being shared by the neighboring unit cells. In general, the ratio $m = M_{\mathrm{A}}^{\#}/M_{\mathrm{C}}^{\#}$ is a fixed constant that results from the given combination of materials. In the case of YSZ, we have $m = 2$. The spacing of the lattice can be described by a number density $n^{\#}$ of unit crystal cells, that may be non-homogeneous in space due to the non-uniformity of the lattice. The densities of the cation lattice sites are then given as $n_{\mathrm{C}}^{\#} = M_{\mathrm{C}}^{\#} n^{\#}$ while for the anion lattice sites is $m\, M_{\mathrm{C}}^{\#}\, n^{\#}$. We assume that all cation lattice sites are actually occupied by either zirconium or yttrium cations whereas some of the anion sites may be left unoccupied. We thus have

$$n_{\mathrm{C}}^{\#} = n_{\mathrm{Zr}} + n_{\mathrm{Y}} \ , \qquad\qquad m\, n_{\mathrm{C}}^{\#} \geq n_{\mathrm{Oi}} + n_{\mathrm{Om}} \ . \tag{2.5}$$

To further specify the state of the YSZ , we introduce the proportion $\nu^{\#}$ of immobile oxide ions and the filling ratio y of the anion lattice sites,

$$\nu^{\#} = \frac{n_{\mathrm{Oi}}}{m\, n_{\mathrm{C}}^{\#}} \ , \qquad\qquad y = \frac{n_{\mathrm{Om}}}{m\, n_{\mathrm{C}}^{\#} - n_{\mathrm{Oi}}} \ . \tag{2.6}$$

In addition, we define the molar fraction $x^{\#}$ of Y_2O_3 in YSZ,

$$x^{\#} = \frac{\frac{1}{2} n_{\mathrm{Y}}}{n_{\mathrm{C}}^{\#} - \frac{1}{2} n_{\mathrm{Y}}} \ , \tag{2.7}$$

To simplify the model, we assume the Zirconium, Yttrium and immobile oxide ions are bound to the lattice and thus all are transported with identical lattice velocity

$$\upsilon_\alpha = \upsilon^{\#} \qquad \text{for} \ \ \alpha \in \{\mathrm{Zr}, \mathrm{Y}, \mathrm{Oi}\} \ . \tag{2.8}$$

2.2.2 Free energy and chemical potentials

The free energy density[2] $\rho\psi$ of YSZ is assumed to be a function of temperature T, partial mass densities ρ_α and the electric field $\boldsymbol{E}$. We suppose that the free

[2]The free energy function is defined here as: $\rho\psi = \rho u - \boldsymbol{P}\cdot\boldsymbol{E} - T\rho s$, where ρu is the density of internal energy.

energy density $\rho\psi(T, \rho_\alpha, \boldsymbol{E})$ can be split into four additive parts: reference energy, entropy of mixing, elastic energy and polarization energy,

$$\rho\psi(T, (\rho_\alpha)_{\alpha\in\mathcal{I}_{\mathrm{YSZ}}}, \boldsymbol{E}) = \rho\psi^{\mathrm{ref}} + \rho\psi^{\mathrm{polar}} + \rho\psi^{\mathrm{mech}} + \rho\psi^{\mathrm{mix}} \ , \tag{2.9}$$

where only $\rho\psi^{\mathrm{polar}}$ depends on the electric field $\boldsymbol{E}$ and only $\rho\psi^{\mathrm{mix}}$ depends on the crystal structure. The entropy density ρs and the chemical potentials of the respective species μ_α are defined with respect to the free energy density as

$$\frac{\partial\rho\psi}{\partial T} = -\rho s \ , \qquad\qquad \frac{\partial\rho\psi}{\partial\rho_\alpha} = \mu_\alpha \ . \tag{2.10}$$

Reference energy. The reference free energy describes a suitable chosen reference state and is assumed to be

$$\rho\psi^{\mathrm{ref}} = \sum_{\alpha\in\mathcal{I}_{\mathrm{YSZ}}} \rho_\alpha \mu_\alpha^{ref} \ . \tag{2.11}$$

Here, μ_α^{ref} denotes the temperature dependent reference chemical of each individual constituent.

Polarization energy. On top of the free charge density n^{F} according to 2.2_{right}, an excess charge density n^{P} may arise in the material due to the presence of the electric field, mechanical strain, etc., see for example [65, Chapter 2]. This excess charge is usually described by a polarization vector $\boldsymbol{P}$ so that

$$-\operatorname{div}\boldsymbol{P} = n^{\mathrm{P}} \ . \tag{2.12}$$

We refrain from a comprehensive discussion of constitutive modeling of polarization like, e.g., in [5] and assume that in bulk YSZ, the relaxation time of the polarization is small and the polarization vector $\boldsymbol{P}$ is proportional to the electric field $\boldsymbol{E}$, i.e.,

$$\frac{\partial\rho\psi}{\partial\boldsymbol{E}} = -\boldsymbol{P} \ , \qquad\qquad \boldsymbol{P} = \chi\varepsilon_0\boldsymbol{E} \ . \tag{2.13}$$

The number χ is the electric susceptibility of YSZ, which for simplicity is assumed spatially homogeneous here. Integrating (2.13) such that $\rho\psi^{\mathrm{polar}}$ vanishes for $\boldsymbol{E} \to 0$ yields the free energy density due to polarization

$$\rho\psi^{\mathrm{polar}} = -\frac{\varepsilon_0\chi}{2}|\boldsymbol{E}|^2 \ . \tag{2.14}$$

Elastic energy. We introduce the material pressure p, which is independent of the electric field $\boldsymbol{E}$, and is defined by the Gibbs-Duhem relation

$$p = -\rho\widetilde{\psi} + \sum_{\alpha\in\mathcal{I}_{\mathrm{YSZ}}} \rho_\alpha\mu_\alpha \ , \tag{2.15}$$

where $\rho\widetilde{\psi} = \rho\psi^{\mathrm{ref}} + \rho\psi^{\mathrm{mix}} + \rho\psi^{\mathrm{mech}}$. The elastic contribution to the free energy is based on a simple linear constitutive relation between the material pressure p and the number densities n_α of YSZ,

$$p = p^{ref} + K\Big(\sum_{\alpha\in\mathcal{I}_{\mathrm{YSZ}}} v_\alpha^{ref} n_\alpha - 1\Big) \ . \tag{2.16}$$

Here K is the bulk modulus of YSZ and v_α^{ref} are the specific volumes of the YSZ species under the reference pressure p^{ref}. In general, the specific volumes are functions of temperature and pressure, but for simplicity we assume v_α^{ref} are constant.

By use of an alternative set of variables for the free energy density $\rho\widetilde{\psi}$ the Gibbs-Duhem relation (2.15) can be written as, cf. [58, equation A.6],

$$\frac{p}{\rho^2} = \frac{\partial \check{\psi}}{\partial \rho} \ . \tag{2.17}$$

Here $\rho\check{\psi}(t, \rho, c_\alpha)$ denotes the free energy density $\rho\widetilde{\psi}$ as a function of the total mass density ρ and the mass fractions $c_\alpha = \frac{\rho_\alpha}{\rho}$.

Insertion of (2.16) into (2.17) and integration such that $\rho\psi^{\mathrm{mech}}$ vanishes for $p \to p^{ref}$ yields the desired elastic contribution to the free energy $\rho\psi^{\mathrm{mech}}$, viz.

$$\rho\psi^{\mathrm{mech}} = (p^{\mathrm{R}} - K)(\rho f - 1) + K\rho f \ln(\rho f) \ , \tag{2.18}$$

where $\rho f = \sum_{\alpha \in \mathcal{I}_{\mathrm{YSZ}}} v_\alpha^{ref} n_\alpha$.

Entropy of mixing. The entropy of mixing depends on the microscopic configuration of the mobile oxide ions in the anion lattice. We therefore consider a YSZ specimen that is homogeneous, so that $n_\alpha = N_\alpha / V$, where N_α is the total number of a species in a volume V. Let W represent the number of possible realizations to arrange the mobile oxide ions on the anion lattice. Then the mixing entropy density, according to Boltzmann's formula, reads

$$\rho\eta^{\mathrm{mix}} = \frac{k_{\mathrm{B}}}{V} \ln(W) \ . \tag{2.19}$$

Every immobile oxide ion is assumed to be fixed at a certain anion lattice site. The number of anion lattice sites available for the mobile oxide ions is therefore $(m\, N_{\mathrm{C}}^{\#} - N_{\mathrm{Oi}})$. Thus, there are

$$W = \frac{(m\, N_{\mathrm{C}}^{\#} - N_{\mathrm{Oi}})!}{N_{\mathrm{Om}}!\ (m\, N_{\mathrm{C}}^{\#} - N_{\mathrm{Oi}} - N_{\mathrm{Om}})!} \tag{2.20}$$

ways to place the mobile oxide ions, which are indistinguishable, at the admissible lattice sites. Using Stirling's formula, we obtain for the mixing entropy density

$$\rho\eta^{\mathrm{mix}} \approx -k_{\mathrm{B}}(m\, n_{\mathrm{C}}^{\#} - n_{\mathrm{Oi}})(y \ln y + (1-y)\ln(1-y)) \ , \tag{2.21}$$

with the filling ratio y according to (2.6). Then the entropic contribution to free energy density follows by integration of $(2.10)_{\mathrm{left}}$ with respect to the temperature,

$$\rho\psi^{\mathrm{mix}} = k_{\mathrm{B}}T(m\, n_{\mathrm{C}}^{\#} - n_{\mathrm{Oi}})(y \ln y + (1-y)\ln(1-y)) \ . \tag{2.22}$$

The integration constant is chosen such that the entropy of mixing contribution to the free energy density vanishes at $T = 0$.

Chemical potentials. The chemical potentials are independent of the electric field due to the choice of a constant susceptibility. With the above contributions to the free energy, the chemical potential are

$$\mu_{\mathrm{Om}} = \mu_{\mathrm{Om}}^{ref} + \tfrac{k_{\mathrm{B}}T}{m_{\mathrm{Om}}} \ln\left(\frac{y}{1-y}\right) + \tfrac{v_{\mathrm{Om}}^{ref}}{m_{\mathrm{Om}}}\left(p^{ref} + K \ln\left(1 + \frac{p-p^{ref}}{K}\right)\right) , \tag{2.23a}$$

$$\mu_{\mathrm{Oi}} = \mu_{\mathrm{Oi}}^{ref} - \tfrac{k_{\mathrm{B}}T}{m_{\mathrm{Oi}}} \ln(1-y) + \tfrac{v_{\mathrm{Oi}}^{ref}}{m_{\mathrm{Oi}}}\left(p^{ref} + K \ln\left(1 + \frac{p-p^{ref}}{K}\right)\right) , \tag{2.23b}$$

$$\mu_{\alpha} = \mu_{\alpha}^{ref} + m\tfrac{k_{\mathrm{B}}T}{m_{\alpha}} \ln(1-y) + \tfrac{v_{\alpha}^{ref}}{m_{\alpha}}\left(p^{ref} + K \ln\left(1 + \frac{p-p^{ref}}{K}\right)\right) \qquad \alpha = \mathrm{Zr}, \mathrm{Y} . \tag{2.23c}$$

2.2.3 Bulk governing equations and constitutive modeling

The electro-thermodynamic state of YSZ, occupying an interval $\Omega_{\mathrm{YSZ}} \subset \mathbb{R}$ at any time t, is described by the number densities n_α ($\alpha \in \mathcal{I}_{\mathrm{YSZ}}$), the barycentric velocity $\boldsymbol{v}$ and the electrostatic potential φ, which all are functions of time and position. In the isothermal electrostatic setting with a constant susceptibility, the evolution equations for the electro-thermodynamic state variables in the bulk are given by the Poisson equation, partial mass balances and the quasi-static momentum balance [45, 5],

$$-\varepsilon_0(1+\chi)\partial_{zz}\varphi = n^{\mathrm{F}} , \tag{2.24a}$$

$$\partial_t \rho_\alpha + \partial_z(\rho_\alpha v + J_\alpha) = 0 , \qquad \alpha \in \mathcal{I}_{\mathrm{YSZ}} , \tag{2.24b}$$

$$\partial_z p + n^{\mathrm{F}} \partial_z \varphi = 0 . \tag{2.24c}$$

The diffusion flux. The constraint $(2.4)_{\mathrm{right}}$ and the constitutive equations (2.8) imply that the diffusion fluxes have to be pairwise linear dependent. We chose J_{Om} as the independent flux and obtain

$$J_\alpha = -\frac{\rho_\alpha}{\rho_{\mathrm{Zr}} + \rho_{\mathrm{Y}} + \rho_{\mathrm{Oi}}} J_{\mathrm{Om}} \qquad \text{for} \quad \alpha \in \{\mathrm{Zr}, \mathrm{Y}, \mathrm{Oi}\} . \tag{2.25}$$

An entropy principle [5] is exploited to obtain the constitutive equation for the flux J_{Om}. To this end, the entropy production due to diffusion is written as a sum of binary products as

$$\xi_D = \sum_{\alpha \in \mathcal{I}_{\mathrm{YSZ}}} J_\alpha D_\alpha \overset{!}{\geq} 0 , \tag{2.26}$$

where the driving forces are

$$D_\alpha = -\left(\partial_z \frac{\mu_\alpha}{T} + \frac{z_\alpha e_0}{m_\alpha}\frac{1}{T}\partial_z\varphi\right) \qquad \text{for} \quad \alpha \in \mathcal{I}_{\mathrm{YSZ}} . \tag{2.27}$$

To satisfy the second law of thermodynamics, i.e., to guarantee that the entropy production is non-negative, we insert the relations (2.25) into the entropy production (2.26) and then chose a linear relation between the diffusion flux J_{Om}

and the resulting term depending on the driving forces. We obtain

$$J_{\mathrm{Om}} = -M\left(\frac{\rho_{\mathrm{Zr}}(D_{\mathrm{Zr}} - D_{\mathrm{Om}}) + \rho_{\mathrm{Y}}(D_{\mathrm{Y}} - D_{\mathrm{Om}}) + \rho_{\mathrm{Oi}}(D_{\mathrm{Oi}} - D_{\mathrm{Om}})}{\rho_{\mathrm{Zr}} + \rho_{\mathrm{Y}} + \rho_{\mathrm{Oi}}}\right) \qquad \text{with} \quad M > 0 \ . \tag{2.28}$$

Here, mobility coefficient M may be a function of the thermodynamic variables and their derivatives, as long as it is guaranteed to be non-negative.

Incompressibility. A useful simplification of the YSZ bulk model is possible when taking the large bulk modulus K of YSZ into account. Hayashi et al. in [66] reported a bulk modulus of YSZ of $K = 205\,\mathrm{GPa}$ at $25\,^{\circ}\mathrm{C}$ and we assume it to be in a comparable order of magnitude at the operating temperature of YSZ at $600\,^{\circ}\mathrm{C}$. This motivates to study the incompressible limit $\frac{K}{p^{ref}} \to \infty$. Under the assumption that the pressure p is bounded, we obtain from the constitutive relation (2.16) the constraint

$$K/p^{ref} \to \infty : \qquad \sum_{\alpha \in \mathcal{I}_{\mathrm{YSZ}}} v_\alpha^{ref} n_\alpha = 1 \ . \tag{2.29}$$

Thus, the pressure p becomes an independent variable of the system and the sum of all number densities is independent of the pressure. For simplicity we assumed that the crystal lattice does not deform over time and that all species except species Om move with the lattice velocity. To be consistent with the incompressibility constraint (2.29), we thus have to require that the specific volume of the mobile oxide ions vanishes, i.e.,

$$v_{\mathrm{Om}}^{ref} = 0 \ . \tag{2.30}$$

In the incompressible limit $K/p^{ref} \to \infty$, the chemical potentials (2.23) are linear in the pressure:

$$\mu_{\mathrm{Om}} = \mu_{\mathrm{Om}}^{ref} + \tfrac{k_{\mathrm{B}}T}{m_{\mathrm{Om}}} \ln\left(\frac{y}{1-y}\right) , \tag{2.31a}$$

$$\mu_{\mathrm{Oi}} = \mu_{\mathrm{Oi}}^{ref} - \tfrac{k_{\mathrm{B}}T}{m_{\mathrm{Oi}}} \ln(1-y) + \tfrac{v_{\mathrm{Oi}}^{ref}}{m_{\mathrm{Oi}}} p \ , \tag{2.31b}$$

$$\mu_\alpha = \mu_\alpha^{ref} + m\tfrac{k_{\mathrm{B}}T}{m_\alpha} \ln(1-y) + \tfrac{v_\alpha^{ref}}{m_\alpha} p \qquad \alpha = \mathrm{Zr}, \mathrm{Y} \ . \tag{2.31c}$$

Vanishing lattice velocity. For further simplification of the YSZ model, we assume that the lattice does not deform over time such that an appropriate reference frame can be chosen where the lattice velocity $v^{\#}$ vanishes,

$$v^{\#} = 0 \ . \tag{2.32}$$

Then the mass balance equations imply constant number densities for the immobile species, i.e., $\partial_t n_\alpha = 0$ for $\alpha = \mathrm{Zr}, \mathrm{Y}, \mathrm{Oi}$, and the barycentric velocity is given by $\rho v = \rho_{\mathrm{Om}} v_{\mathrm{Om}}$ which can be expressed in terms of the diffusion flux of the mobile oxide ions as

$$(\rho_{\mathrm{Zr}} + \rho_{\mathrm{Y}} + \rho_{\mathrm{Oi}}) v = J_{\mathrm{Om}} \ . \tag{2.33}$$

The assumptions of incompressibility and vanishing lattice velocity may be also viewed alternatively as a description of the charge transport in the reference frame of the cation lattice which does not undergo any deformation.

2.2.4 Summary of the bulk YSZ model

The constitutive modeling above motivates to change the set of variables from the number densities $(n_\alpha)_{\alpha\in\mathcal{I}}$ to $\{n_\mathrm{C}^\#, \nu^\#, x^\#, y\}$. Due to the vanishing lattice velocity the quantities $n_\mathrm{C}^\#$, $x^\#$ and $\nu^\#$ are constant in time and are further considered as model parameters. Therefore, the thermodynamic state of the bulk YSZ is described by three quantities: filling ratio y, electrostatic potential φ and pressure p. In addition, we define the lattice volume $V^\#$, lattice mass $m^\#$ and lattice charge number $z^\#$ as

$$\begin{aligned} V^\# n_\mathrm{C}^\# &= n_\mathrm{Zr} v_\mathrm{Zr}^{ref} + n_\mathrm{Y} v_\mathrm{Y}^{ref} + n_\mathrm{Oi} v_\mathrm{O}^{ref} \\ &= n_\mathrm{C}^\# \left(\frac{1-x^\#}{1+x^\#} v_\mathrm{Zr}^{ref} + \frac{2x^\#}{1+x^\#} v_\mathrm{Y}^{ref} + m\,\nu^\#\, v_\mathrm{O}^{ref} \right) , \qquad (2.34a) \\ m^\# n_\mathrm{C}^\# &= n_\mathrm{C}^\# \left(\frac{1-x^\#}{1+x^\#} m_\mathrm{Zr} + \frac{2x^\#}{1+x^\#} m_\mathrm{Y} + m\,\nu^\#\, m_\mathrm{O} \right) , \qquad (2.34b) \\ z^\# n_\mathrm{C}^\# &= n_\mathrm{C}^\# \left(\frac{1-x^\#}{1+x^\#} z_\mathrm{Zr} + \frac{2x^\#}{1+x^\#} z_\mathrm{Y} + m\,\nu^\#\, z_\mathrm{O} \right) , \qquad (2.34c) \end{aligned}$$

respectively.

The evolution of the thermodynamic state is then described by

$$\begin{aligned} -\varepsilon_0(1+\chi)\partial_{zz}\varphi &= n^\mathrm{F} , \qquad (2.35a) \\ m_\mathrm{Om}\frac{(1-\nu^\#)m}{V^\#}\partial_t y + \partial_z \left(\left(1 + m_\mathrm{Om}\tfrac{(1-\nu^\#)m}{m^\#} y\right) J_\mathrm{Om} \right) &= 0 , \qquad (2.35b) \\ \partial_z p + n^\mathrm{F}\partial_z\varphi &= 0 . \qquad (2.35c) \end{aligned}$$

Let us assume M linearly dependent [67] on ρ_Om as $M = D\frac{m_\mathrm{Om}}{k_\mathrm{B}}\rho_\mathrm{Om}$. Eventually, the free charge and the diffusion flux of mobile oxide ions are given as

$$\begin{aligned} n^\mathrm{F} &= e_0 n_\mathrm{C}^\# (z^\# + z_\mathrm{O}(1-\nu^\#)m\ y) , \qquad (2.36a) \\ J_\mathrm{Om} &= -m_\mathrm{Om}\, D\, \tfrac{(1-\nu^\#)m}{V^\#} \left(1 + m_\mathrm{Om}\tfrac{(1-\nu^\#)m}{m^\#}\, y\right) \left(\frac{\partial_z y}{1-y} + y\tfrac{e_0 z_\mathrm{Om}}{k_\mathrm{B}T}\partial_z\varphi \right) , \qquad (2.36b) \end{aligned}$$

where (2.35c) was used in place of the pressure gradient term. The parameter $x^\#$ has usually values in the range of $[0, 0.2]$ and we have $\nu^\# \in [0, \frac{1}{m}\frac{2+x^\#}{1+x^\#}]$. The remaining parameters of the YSZ model are given in Tab. 2.4.1 .

2.3 Bulk metal and gas phase

In order to act as an electrolyte in a SOEC, the YSZ has to be connected to two different materials: a gas phase and some electric conductor. In this paper, we do no consider the internal structure of these parts of the SOEC. Therefore, we assume the gas to be equilibrated such that boundary conditions at the gas-YSZ surface can be determined easily. Although not appropriate for the use in real SOEC, we will treat the conductor as a pure metal, since this way the conductor can be almost completely removed from the model.

temperature	T	$800\,°\mathrm{C}$
dielectric constant	χ	40
Zr cation charge number	z_{Zr}	$+4$
Y cation charge number	z_{Y}	$+3$
oxide ion charge number	$z_{\mathrm{Om}}, z_{\mathrm{Oi}}$	-2
Zr molar mass	M_{Zr}	$91.22\,\mathrm{g\,mol^{-1}}$
Y molar mass	M_{Y}	$88.91\,\mathrm{g\,mol^{-1}}$
O molar mass	M_{O}	$16\,\mathrm{g\,mol^{-1}}$
ratio of C/A lattices	m	2
YSZ molar fraction	$x^{\#}$	0.08
ratio of immobile O^{2-}	$\nu^{\#}$	$[0, \frac{1}{m}\frac{2+x^{\#}}{1+x^{\#}}]$
specific lattice volume of YSZ	$V^{\#}$	$3.35 \times 10^{-29}\,\mathrm{m}^3$
lattice cation number density	$n_{\mathrm{C}}^{\#}$	$(V^{\#})^{-1}$
diffusion coefficient	D	$1 \times 10^{-11}\,\mathrm{m}^2/\mathrm{s}$

Table 2.2.1: Characteristic values. Per-particle masses m_α are used in the calculations.

2.3.1 Bulk gas

The gas in the bulk is assumed to behave as an ideal mixture of ideal gases. We introduce the index set $\mathcal{I}_{\mathrm{gas}}$ of the constituents of the gas phase. For each constituent, the partial pressure is $p_\alpha = c_\alpha RT$. The chemical potential of a gaseous species reads

$$\mu_\alpha(p_\alpha, T) = \mu_\alpha^{ref}(T) + \frac{k_{\mathrm{B}}T}{m_\alpha} \ln\left(\frac{p_\alpha}{p^{ref}}\right) \qquad \text{for } \alpha \in \mathcal{I}_{\mathrm{gas}}, \tag{2.37}$$

where the reference pressure is given by the standard atmospheric pressure $p^{ref} = 100\,\mathrm{kPa}$ and μ_α^{ref} is the chemical potential of the pure substance.

In the bulk domain $\Omega_{\mathrm{gas}} \subset \mathbb{R}^3$, we assume that the diffusion is fast such that the chemical potentials are homogeneous in space, i.e., $\nabla\mu_\alpha = 0$ for $\alpha \in \mathcal{I}_{\mathrm{gas}}$. Since there are no charge carriers in the gas, we assume that the electric potential φ is also homogeneous in the gas phase.

2.3.2 Bulk metal

For the description of the conductor, we apply the Sommerfeld model of metals, cf. [68]. The metal is considered as a mixture of positively charged metal ions M^+ and free electrons e^- with negligible volume and high mobility. Thus, we use the index set $\mathcal{I}_{\mathrm{metal}} = \{\mathrm{M}^+, \mathrm{e}^-\}$ for the constituents. We assume the metal ions to be incompressible and thus the density of metal ions to be homogeneous in the whole metal domain $\Omega_{\mathrm{metal}} \subset \mathbb{R}^3$, cf. [58]. Sufficiently far away from the metal boundary, i.e., outside of double layers, the metal is electroneutral and therefore the bulk number density n_{e^-} of the electrons and the corresponding bulk chemical potential μ_{e^-} are material dependent constants. Neglecting electric resistance, the electric potential φ is homogeneous in the metal bulk. Moreover, we assume quasi-equilibrium in the metal such that in particular the electrochemical potential of

the electrons is constant not only in the bulk but also inside double layers, i.e.,

$$\nabla(m_{\mathrm{e}^-}\mu_{\mathrm{e}^-} - e_0\varphi) = 0 \ . \tag{2.38}$$

2.4 Surface – triple phase boundary

The electrodes in solid oxide cells are combined of YSZ, metal and the gas phase. Thus, an interface model should, in principle, treat three thermodynamically distinct surfaces and one triple phase line present in the electrode. For a start, in this work, we aim at a strongly simplified 1D model of the electrodes. To incorporate the triple phase boundary into such a 1D model, we assume that the only contribution of the metal as an electric conductor is to provide free electrons for the charge transport. We make the following assumptions:

i) The YSZ surface is endowed with a thin layer of metal ions and their corresponding free electrons.

ii) The tangential diffusion of electrons along the surface is assumed to be fast compared to all the other treated kinetic processes.

iii) The metal ions and electrons do not contribute to the internal energy and entropy of the surface.

Due to the first assumption, the electrons are transported only tangentially to the surface. The second assumption implies spatially homogeneous surface electrochemical potentials which only may change in time. The last assumptions allows to approximate the triple phase boundary by a simple surface model, which can be reduced to a 1D model in a straightforward way. A more detailed derivation of this reduction of a triple phase line into a 1D model can be found in the context of intercalation electrodes in [69].

The following derivation of the YSZ surface model is based on the general approach developed in [45, 5].

2.4.1 Surface constituents and basic quantities.

As in the bulk, we describe the YSZ surface as a mixture of different surface constituents and apply for the surface quantities analogous notation with an underset 's' added. In the isothermal case, the surface temperature $\underset{\mathrm{s}}{T}$ is identical to the constant bulk temperature T and appears in the equations only as a parameter. In addition to the constituents from the metal and the bulk phases of the gas and YSZ bulk, surface reaction products may be present on the surface. Thus, the index set of all surface constituents is of the form $\mathcal{I}_S = \mathcal{I}_{\mathrm{YSZ}} \cup \mathcal{I}_{\mathrm{gas}} \cup \mathcal{I}_{\mathrm{metal}} \cup \mathcal{I}_{\mathrm{react}}$, where $\mathcal{I}_{\mathrm{react}}$ is the index set of surface reaction products.

Each surface constituent is characterized by its surface number density $\underset{\mathrm{s}}{n_\alpha}$, atomic mass m_α and electric charge number z_α. The partial mass densities $\underset{\mathrm{s}}{\rho_\alpha}$, the total mass density $\underset{\mathrm{s}}{\rho}$ and the free electric charge density for the surface are defined by

$$\underset{\mathrm{s}}{\rho_\alpha} = m_\alpha \underset{\mathrm{s}}{n_\alpha} \ , \qquad \underset{\mathrm{s}}{\rho} = \sum_{\alpha\in\mathcal{I}_S} \underset{\mathrm{s}}{\rho_\alpha} \ , \qquad \underset{\mathrm{s}}{n^{\mathrm{F}}} = \sum_{\alpha\in\mathcal{I}_S} z_\alpha e_0 \underset{\mathrm{s}}{n_\alpha} \ . \tag{2.39}$$

We assume that proper preparation and cutting of the bulk YSZ crystal results in the formation of a planar face which can be represented by our surface model. Therefore, as in the bulk YSZ case, the surface lattice density of cations is in certain relation to the surface density of anion lattice, i.e., the surface anion density is $\underset{\mathrm{s}}{m}\, \underset{\mathrm{s}}{n}{}^{\#}_{\mathrm{C}}$. The surface cation lattice is assumed to be fully occupied by zirconium and yttrium cations, whereas the anion lattice is partially occupied by mobile and immobile oxide ions.

$$\underset{\mathrm{s}}{n}{}^{\#}_{\mathrm{C}} = \underset{\mathrm{s}}{n}_{\mathrm{Zr}} + \underset{\mathrm{s}}{n}_{\mathrm{Y}} \ , \qquad\qquad \underset{\mathrm{s}}{m}\, \underset{\mathrm{s}}{n}{}^{\#}_{\mathrm{C}} \geq \underset{\mathrm{s}}{n}_{\mathrm{Oi}} + \underset{\mathrm{s}}{n}_{\mathrm{Om}} \ . \tag{2.40}$$

The surface model needs to reflect the structure of the bulk YSZ model. The YSZ surface is defined by the cation crystal lattice. The deformation of the cation lattice therefore prescribes the surface velocity. In order to maintain the compatibility of the bulk model and the surface model, we have

$$\underset{\mathrm{s}}{v} = v^{\#} \ . \tag{2.41}$$

On the YSZ surface gaseous species may adsorb and some reaction products may be formed. The admissible adsorption sites for gaseous species and reaction products in general depend on the lattice sites of the YSZ crystal. We assume that these adsorption sites coincide with the anion surface lattice sites of YSZ. Several chemical reactions may occur. Denoting the constituents by A_α for $\alpha \in \mathcal{I}_S$, the reactions can be written in the form

$$\sum_{\alpha\in\mathcal{I}_S} \mathrm{a}^i_\alpha \mathrm{A}_\alpha \underset{\underset{\mathrm{s}}{\mathrm{R}^{\mathrm{i}}_{\mathrm{b}}}}{\overset{\underset{\mathrm{s}}{\mathrm{R}^{\mathrm{i}}_{\mathrm{f}}}}{\rightleftharpoons}} \sum_{\alpha\in\mathcal{I}_S} \mathrm{b}^i_\alpha \mathrm{A}_\alpha \qquad\qquad \text{for} \qquad i = 1, \ldots, M. \tag{2.42}$$

The constants a^i_α, b^i_α are positive integers and $\gamma^i_\alpha := \mathrm{b}^i_\alpha - \mathrm{a}^i_\alpha$ denote the stoichiometric coefficients of the reactions. Here $R^i_f > 0$ denotes the forward reaction rate and accordingly $R^i_b > 0$ denotes the backward reaction rate. The net reaction rate is defined as $R^i = R^i_f - R^i_b$. Since charge and mass have to be conserved in every single reaction, we have

$$\sum_{\alpha\in\mathcal{I}_S} m_\alpha \gamma^i_\alpha = 0 \qquad \text{and} \qquad \sum_{\alpha\in\mathcal{I}_S} z_\alpha \gamma^i_\alpha = 0 \qquad \text{for} \qquad i = 1, \ldots, M \ . \tag{2.43}$$

2.4.2 Surface free energy

The surface free energy can in general be assumed to be independent of the electric field. Here, we also assume that there is no elastic energy contribution and we distinguish two different entropic contributions to the free energy density. One takes into account the entropy of mixing of the mobile oxide ions on the anion lattice and the other is due to for the mixing of adsorbed gas species and reaction products on the adsorption sites. The metal ions and electrons only contribute to the reference energy. The free energy density for the surface is of the form

$$\underset{\mathrm{s}}{\rho}\underset{\mathrm{s}}{\psi}(\underset{\mathrm{s}}{T}, (\underset{\mathrm{s}}{\rho}_\alpha)_{\alpha\in\mathcal{I}_S}) = \underset{\mathrm{s}}{\rho}\underset{\mathrm{s}}{\psi}^{ref} + \underset{\mathrm{s}}{\rho}\underset{\mathrm{s}}{\psi}^{\text{mix, anions}} + \underset{\mathrm{s}}{\rho}\underset{\mathrm{s}}{\psi}^{\text{mix, adsorbates}} \ . \tag{2.44}$$

The surface entropy and the surface chemical potentials are defined as

$$\left(\frac{\partial \underset{\mathrm{s}}{\rho}\underset{\mathrm{s}}{\psi}}{\partial \underset{\mathrm{s}}{T}}\right) = -\underset{\mathrm{s}}{\rho}\underset{\mathrm{s}}{s} \ , \qquad \left(\frac{\partial \underset{\mathrm{s}}{\rho}\underset{\mathrm{s}}{\psi}}{\partial \underset{\mathrm{s}}{\rho_\alpha}}\right) = \underset{\mathrm{s}}{\mu_\alpha} \qquad \alpha \in \mathcal{I}_S \ . \tag{2.45}$$

In general an elastic energy contribution has to be taken into account. The derivation of the energy is quite similar to the bulk. In [58] an example for a metal-electrolyte interface can be found. It turns out that if the constitutive equation of the surface tension depends only on the immobile YSZ species, and the lattice velocity $v^{\#}$ is equal to the surface velocity, then the remaining equations for the adsorption and surface reaction are independent of the elastic contribution. Therefore, for simplicity, we ignore the surface elasticity.

Surface mixing of oxide ions. On the surface we introduce the coverage of anion lattice sites as

$$\underset{\mathrm{s}}{y} = \frac{\underset{\mathrm{s}}{n_{\mathrm{Om}}}}{\underset{\mathrm{s}}{m}\,\underset{\mathrm{s}}{n_{\mathrm{C}}^{\#}} - \underset{\mathrm{s}}{n_{\mathrm{Oi}}}} \ . \tag{2.46}$$

Then, the free energy contribution due to the mixing entropy of the oxide ions can be derived in analogous way like in the bulk as

$$\underset{\mathrm{s}}{\rho}\underset{\mathrm{s}}{\psi}^{\mathrm{mix,anions}} = k_{\mathrm{B}}\underset{\mathrm{s}}{T}\,(\underset{\mathrm{s}}{m}\,\underset{\mathrm{s}}{n_{\mathrm{C}}^{\#}} - \underset{\mathrm{s}}{n_{\mathrm{Oi}}})\Big(\underset{\mathrm{s}}{y}\ln(\underset{\mathrm{s}}{y}) + (1-\underset{\mathrm{s}}{y})\ln(1-\underset{\mathrm{s}}{y})\Big) \tag{2.47}$$

Surface mixing of gaseous adsorbates and reaction products. Since some of the adsorption sites for gaseous constituents might not be occupied, we can define the number density of vacancies and the surface coverage of the gaseous species as

$$\underset{\mathrm{s}}{n_V} = \underset{\mathrm{s}}{m}\,\underset{\mathrm{s}}{n_{\mathrm{C}}^{\#}} - \sum_{\alpha\in\mathcal{I}_{\mathrm{gas}}\cup\mathcal{I}_{\mathrm{react}}} \underset{\mathrm{s}}{n_\alpha} \ , \tag{2.48}$$

$$\underset{\mathrm{s}}{y_\alpha} = \frac{\underset{\mathrm{s}}{n_\alpha}}{\underset{\mathrm{s}}{m}\,\underset{\mathrm{s}}{n_{\mathrm{C}}^{\#}}} \quad \text{for } \alpha \in \mathcal{I}_{\mathrm{gas}} \cup \mathcal{I}_{\mathrm{react}} \cup \{V\} \ . \tag{2.49}$$

The free energy contribution due to the configuration of adsorbed gaseous species can be derived by Boltzmann's formula where the vacancies are taken into account. We obtain

$$\underset{\mathrm{s}}{\rho}\underset{\mathrm{s}}{\psi}^{\mathrm{mix,adsorbates}} = k_{\mathrm{B}}\underset{\mathrm{s}}{T}\,\underset{\mathrm{s}}{m}\,\underset{\mathrm{s}}{n_{\mathrm{C}}^{\#}} \sum_{\alpha\in\mathcal{I}_{\mathrm{gas}}\cup\mathcal{I}_{\mathrm{react}}\cup\{V\}} \underset{\mathrm{s}}{y_\alpha}\ln\underset{\mathrm{s}}{y_\alpha} \ . \tag{2.50}$$

Reference surface energy. As in the bulk, the reference surface free energy describes a suitable chosen reference state of the surface and is assumed to be

$$\underset{\mathrm{s}}{\rho}\underset{\mathrm{s}}{\psi}^{ref} = \sum_{\alpha\in\mathcal{I}_S} \rho_\alpha \underset{\mathrm{s}}{\mu_\alpha^{ref}} \ . \tag{2.51}$$

μ_α^{ref} denotes the temperature dependent reference chemical potential of each individual constituent.

Surface chemical potentials. The surface chemical potentials are given in terms of the surface number densities according to definition $(2.45)_{\text{right}}$ as

$$\underset{\text{s}}{\mu}_{\text{Om}} = \mu^{ref}_{\text{Om}} + \frac{k_{\text{B}}\underset{\text{s}}{T}}{m_{\text{Om}}} \ln\left(\frac{\underset{\text{s}}{y}}{1-\underset{\text{s}}{y}}\right) , \tag{2.52a}$$

$$\underset{\text{s}}{\mu}_{\text{Oi}} = \mu^{ref}_{\text{Oi}} - \frac{k_{\text{B}}\underset{\text{s}}{T}}{m_{\text{Oi}}} \ln\left(1-\underset{\text{s}}{y}\right) , \tag{2.52b}$$

$$\underset{\text{s}}{\mu}_{\alpha} = \mu^{ref}_{\alpha} + \frac{m k_{\text{B}}\underset{\text{s}}{T}}{m_{\alpha}}\Big(\ln\left(1-\underset{\text{s}}{y}\right) + \ln \underset{\text{s}}{y}_V\Big), \qquad \alpha = \text{Zr}, \text{Y} , \tag{2.52c}$$

$$\underset{\text{s}}{\mu}_{\alpha} = \mu^{ref}_{\alpha} + \frac{k_{\text{B}}\underset{\text{s}}{T}}{m_{\alpha}} \ln\left(\frac{\underset{\text{s}}{y}_{\alpha}}{\underset{\text{s}}{y}_V}\right) , \qquad \alpha \in \mathcal{I}_{\text{gas}} \cup \mathcal{I}_{\text{react}} , \tag{2.52d}$$

$$\underset{\text{s}}{\mu}_{\alpha} = \mu^{ref}_{\alpha} , \qquad \alpha \in \mathcal{I}_{\text{metal}} . \tag{2.52e}$$

2.4.3 Governing equations, constitutive modeling and coupling to the bulk

For the coupling of bulk and surface, we have to introduce the boundary traces of the bulk quantities. For a generic function $u(t,x)$ in the YSZ bulk, we define

$$u|_S^{\text{YSZ}} = \lim_{x \in \Omega_{\text{YSZ}} \to S} u \, . \tag{2.53}$$

In analogous way, traces for functions in the gas bulk domain can be defined. Due to the choice of pairwise disjoint index sets for the bulk domains, most of the quantities are only defined in one of the subdomains. Therefore, we assume the simplification $u|_S = \lim_{x\to S} u$. By convention, we let ν denote the outer normal of the YSZ domain.

In the planar one-dimensional approximation of the general surface mass balance equation, cf. [45, 5], the tangential transport and the curvature related terms vanish. Only the surface chemical reactions (2.42) and mass transport normal to the surface can change the surface densities of the constituents. The surface mass balances and the remaining surface equation for the electric field in the electrostatic approximation read

$$\partial_t \underset{\text{s}}{\rho}_{\alpha} = \sum_{i=1}^{M} \gamma^i_{\alpha} m_{\alpha} R^i + \Big(\Big(J_{\alpha} + \rho_{\alpha}(\upsilon - \underset{\text{s}}{\upsilon}) \Big) \nu \Big) \Big|_S , \quad \alpha \in \mathcal{I}_{\text{YSZ}} . \tag{2.54a}$$

$$\partial_t \underset{\text{s}}{\rho}_{\alpha} = \sum_{i=1}^{M} \gamma^i_{\alpha} m_{\alpha} R^i - \Big(\Big(J_{\alpha} + \rho_{\alpha}(\upsilon - \underset{\text{s}}{\upsilon}) \Big) \nu \Big) \Big|_S , \quad \alpha \in \mathcal{I}_{\text{gas}} . \tag{2.54b}$$

$$\partial_t \underset{\text{s}}{\rho}_{\alpha} = \sum_{i=1}^{M} \gamma^i_{\alpha} m_{\alpha} R^i , \qquad \alpha \in \mathcal{I}_{\text{react}} . \tag{2.54c}$$

$$\varepsilon_0 \Big((1+\chi) \nabla \varphi \, \nu \Big) |_S^{\text{YSZ}} = \underset{\text{s}}{n}^{\text{F}} \, . \tag{2.54d}$$

We assume that $\text{Zr}, \text{Y}, \text{Oi}$ are not involved in any surface reaction. Since $\upsilon_{\alpha} = \upsilon^{\#} = \underset{\text{s}}{\upsilon}$ for $\alpha \in \{\text{Zr}, \text{Y}, \text{Oi}\}$ according to (2.8) and (2.55), the surface mass balance equations (2.54a) imply that the corresponding surface number densities

are constant, i.e.,

$$0 = \rho_\alpha(v^\# - \underset{\mathrm{s}}{v})|_S = \Big(J_\alpha + \rho_\alpha(v - \underset{\mathrm{s}}{v})\Big)\Big|_S = \partial_t \underset{\mathrm{s}}{n}_\alpha \qquad \text{for } \alpha = \mathrm{Zr}, \mathrm{Y}, \mathrm{Oi}\ . \tag{2.55}$$

Maxwell's surface equations in the electrostatic setting imply that the electrostatic potential is continuous at the gas-YSZ interface, see, e.g. [65]. for further details. This allows us to introduce the surface electrostatic potential,

$$\underset{\mathrm{s}}{\varphi} = \varphi|_S^{\mathrm{YSZ}} = \varphi|_S^{\mathrm{gas}}\ . \tag{2.56}$$

2.4.4 Constitutive modeling

To derive constitutive equations for the normal mass fluxes and surface reaction rates, we apply the entropy principle according to [5]. At first, we reduce the entropy production $\underset{\mathrm{s}}{\xi}$ derived in [5, eqn. (6.14)] to the isothermal electrostatic one-dimensional setting [3], viz.,

$$\begin{aligned}
\underset{\mathrm{s}}{\xi} = & \underbrace{-\frac{1}{\underset{\mathrm{s}}{T}} \sum_{k=1}^{M} \Big(\sum_{\beta \in \mathcal{I}_S} \gamma_\beta^k m_\beta \underset{\mathrm{s}}{\mu}_\beta \Big) R^k}_{\underset{\mathrm{s}}{\xi}_{\mathrm{react}}} \\
& \underbrace{+ \sum_{\alpha \in \mathcal{I}_{\mathrm{YSZ}}} \Big(\Big(J_\alpha \nu + \rho_\alpha (v - \underset{\mathrm{s}}{v}) \nu \Big) \Big(\frac{\mu_\alpha}{T} - \frac{\underset{\mathrm{s}}{\mu}_\alpha}{\underset{\mathrm{s}}{T}} \Big) \Big) \Big|_S^{\mathrm{YSZ}}}_{\underset{\mathrm{s}}{\xi}_{\mathrm{YSZ}}} \\
& \underbrace{+ \sum_{\alpha \in \mathcal{I}_{\mathrm{gas}}} \Big(- \Big(J_\alpha \nu + \rho_\alpha (v - \underset{\mathrm{s}}{v}) \nu \Big) \Big(\frac{\mu_\alpha}{T} - \frac{\underset{\mathrm{s}}{\mu}_\alpha}{\underset{\mathrm{s}}{T}} \Big) \Big) \Big|_S^{\mathrm{gas}}}_{\underset{\mathrm{s}}{\xi}_{\mathrm{gas}}} \overset{!}{\geq} 0 \qquad \text{on} \quad S\ .
\end{aligned} \tag{2.57}$$

The entropy production can be split into the three contributions: $\underset{\mathrm{s}}{\xi}_{\mathrm{react}}$, $\underset{\mathrm{s}}{\xi}_{\mathrm{YSZ}}$ and $\underset{\mathrm{s}}{\xi}_{\mathrm{gas}}$, stemming from surface the reactions (2.42), adsorption from the bulk YSZ and adsorption from the gas phase, respectively. In analogous way like in the bulk, the structure of the entropy production (2.57) allows to derive constitutive equations such that the second law of thermodynamics is satisfied, i.e., the entropy production is non-negative.

Adsorption from YSZ bulk. Let us define the adsorption of oxide ions from the bulk to the surface as

$$\mathrm{O}^{2-}(\mathrm{YSZ}) \longrightarrow \mathrm{O}^{2-}(\mathrm{s})\ . \tag{2.58}$$

[3] For the representation of the entropy production, we assumed that the kinetic term $\frac{1}{2}\rho(\underset{\mathrm{s}}{v} - v)^2$ is small and can be ignored.

According to (2.55), $\underset{\mathrm{s}}{\xi}_{\mathrm{YSZ}}$ contains only the term with normal flux of mobile oxide ions, i.e.,

$$\underset{\mathrm{s}}{\xi}_{\mathrm{YSZ}} = \Big(J_{\mathrm{Om}}\nu + \rho_{\mathrm{Om}}(\upsilon - \underset{\mathrm{s}}{\upsilon})\nu\Big)\left(\frac{\mu_{\mathrm{Om}}}{T} - \frac{\underset{\mathrm{s}}{\mu}_{\mathrm{Om}}}{\underset{\mathrm{s}}{T}}\right)\Big|_S^{\mathrm{YSZ}} , \tag{2.59}$$

where the second bracket on the right hand side is equal to affinity of (2.58). By using a linear relation between the differences of chemical potentials and the mass flux, the entropy production $\underset{\mathrm{s}}{\xi}_{\mathrm{YSZ}}$ is guaranteed to be non-negative,

$$(J_{\mathrm{Om}}\nu + \rho_{\mathrm{Om}}(\upsilon - \underset{\mathrm{s}}{\upsilon})\nu)\Big|_S^{\mathrm{YSZ}} = \underset{\mathrm{s}}{D}\left(\frac{\mu_{\mathrm{Om}}}{T} - \frac{\underset{\mathrm{s}}{\mu}_{\mathrm{Om}}}{\underset{\mathrm{s}}{T}}\right)\Big|_S^{\mathrm{YSZ}} \quad \text{with} \quad \underset{\mathrm{s}}{D} \geq 0 \ . \tag{2.60}$$

Adsorption from gas phase. In the bulk gas phase, the fluxes are restricted by the constraint $\sum_{\alpha\in\mathcal{I}_{\mathrm{gas}}} J_\alpha = 0$ and on the surface, (2.41) has to be satisfied. Therefore, we reformulate the entropy production due to the gas adsorption, as

$$\begin{aligned}\underset{\mathrm{s}}{\xi}_{\mathrm{gas}} = &-\rho(\upsilon - \underset{\mathrm{s}}{\upsilon})\nu\Big|_S\left(\frac{\mu_0}{T} - \frac{\underset{\mathrm{s}}{\mu}_0}{\underset{\mathrm{s}}{T}}\right)\Big|_S^{\mathrm{gas}} \\ &+ \sum_{\alpha\in\mathcal{I}_{\mathrm{gas}}\setminus\{0\}} \Big(-\Big(J_\alpha\nu + \rho_\alpha(\upsilon - \underset{\mathrm{s}}{\upsilon})\nu\Big)\Big)\left(\frac{\mu_\alpha - \mu_0}{T} - \frac{\underset{\mathrm{s}}{\mu}_\alpha - \underset{\mathrm{s}}{\mu}_0}{\underset{\mathrm{s}}{T}}\right)\Big|_S^{\mathrm{gas}} ,\end{aligned} \tag{2.61}$$

where an arbitrary species is selected and denoted by the index 0. Linear relations are employed to define the constitutive relations for the mass fluxes of the gas species on S,

$$-\Big(J_\alpha\nu + \rho_\alpha(\upsilon - \underset{\mathrm{s}}{\upsilon})\nu\Big)\Big|_S^{\mathrm{gas}} = \underset{\mathrm{s}}{M}_\alpha\left(\frac{\mu_\alpha - \mu_0}{T} - \frac{\underset{\mathrm{s}}{\mu}_\alpha - \underset{\mathrm{s}}{\mu}_0}{\underset{\mathrm{s}}{T}}\right)\Big|_S^{\mathrm{gas}} \tag{2.62a}$$

$$\text{for } \alpha \in \mathcal{I}_{\mathrm{gas}} \setminus \{0\} ,$$

$$-\rho(\upsilon - \underset{\mathrm{s}}{\upsilon})\nu\Big|_S^{\mathrm{gas}} = \underset{\mathrm{s}}{M}\left(\frac{\mu_0}{T} - \frac{\underset{\mathrm{s}}{\mu}_0}{\underset{\mathrm{s}}{T}}\right)\Big|_S^{\mathrm{gas}} \quad \text{with } \underset{\mathrm{s}}{M}_\alpha, \underset{\mathrm{s}}{M} \geq 0 \ . \tag{2.62b}$$

The phenomenological coefficients $\underset{\mathrm{s}}{M}_\alpha$ and $\underset{\mathrm{s}}{M}$ are positive to guarantee a non-negative entropy production.

Surface reactions. For the surface reactions, we use the nonlinear closure developed in [45]

$$R^i = R_0^i\left[\exp\left(-\frac{\beta^i}{k_{\mathrm{B}}\underset{\mathrm{s}}{T}}\sum_{\alpha\in\mathcal{I}_S}\gamma_\alpha^i m_\alpha \underset{\mathrm{s}}{\mu}_\alpha\right) - \exp\left(\frac{(1-\beta^i)}{k_{\mathrm{B}}\underset{\mathrm{s}}{T}}\sum_{\alpha\in\mathcal{I}_S}\gamma_\alpha^i m_\alpha \underset{\mathrm{s}}{\mu}_\alpha\right)\right] , \tag{2.63}$$

with $R_0^i \geq 0$. The constants $\beta^i \in (0,1)$ are called symmetry factors. In an asymptotic limit of vanishing double layer width the constitutive equation (2.63) allows to derive generalized Butler-Volmer equations for the surface reactions, see [48].

2.4.5 Summary of the surface model

On the surface, we consider a single surface net reaction $(2.69)_{\text{right}}$ with $\beta = 1/2$. From the YSZ phase only the mobile oxide ions and from the conductor only the surface electrons are allowed to participate in this reaction. We assume fast adsorption from the gas phase, i.e., $\mu_\alpha|_S = \underset{\text{s}}{\mu_\alpha}$ for $\alpha \in \mathcal{I}_{\text{gas}}$.

$$\underset{\text{s}}{R} = -2\underset{\text{s}}{R_0}\sinh\left(\frac{1}{2}\left[\frac{\Delta G_R}{k_\text{B}T} + \gamma_{\text{Om}}\ln\left(\frac{\underset{\text{s}}{y}}{1-\underset{\text{s}}{y}}\right) + \sum_{\alpha\in\mathcal{I}_{\text{gas}}}\gamma_\alpha\ln\left(\frac{p_\alpha}{p^{ref}}\right) + \sum_{\alpha\in\mathcal{I}_{\text{react}}}\gamma_\alpha\ln\left(\frac{\underset{\text{s}}{y_\alpha}}{\underset{\text{s}}{y_V}}\right)\right]\right), \quad (2.64a)$$

$$\Delta G_R = \gamma_{\text{Om}}m_{\text{Om}}\underset{\text{s}}{\mu^{ref}_{\text{Om}}} + \gamma_{\text{e}^-}m_{\text{e}^-}\underset{\text{s}}{\mu^{ref}_{\text{e}^-}} + \sum_{\alpha\in\mathcal{I}_{\text{gas}}}\gamma_\alpha m_\alpha\mu^{ref}_\alpha + \sum_{\alpha\in\mathcal{I}_{\text{react}}}\gamma_\alpha m_\alpha\underset{\text{s}}{\mu^{ref}_\alpha} \quad (2.64b)$$

Moreover, we choose

$$\underset{\text{s}}{D} = \underset{\text{s}}{A_0}\frac{m_\text{O}^2}{k_\text{B}}\,, \quad (2.65)$$

so that $[\underset{\text{s}}{A_0}] = 1/\text{m}^2/\text{s}$. Finally, only the following evolution equation is solved for on the surface,

$$m_\text{O}\partial_t\frac{(1-\underset{\text{s}}{\nu^\#})\underset{\text{s}}{m}}{a^\#}\underset{\text{s}}{y} - \underset{\text{s}}{A_0}m_\text{O}\left[-\frac{\Delta G_A}{k_\text{B}T} + \ln\left(\frac{y|_S}{1-y|_S}\frac{1-\underset{\text{s}}{y}}{\underset{\text{s}}{y}}\right)\right] = m_\text{O}\gamma_{\text{Om}}\underset{\text{s}}{R}\,, \quad (2.66)$$

with

$$\Delta G_A = m_{\text{Om}}\underset{\text{s}}{\mu^{ref}_{\text{Om}}} - m_{\text{Om}}\mu^{ref}_{\text{Om}}\big|_S\,. \quad (2.67)$$

reaction kin. coef.	$\underset{\text{s}}{R_0}$	$1\times10^{10}\,/\text{m}^2/\text{s}$
oxide ion adsorption coef.	$\underset{\text{s}}{A_0}$	$1\times10^{17}\,/\text{m}^2/\text{s}$
surface density of cations	$\underset{\text{s}}{a^\#}$	$\sqrt[3]{V^\#} \approx 1.04\times10^{-19}\,\text{m}^2$
surface ratio of imm. ox. ions	$\underset{\text{s}}{\nu^\#}$	0.9
surface anion lattice num.	$\underset{\text{s}}{m}$	[0,4]
gibbs energy of adsorption	ΔG_A	0.2 eV
gibbs energy of reaction	ΔG_R	0.2 eV
partial pressure of O_2	p_{O_2}	21 kPa
standard pressure	p^{ref}	100 kPa

Table 2.4.1: Characteristic values and parameters for the surface part of the model.

2.5 Simulation of a SOC half-cell

We consider an YSZ-air electrode that contains the YSZ and gas bulk domains and the YSZ-gas surface S located at x_S. We chose a point $x_B > x_S$ outside of the double layer, located in the bulk YSZ sufficiently far away from S. Thus, the YSZ can be assumed to be electroneutral and consequently also isobaric in the YSZ bulk including x_B. We assume that the pressure at x_B corresponds to the outer pressure[4] and the filling ratio of the anion lattice sites y at x_B is determined by the crystal lattice, i.e.,

$$y_B = y(t, x_B) = -\frac{z^\#}{z_{\mathrm{Om}}\,(1-\nu^\#)m}\ , \tag{2.68a}$$

$$p(t, x_B) = 100\,\mathrm{kPa}\ . \tag{2.68b}$$

The gas phase consists of nitrogen[5] $\mathrm{N_2}$ and oxygen $\mathrm{O_2}$ and values for the spatially homogeneous chemical potentials $\mu_{\mathrm{N_2}}$ and $\mu_{\mathrm{O_2}}$ are prescribed.

On the YSZ surface, two reaction take place: dissociation of oxygen molecules and electron transfer to form oxide anions, viz.,

$$\mathrm{O_2} \rightleftharpoons 2\,\mathrm{O} \qquad \text{and} \qquad \mathrm{O} + 2\,\mathrm{e^-} \rightleftharpoons \mathrm{O^{2-}}\ . \tag{2.69}$$

The adsorption of gaseous species is assumed to be considerably faster than the reaction and diffusion processes. Hence, the phenomenological coefficients in equations (2.62) for gaseous adsorbates are large, implying that the surface chemical potential and bulk chemical potential of the gas species are equal. Moreover, we assume fast dissociation, i.e., the reaction rate for the dissociation reaction (2.69) is large, and we obtain from (2.63)

$$\text{fast adsorption:} \qquad \mu_{\mathrm{N_2}}|_S = \underset{\mathrm{s}}{\mu_{\mathrm{N_2}}}\ , \qquad \mu_{\mathrm{O_2}}|_S = \underset{\mathrm{s}}{\mu_{\mathrm{O_2}}}\ , \tag{2.70a}$$

$$\text{fast dissociation of } \mathrm{O_2}: \qquad 2m_{\mathrm{O}}\underset{\mathrm{s}}{\mu_{\mathrm{O}}} = m_{\mathrm{O_2}}\underset{\mathrm{s}}{\mu_{\mathrm{O_2}}}\ . \tag{2.70b}$$

Cell potential. The thin metal layer on the YSZ surface is assumed to be connected to a metal current collector, e.g., a wire. Therefore, there is an electric contact at the YSZ surface to an external circuit. Let $\mu_{\mathrm{e^-}}^{\mathrm{ext}}$ and φ_{ext} denote the (spatially homogeneous) chemical and the electrostatic potential in the current collector bulk, respectively. Assuming, that the electrochemical potential of the electrons is continuous at the surface, we can determine the contact potential $U_0^{ref} = \varphi_{\mathrm{ext}} - \underset{\mathrm{s}}{\varphi}$ as

$$U_0^{ref} = \tfrac{k_{\mathrm{B}}T}{e_0} m_{\mathrm{e^-}} \left(\mu_{\mathrm{e^-}}^{\mathrm{ext}} - \underset{\mathrm{s}}{\mu_{\mathrm{e^-}}}\right)\ . \tag{2.71}$$

Due to the incompressibility of the metal bulk and the constitutive equation (2.52e) on the surface, the contact potential is a material dependent constant, i.e., $\partial_t U_0^{ref} = 0$.

[4] In general, the total stress has to specified, but due to electroneutrality assumption at x_B and the one dimensional approximation, the total stress and material pressure p coincide.

[5] We chose nitrogen as the reference species for the gas phase, i.e., $A_0 = \mathrm{N_2}$.

In principle, we are capable to measure the electrostatic potential φ_B at x_B, e.g., with a suitable reference electrode. We define the half cell potential U of the solid oxide half-cell as

$$U = \varphi_{\text{ext}} - \varphi_B = U_0^{ref} + \underset{\text{s}}{\varphi} - \varphi_B \ . \tag{2.72}$$

Thus, boundary condition for the electrostatic potential in the YSZ domain is given by the half cell potential U, and a normalization condition for φ_B, e.g., $\varphi_B = 0$.

Electric current. We are interested in the electric current I flowing through the electric wire contacted to the SOC electrode. The global mass balance equations allows us to relate the electric current I, flowing through the wire, to the quantities of the SOC electrode model as follows,

$$\frac{I}{A} = -\frac{\mathrm{d}}{\mathrm{d}t}\Big(e_0 z_{\text{Om}} \underset{\text{s}}{n}_{\text{Om}}\Big) + \frac{\mathrm{d}}{\mathrm{d}t}\Big((1+\chi)\varepsilon_0 \nabla\varphi\nu\Big)\Big|_S^{\text{YSZ}} - z_{\text{e}^-} e_0 \sum_{i=1}^{M} \gamma_{\text{e}^-}^i R^i \ , \tag{2.73}$$

where A is the area of the cross section of the gas-YSZ interface. The derivation of formula (2.73) is summarized in section 2.A.

2.5.1 Double layer capacitance of blocking electrode

First, we want to investigate the equilibrium properties of the model derived above and therefore assume that no electron transfer reaction take place on the surface. This situation can be met if the contact of gas phase and YSZ is prevented by e.g., continuous metal layer. When an applied voltage is sustained so that the system is allowed to relax to an equilibrium state, and mobile oxide ions adsorb or desorb between the bulk and the surface and a charged layer in the bulk of YSZ is formed. We introduce the boundary layer charge Q_{BL} and the surface charge Q_{S} of the gas-YSZ interface as

$$Q_{\text{BL}} = -\int_{x_S}^{x_B} n^{\text{F}} \, \mathrm{d}z \tag{2.74}$$

$$Q_{\text{S}} = -z_{\text{Om}} e_0 \underset{\text{s}}{n}_{\text{Om}} \ . \tag{2.75}$$

In equilibrium both the surface charge and the boundary layer charge are function of the applied half cell potential U, or – equally well – of the voltage $U - U_0^{ref} = \underset{\text{s}}{\varphi} - \varphi_B$, cf. [58]. This allows us to define the corresponding surface, boundary layer and double layer capacitance as

$$C_{\text{S}} = \frac{\mathrm{d}}{\mathrm{d}(U - U_0^{ref})} Q_{\text{S}} \ , \quad C_{\text{BL}} = \frac{\mathrm{d}}{\mathrm{d}(U - U_0^{ref})} Q_{\text{BL}} \ , \quad C_{\text{DL}} = C_{\text{S}} + C_{\text{BL}} \ , \tag{2.76}$$

respectively. Due to the 1D approximation, we are able to derive explicit representations of the bulk and surface capacitance as functions of the potential difference $U - U_0^{ref}$. The homogeneity of the electrochemical potential in equilibrium, i.e.,

$$\mu_{\text{Om}} + z_{\text{Om}} \tfrac{e_0}{m_{\text{Om}}} \varphi = \mu_{\text{Om}}(x_B) + z_{\text{Om}} \tfrac{e_0}{m_{\text{Om}}} \varphi(x_B) \ , \tag{2.77}$$

allows to express the filling ratio and the free charge dependence on $\varphi - \varphi_B$ as

$$n^{\mathrm{F}}(\varphi - \varphi_B) = e_0 n_{\mathrm{C}}^{\#}(z^{\#} + z_{\mathrm{Om}}(1-\nu^{\#})m\ y(\varphi - \varphi_B)) \tag{2.78}$$

$$y(\varphi - \varphi_B) = \frac{X(\varphi - \varphi_B)}{1 + X(\varphi - \varphi_B)} \text{with } X(\varphi - \varphi_B) = \frac{y_B}{1 - y_B} \exp\left(-\tfrac{z_{\mathrm{Om}} e_0}{k_{\mathrm{B}} T}(\varphi - \varphi_B)\right). \tag{2.79}$$

Then multiplication of the Poisson equation (2.24a) with $\partial_x \varphi$ and integration yields, assuming vanishing $\partial_x \varphi$ in the bulk,

$$\begin{aligned}\partial_x \varphi = &- \operatorname{sign}(\varphi - \varphi_B)\sqrt{\frac{2 e_0 n_{\mathrm{C}}^{\#}}{(1+\chi)\varepsilon_0}} \\ &\times \sqrt{\frac{k_{\mathrm{B}} T}{e_0}(1-\nu^{\#})m \ln\Big((1-y_B)(1+X(\varphi-\varphi_B))\Big) - (\varphi - \varphi_B) z^{\#}} \\ &=: F(\varphi - \varphi_B)\ . \end{aligned} \tag{2.80}$$

Clearly, the derivative of the potential is a monotonous function, thus, we can express the boundary layer charge and capacitance as

$$Q_{\mathrm{BL}} = \int_0^{\varphi_S - \varphi_B} \frac{n^{\mathrm{F}}(\widetilde{\varphi})}{F(\widetilde{\varphi})}\, d\widetilde{\varphi}\ , \qquad C_{\mathrm{BL}} = \frac{n^{\mathrm{F}}(\varphi_S - \varphi_B)}{F(\varphi_S - \varphi_B)}\ . \tag{2.81}$$

The impact of the mobility ratio $\nu^{\#}$ and of dielectric constant χ on the bulk layer capacitance is shown in Fig. 2.5.1. To screen a positive surface potential, a negatively charged layer in the YSZ has to be formed by occupying available anion lattice sites. Clearly, this number of available anion lattice sites is independent of the mobility ratio $\nu^{\#}$ and thus, the charge layer profile and the double layer capacitance C_{BL} have to be independent of $\nu^{\#}$ for positive applied potentials. To the contrary, when the surface potential is more negative than the bulk, a small $\nu^{\#}$, i.e., a large portion of the oxide anions is mobile, allows to vacate many anion lattice sides near the surface, leading to effective screening of the surface potential by a high negative charge density in the boundary layer and resulting in high capacity. The growth of the double layer capacitance for increasing χ, can be attributed to a spreading of the boundary layer due to the greater amount of the polarized charge. We fix $\chi = 27$ and $\nu^{\#} = \underset{\mathrm{s}}{\nu^{\#}} = 0.9$ for all the following numerical simulations if not stated otherwise. On the surface, we have

$$\underset{\mathrm{s}}{y}(\underset{\mathrm{s}}{\varphi} - \varphi_B) = \frac{\underset{\mathrm{s}}{Y}(\underset{\mathrm{s}}{\varphi} - \varphi_B)}{1 + \underset{\mathrm{s}}{Y}(\underset{\mathrm{s}}{\varphi} - \varphi_B)} \tag{2.82}$$

$$\text{with } \underset{\mathrm{s}}{Y}(\underset{\mathrm{s}}{\varphi} - \varphi_B) = \frac{y_B}{1 - y_B} \exp\left(-\frac{\Delta G_A}{k_{\mathrm{B}} T} - \tfrac{z_{\mathrm{Om}} e_0}{k_{\mathrm{B}} T}(\underset{\mathrm{s}}{\varphi} - \varphi_B)\right)\ . \tag{2.83}$$

Thus, we can express the surface charge and capacitance as

$$Q_{\mathrm{S}} = -z_{\mathrm{Om}} e_0 \Big((1 - \underset{\mathrm{s}}{\nu^{\#}}) \underset{\mathrm{s}}{m}\, \underset{\mathrm{s}}{n_{\mathrm{C}}^{\#}}\Big) \underset{\mathrm{s}}{y}\ , \tag{2.84a}$$

$$C_{\mathrm{S}} = \frac{z_{\mathrm{Om}}^2 e_0^2}{k_{\mathrm{B}} T}(1 - \underset{\mathrm{s}}{\nu^{\#}}) \underset{\mathrm{s}}{m}\, \underset{\mathrm{s}}{n_{\mathrm{C}}^{\#}}\ \frac{\underset{\mathrm{s}}{Y}(\underset{\mathrm{s}}{\varphi} - \varphi_B)}{\Big(1 + \underset{\mathrm{s}}{Y}(\underset{\mathrm{s}}{\varphi} - \varphi_B)\Big)^2}\ , \tag{2.84b}$$

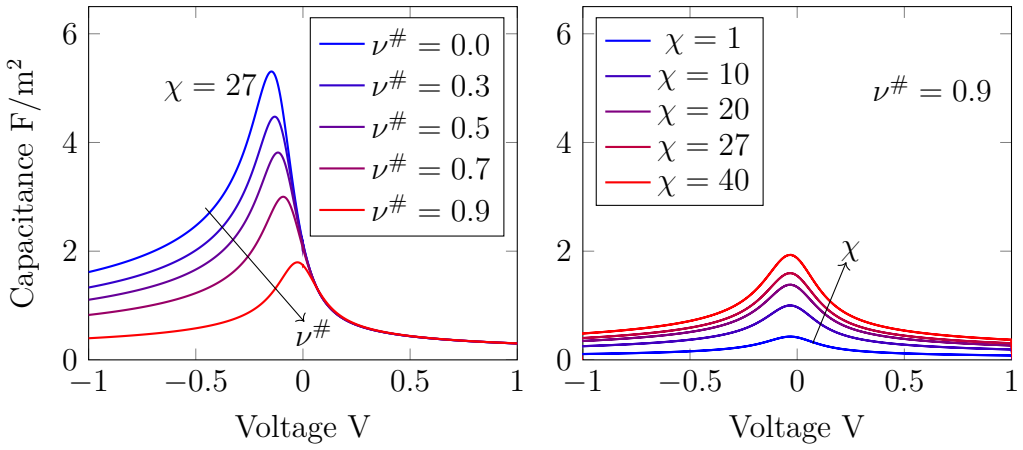

Figure 2.5.1: Dependence of the double layer capacitance C_{DL} as a function of the applied half cell potential U on the mobility ratio $\nu^{\#}$ (left) and on the dielectric constant χ (right).

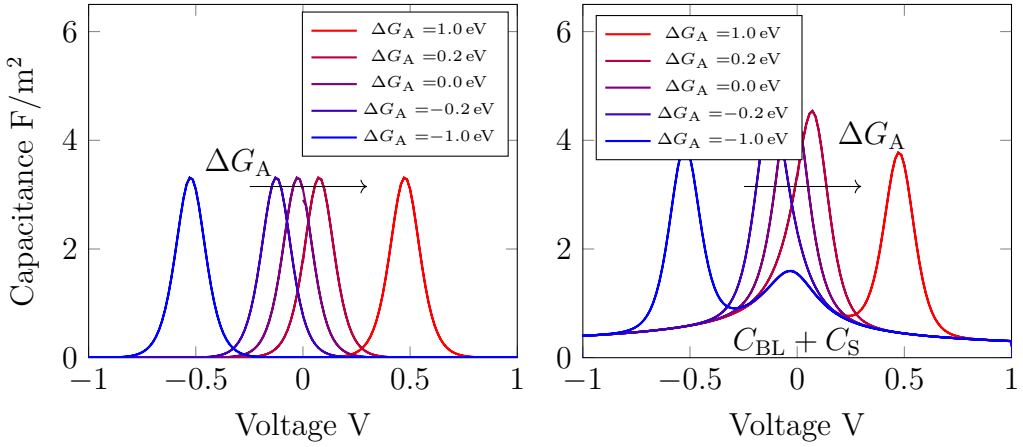

Figure 2.5.2: Left: surface capacitance C_{S} for different values of ΔG_{A}. Right: the combined double layer capacitance C_{DL} Remaining parameters are $\chi = 27$, $\nu^{\#} = \underset{\mathrm{s}}{\nu^{\#}} = 0.9$.

Fig. 2.5.2 shows the influence of ΔG_{A} on the double layer capacitance of a blocking electrode. Negatively charged oxide ions tend to move into higher electric potential. If the adsorption energy, $\Delta G_{\mathrm{A}} = m_{\mathrm{Om}}\underset{\mathrm{s}}{\mu}{}^{ref}_{\mathrm{Om}} - m_{\mathrm{Om}}\mu^{ref}_{\mathrm{Om}}$, is positive, then energy is required to for oxide ion to pass from the bulk to the surface. Stronger negative values of ΔG_{A} foster the adsorption of oxide anions to the surface and thereby shift the surface capacitance maximum to more negative potentials. This can be seen most clearly in Fig. $2.5.2_{\mathrm{left}}$ where only the surface contribution is shown. Comparison of the Fig. 2.5.1 and Fig. 2.5.2 suggests that the bulk contribution remains undisturbed. The maxima of surface capacitance in $2.5.2_{\mathrm{left}}$ are due to the saturation of the surface for growing potential difference. The position of the maxima occurs for

$$(\underset{\mathrm{s}}{\varphi}{}^{\max} - \varphi_B) = \frac{\Delta G_{\mathrm{A}}}{2e_0} - \frac{k_{\mathrm{B}}T}{2e_0}\ln\left(\frac{y_B}{1-y_B}\right) . \tag{2.85}$$

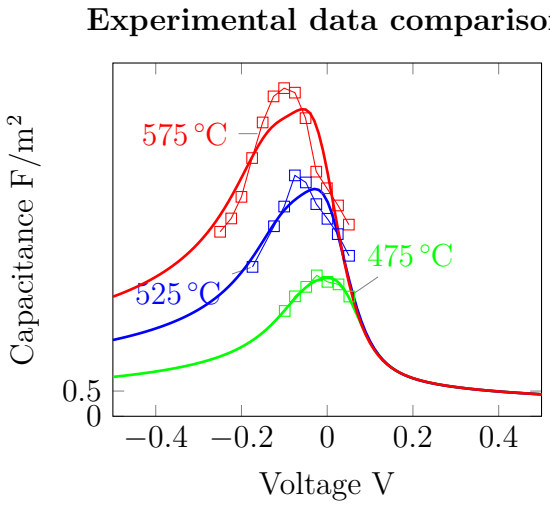

Figure 2.5.3: Blocking electrode capacitance, marked plots: experimental 8 % mol polycrystalline YSZ [70], solid: fit of the blocking electrode model.

Comparison to experiment Fig. 2.5.3 compares simulations with fitted data to experimentally measured capacitance curves for different temperatures [70]. We do not attempt to systematically adjust the model parameters to the data due to the polycrystalline nature of the YSZ studied in the experiment, instead, we try to illustrate the possible temperature dependence and the effect of the fitted parameters. As the temperature dependencies would need additional modeling efforts, as a first step, for this thesis, we performed the fit separately for each temperature.

It is difficult to assert that a particular oxide ion is mobile or immobile in the microscopic picture. It is suitable to consider the parameters $\nu^{\#}$ and $\underset{\mathrm{s}}{\nu}^{\#}$ determining certain (dynamic) equilibrium between the admissible and occupied vacancies in state with vanishing macroscopic free charge density. As this is usually an effect of thermal excitations, the values of $\nu^{\#}$ and $\underset{\mathrm{s}}{\nu}^{\#}$ should depend on temperature. Also ΔG_{A} presumably depends on the temperature.

To this end also $\underset{\mathrm{s}}{m}$ was treated as a fitting parameter shared for the three cases.

temperature	T	475 °C	525 °C	575 °C
Gibbs adsorption energy	ΔG_{A}	0.14 eV	0.16 eV	0.18 eV
bulk immobiles ratio	$\nu^{\#}$	0.85	0.57	0.07
surf. immobiles ratio	$\underset{\mathrm{s}}{\nu}^{\#}$	0.85	0.64	0.44
surf. lattice ratio	$\underset{\mathrm{s}}{m}$	0.26	0.26	0.26

Table 2.5.1: Fitted parameters, see Fig. 2.5.3

2.5.2 Capacitive currents

In the case of time dependent applied voltages, the current representation (2.73) simplifies in the absence of reactions to the case of no electron transfer:

$$\frac{I}{A} = -\frac{\mathrm{d}}{\mathrm{d}t}\left(z_{\mathrm{Om}} e_0 n_{\mathrm{s}}^{\mathrm{Om}}\right) + \frac{\mathrm{d}}{\mathrm{d}t}\left((1+\chi)\varepsilon_0 \nabla\varphi\nu\right)\Big|_S^{\mathrm{YSZ}} = \frac{\mathrm{d}}{\mathrm{d}t} Q_{\mathrm{S}} + \frac{\mathrm{d}}{\mathrm{d}t} Q_{\mathrm{BL}} \ . \tag{2.86}$$

Thus, the current is composed of two contributions describing the change of the surface charge and the boundary layer charge, respectively. However, unlike in the equilibrium case, Q_{S} and Q_{BL} are not uniquely determined by the applied voltage. Consider a small time depending perturbation around the half cell equilibrium potential $\bar{U}$, i.e., the applied voltage is $U(t) = \bar{U} + \Delta U(t)$. For a time scale of the perturbation considerably slower than the diffusion and adsorption, the system can be assumed to behave quasi-static and the current I can be linearised at $\bar{U}$ such that

$$I \approx C_{\mathrm{DL}}(\bar{U}) \frac{d\Delta U}{dt} \ . \tag{2.87}$$

Thus, the double layer capacitance can be measured at low frequencies using impedance spectroscopy, or with cyclic voltammetry (CV) at low sweep rate. Here, sweep rate refers to the slope of voltage change during one linear cycle.

Kinetic coefficients The blocking electrode model contains two kinetic parameters: diffusion coefficient D and adsorption rate A_{s}^{0}. If one of those parameters is small w.r.t. sweep rate, a limitation of the total current occurs. To this end the sweep rate is fixed to $1\,\mathrm{mV\,s^{-1}}$ in this paragraph. Small values of adsorption coefficient limit charging and discharging of the surface oxide ions as it is shown in Fig. 2.5.4. The current due to charging of the bulk double layer is not affected by this.

Similarly, small values of D lead to limitation of the rate of charging the bulk double as documented in Fig. 2.5.5. In this case, the charging of the surface is affected, because the bulk diffusion limits the supply of the oxide ions.

Length of domain and sweep rate Faster sweep rates affect the current response of the blocking electrode similarly as small values of the kinetic coefficients. Fast-changing voltage unveils limited rates of oxide ion transportation that can be attributed to concrete mechanisms. Figures 2.5.6 illustrate this for the oxide ion adsorption. Fig. $2.5.6_{\mathrm{right}}$ in particular shows that the rate of the surface charging is limited due to the adsorption. For even greater sweep rates, the decreasing rates of current to the bulk diffusion limitation are displayed in Figure $2.5.7_{\mathrm{left}}$.

The bulk diffusion limitation depends also on the domain length, see Figure $2.5.7_{\mathrm{right}}$.

2.5.3 Currents of full half cell

Let us now investigate a scenario where on the surface the electrochemical reaction 2.69_{right} proceeds. In the constitutive relation for the reaction rate according

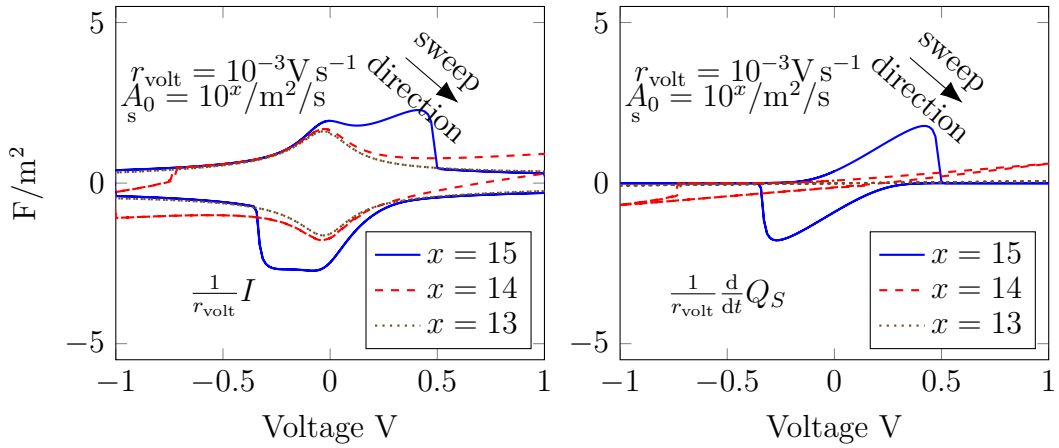

Figure 2.5.4: Voltammetry of blocking electrode varying adsorption coefficient A_0. The current is scaled by the respective rate of voltage change. Left: total current. Right: surface contribution to the current. The additional parameters are: $\Delta G_{\text{A}} = 0.2\,\text{eV}$, $D = 1 \times 10^{-11}\,\text{m}^2/\text{s}$.

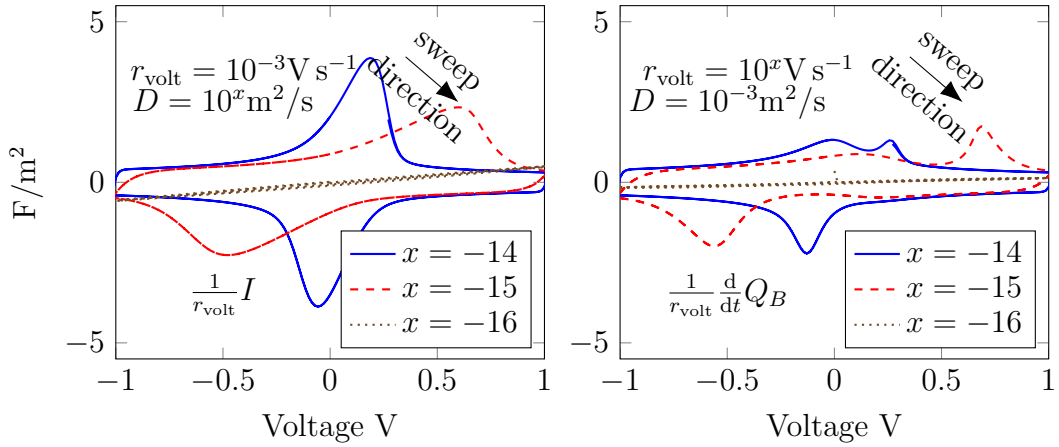

Figure 2.5.5: Voltammetry of blocking electrode varying bulk diffusion coefficient D. The current is scaled by the respective rate of voltage change. Left: total current. Right: bulk contribution to the current. The additional parameters are: $\Delta G_{\text{A}} = 0.2\,\text{eV}$, $A_0 = 1 \times 10^{17}\,/\text{m}^2/\text{s}$.

to (2.63), we choose the symmetry factor $\beta = \frac{1}{2}$, yielding

$$R = -2R_0 \sinh\left(\frac{1}{2k_{\text{B}}T}(m_{\text{Om}}\mu_{\text{Om}} - 2m_{\text{e}^-}\mu_{\text{e}^-} - \frac{1}{2}m_{\text{O}_2}\mu_{\text{O}_2})\right) \tag{2.88}$$

With the chemical potential (2.52) and $\Delta G_R = m_{\text{Om}}\mu^{ref}_{\text{Om}} - 2m_{\text{e}^-}\mu^{ref}_{\text{e}^-} - \frac{1}{2}m_{\text{O}_2}\mu^{ref}_{\text{O}_2}$ we get

$$R = -2R_0 \sinh\left(\frac{1}{2k_{\text{B}}T}\left(\Delta G_R + \ln\frac{y}{1-y} - \frac{1}{2}\ln\frac{p_{\text{O}_2}}{p^{ref}}\right)\right)\,, \tag{2.89}$$

Cyclic voltammetry with realistic sweep rate $r_{\text{volt}} = 1\,\text{mV}\,\text{s}^{-1}$ is fixed in further demonstration of the basic features of the investigated system with the reaction.

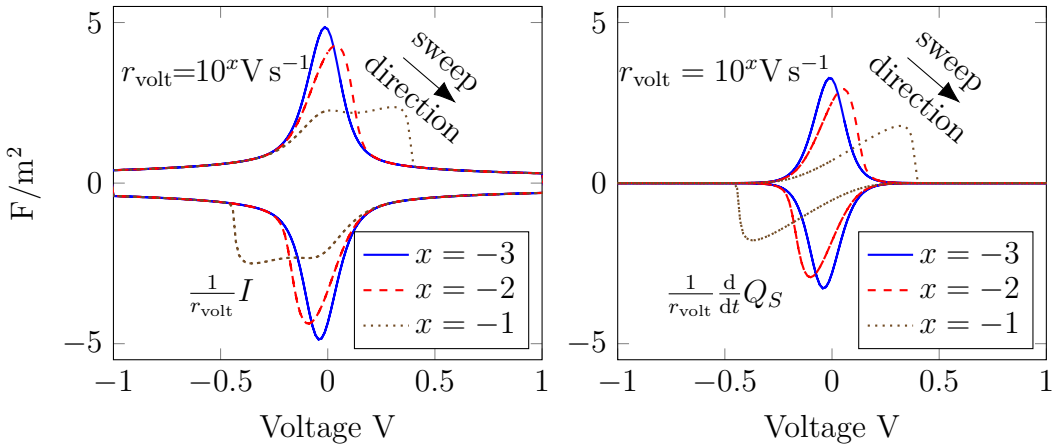

Figure 2.5.6: Voltammetry of blocking electrode varying sweep rates. The current is scaled by the respective rate of voltage change. Left: increasing sweep rates distinguish the charging of surface and bulk double layers. Right: the surface charging contribution to the current. The additional parameters are: $\Delta G_{\text{A}} = 0.2\,\text{eV}$, $D = 1 \times 10^{-11}\,\text{m}^2/\text{s}$, $A_{0\atop \text{s}} = 1 \times 10^{17}\,/\text{m}^2/\text{s}$.

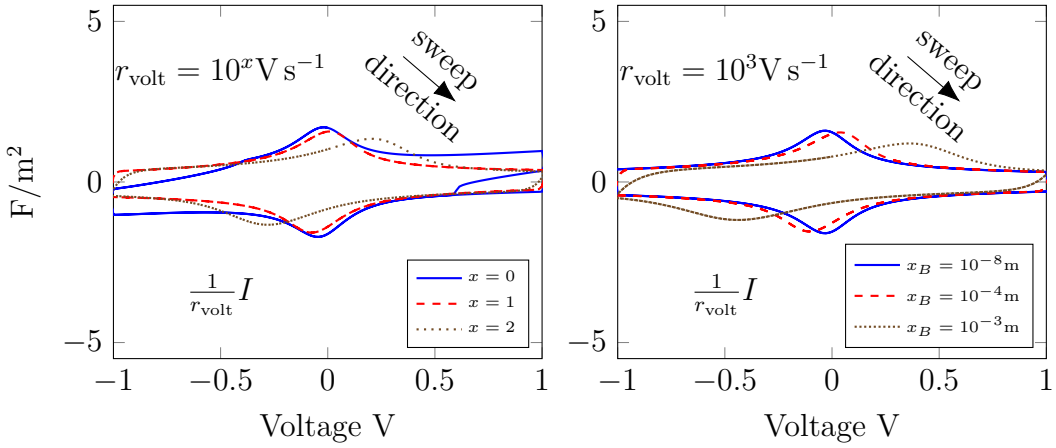

Figure 2.5.7: Linear-sweep voltammetry of blocking electrode. Left: increasing sweep rates for thick electrolyte $x_B = 5 \times 10^{-3}\,\text{m}$. Right: Fixed fast sweep rate, varying electrolyte thickness.

Free energy parameters

Gibbs energy of reaction ΔG_R is treated as an additional free energy parameter entering the model with the surface chemical reaction. The different ΔG_R values, see Fig. $2.5.8_{\text{left}}$, do not alter the charging of the double layer but lead to the shift of the onset of the reaction current. Gibbs energy of adsorption ΔG_{A}, see Fig. $2.5.8_{\text{right}}$, shifts, consistently with the blocking electrode case, cf. Fig. 2.5.2, charging of bulk a surface layer. The shift of the reaction onset occurs because ΔG_{A} shifts the chemical potential of the surface oxide ions, cf. (2.88). The reaction current is for either non-zero ΔG_{A} or ΔG_R in the depicted range much greater then the bulk and surface contributions.

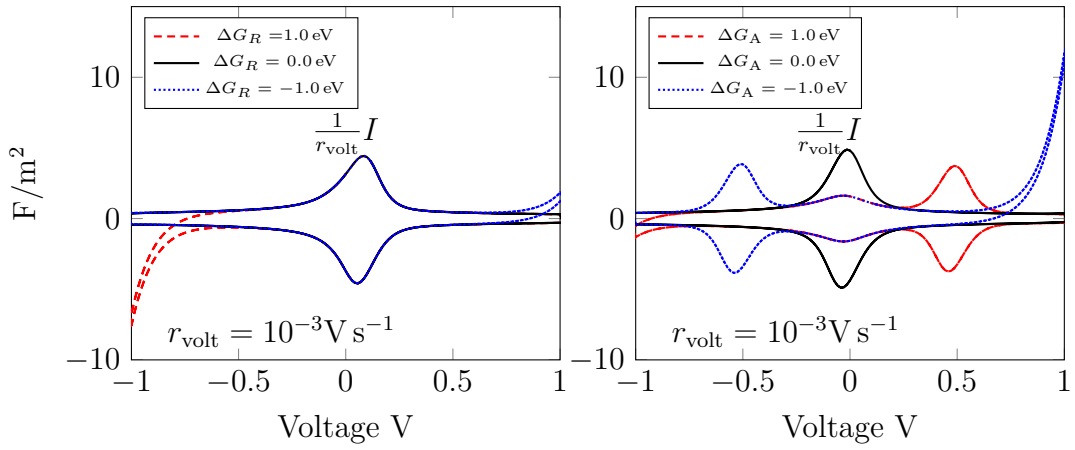

Figure 2.5.8: Linear-sweep voltammetry different values of ΔG_R (left) and ΔG_A (right). With reaction rate $R_0^{\text{s}} = 1 \times 10^8\,/\text{m}^2/\text{s}$ and adsorption rate $A_0^{\text{s}} = 1 \times 10^{17}\,/\text{m}^2/\text{s}$.

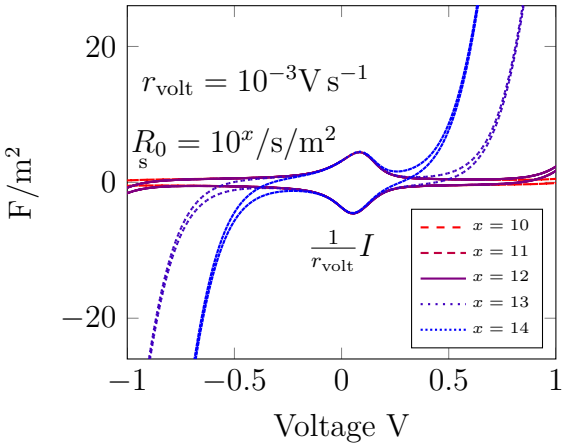

Figure 2.5.9: Linear-sweep voltammetry for different values of reaction coefficient R_0. For $\Delta G_R = 0.2\,\text{eV}$, $\Delta G_\text{A} = 0.2\,\text{eV}$ and $A_0^{\text{s}} = 1 \times 10^{17}\,/\text{m}^2/\text{s}$.

Reaction rate

According to (2.73) surface reaction rate R_0^{s} changes the relative magnitude of the reaction current, hence it also changes the relative onset of the reaction current w.r.t bulk and surface contributions as it shown in Fig. 2.5.9. The limiting case of a small R_0^{s} is the blocking electrode. The effects of D and A_0^{s} are for the open system similar as for the blocking electrode case. Small values would lead to surface charging and consequently to bulk charging limitations thus hindering the reaction.

2.6 Discussion

The representation of the interface was chosen as uncomplicated as possible so that the behavior of oxide ions double layer dynamics remains unobscured. This was achieved, however, let us discuss the drawbacks of the treatment. First, in a real electrode two distinguished surfaces (YSZ, metal) are present and the

electron-transfer reaction occurs near their intersection. Hence, tangential diffusion of the surface species comes into play together with the particular geometrical realization. To this end a two or three dimensional model would be required including the in-plane transport of the species. A question that naturally follows is: where exactly does the electron-transfer reaction occur, at the contact line or on one of the surfaces? Second, behavior of the metal electrons may in the close vicinity of the contact line start to display quantum effects that may result in richer behavior of the electron-transfer reaction. Third, the adsorption of gaseous species may under some circumstances limit the supply of gaseous species to the surface. Fourth, the appearing surface species depend on the particular electrode material. In particular, the nature and amount of the surface species will be different for Pt, Au or LSM electrodes. Also and additional phase of surface oxide ions with different adsorption energy might also be present. Finally, one might also consider production of surface oxygen $\mathrm{O(s)}$ for the blocking electrode (although no desorption to the gas phase is possible) and investigate the mechanical strain to the interfaces due to this.

2.7 Summary and Conclusions

A generalized Poisson-Nernst-Planck system describing YSZ|gas|metal-interface has been derived from first principles of nonequilibrium thermodynamics and numerically solved for simulating double layer capacitance and cyclic voltammetry measurements.

The core of the gPNP system is due to carefully derived free energy densities for the bulk YSZ and the YSZ|metal|gas surface capturing the main features of the YSZ crystalline nature. It is assumed that the described species, except for mobile oxide ions, are bound to the crystalline lattice. These assumptions result, using the entropy principle, in a novel form of the mobile oxide ion flux, which is a certain combination of the electrochemical potentials of all species. The charged layer in the metal is assumed to be in a diffusional equilibrium, since no transport limitations of the electrons is assumed. Finally, the formula for the electric current measured in the apparatus is derived.

A numerical model for the system has been derived and implemented in one spatial dimension using the finite volume method, specifically a variant of the Scharfetter-Gummel scheme, in the Julia programming language [71].

Although the model is strictly developed as isothermal, most of its parameters may depend on the temperature. Therefore, the parametric study is also aimed to demonstrate the scenarios where some of the parameters become limiting to the charge transfer of the system. Finally, the capacitance of blocking YSZ electrode taken from literature [70] is fitted with the model, the quality of the fit relies heavily on the newly introduced ratios of immobile oxide ions $\nu^{\#}$ and $\underset{\mathrm{s}}{\nu^{\#}}$. For each temperature these can be fitted alongside with $\Delta \mathrm{G_A}$ to the measured data. While the derivation of the model assumed a single crystal, the measurements had been obtained for polycrystalline YSZ. Therefore, the presented fitting results can be seen only as a first step towards a model for polycrystalline YSZ which ideally should be derived from the presented model using homogenization techniques. Moreover, the presented model can serve as a starting point for further extensions

containing more sophisticated surface chemistry capable of describing the anodic and cathodic within one kinetic model.

Appendix

The quantities used troughout the section are listed below. The undersetted letter s denotes surface quantities, which were omitted.

Quantity	Symbol	SI units
electric field	$\boldsymbol{E}$	$\mathrm{V\,m^{-1}}$
electric potential	φ	V
polarization density	$\boldsymbol{P}$	$\mathrm{C/m^2}$
partial mass density	ρ_α	$\mathrm{kg/m^3}$
total mass density	ρ	$\mathrm{kg/m^3}$
number density	n_α	$1\,/\mathrm{m^3}$
free charge density	n^F	$\mathrm{C/m^3}$
polar. charge density	n^P	$\mathrm{C/m^3}$
barycentric velocity	$\boldsymbol{v}$	$\mathrm{m\,s^{-1}}$
partial velocity	$\boldsymbol{v}_\alpha$	$\mathrm{m\,s^{-1}}$
partial mass flux	$\boldsymbol{J}_\alpha$	$\mathrm{kg/m^2/s}$
partial velocity	$\boldsymbol{v}_\alpha$	$\mathrm{m\,s^{-1}}$
free energy dens.	$\rho\psi$	$\mathrm{J/m^3}$
entropy dens.	ρs	$\mathrm{J/m^3/K}$
chemical potential	μ_α	$\mathrm{J\,kg^{-1}}$
pressure	p	Pa
temperature	T	K

2.A Electric current

Let I be the electric current flowing through an electric wire to the gas-YSZ surface, which can be measured by an amperemeter. The current is related to the temporal change of the surface electron density and electron production on the gas-YSZ surface. For spatially homogeneous fields on a gas-YSZ surface with the area A, we have

$$\frac{I}{A} = z_{\mathrm{e}^-} e_0 \Big(\frac{\mathrm{d}}{\mathrm{d}t} n_{\mathrm{s}}^{\mathrm{e}^-} - \sum_{k=1}^{M} \gamma_{\mathrm{e}^-}^k R_{\mathrm{s}}^k \Big) \,. \tag{2.90}$$

The derivation based on surface and bulk balance equations, see [5], the metal model proposed in [58] and that the atomic mass of electrons are much smaller than the atomic mass of metal atoms, i.e. $m_{\mathrm{e}^-}/m_M \approx 0$.

To express the electron number density $n_{\mathrm{s}}^{\mathrm{e}^-}$ in (2.90) we use the identity

$$\frac{\mathrm{d}}{\mathrm{d}t} n_{\mathrm{s}}^{\mathrm{F}} = \frac{\mathrm{d}}{\mathrm{d}t} \left(e_0 z_{\mathrm{e}^-} n_{\mathrm{s}}^{\mathrm{e}^-} + e_0 z_{\mathrm{Om}} n_{\mathrm{s}}^{\mathrm{Om}} \right) \,, \tag{2.91}$$

which follows from equation (2.55) and that the surface number density of metal ions is constant. Then, with

$$n_{\mathrm{s}}^{\mathrm{F}} = \left((1+\chi) \varepsilon_0 \nabla\varphi\nu \right) \Big|_S^{\mathrm{YSZ}} \,, \tag{2.92}$$

Introducing (2.91),(2.92) into (2.90) yields the identity (2.73).

2.B Summary of the model

For easy reference, we summarize the model equations which have been implemented.

$$-\varepsilon_0(1+\chi)\partial_{zz}\varphi = n^{\mathrm{F}} \ , \tag{2.93a}$$

$$m_{\mathrm{Om}}\partial_t \frac{(1-\nu^{\#})m}{V^{\#}} y + \partial_z \left(\left(1 + m_{\mathrm{Om}} \frac{(1-\nu^{\#})m}{m^{\#}} y \right) \boldsymbol{J}_{\mathrm{Om}} \right) = 0 \tag{2.93b}$$

with

$$\begin{aligned} \boldsymbol{J}_{\mathrm{Om}} = &- D\ m_{\mathrm{Om}} \frac{(1-\nu^{\#})m}{V^{\#}} \left(1 + m_{\mathrm{Om}} \frac{(1-\nu^{\#})m}{m^{\#}} y \right) \\ &\times \left[\frac{\partial_z y}{(1-y)} + y \frac{z_{\mathrm{Om}} e_0}{k_{\mathrm{B}}T} \partial_z \varphi \right], \end{aligned} \tag{2.93c}$$

$$n^{\mathrm{F}} = \frac{e_0}{V^{\#}} \left(z_{\mathrm{Om}} (1-\nu^{\#}) m\ y + z^{\#} \right) \tag{2.93d}$$

for bulk with the choice of mobility coefficient

$$M = D \frac{m_{\mathrm{Om}}}{k_{\mathrm{B}}} \rho_{\mathrm{Om}} = D\, m_{\mathrm{Om}}^2 \frac{(1-\nu^{\#})m}{V^{\#}\ k_{\mathrm{B}}} y, \tag{2.94}$$

where $[D] = \mathrm{m}^2\mathrm{s}^{-1}$ is a diffusion coefficient.

On the surface, we have with $\beta = 1/2$ The electrochemical reaction is supposed to be

$$\frac{1}{2}\mathrm{O}_2 + 2\mathrm{e}^- \rightleftharpoons \mathrm{O}^{2-} \tag{2.95}$$

and we define

$$\Delta G_{\mathrm{A}} = m_{\mathrm{Om}} \underset{\mathrm{s}}{\mu}{}^{ref}_{\mathrm{Om}} - m_{\mathrm{Om}} \mu^{ref}_{\mathrm{Om}} \Big|_S \ , \tag{2.96a}$$

$$\Delta G_{\mathrm{R}} = m_{\mathrm{Om}} \underset{\mathrm{s}}{\mu}{}^{ref}_{\mathrm{Om}} - m_{\mathrm{O}_2} \frac{\mu^{ref}_{\mathrm{O}_2}}{2} - 2 m_{\mathrm{e}^-} \mu^{ref}_{\mathrm{e}^-} \ . \tag{2.96b}$$

This leads to the surface equations in the form

$$m_{\mathrm{Om}} \partial_t \frac{(1-\underset{\mathrm{s}}{\nu}{}^{\#})\underset{\mathrm{s}}{m}}{a^{\#}} \underset{\mathrm{s}}{y} = m_{\mathrm{Om}} \underset{\mathrm{s}}{A}_0 \left(-\frac{\Delta G_{\mathrm{A}}}{k_{\mathrm{B}}T} + \ln \frac{y|_S\ (1-\underset{\mathrm{s}}{y})}{(1-y|_S)\ \underset{\mathrm{s}}{y}} \right) + m_{\mathrm{Om}} \underset{\mathrm{s}}{R}, \tag{2.97a}$$

with

$$\begin{aligned} \underset{\mathrm{s}}{R} = \underset{\mathrm{s}}{R}_0 \Bigg[&\exp\left(-\beta \frac{\Delta G_{\mathrm{R}}}{k_{\mathrm{B}}T} \right) \left(\frac{\underset{\mathrm{s}}{y}}{1-\underset{\mathrm{s}}{y}} \right)^{-\beta} \left(\frac{p_{\mathrm{O}_2}}{p^{ref}} \right)^{\frac{\beta}{2}} \\ &- \exp\left((1-\beta) \frac{\Delta G_{\mathrm{R}}}{k_{\mathrm{B}}T} \right) \left(\frac{\underset{\mathrm{s}}{y}}{1-\underset{\mathrm{s}}{y}} \right)^{(1-\beta)} \left(\frac{p_{\mathrm{O}_2}}{p^{ref}} \right)^{-\frac{(1-\beta)}{2}} \Bigg], \end{aligned} \tag{2.97b}$$

$$= -2R_0 \sinh\left(\frac{1}{2} \frac{\Delta G_{\mathrm{R}}}{k_{\mathrm{B}}T} + \frac{1}{2} \ln\left(\frac{\underset{\mathrm{s}}{y}}{1-\underset{\mathrm{s}}{y}} \right) - \frac{1}{4} \ln\left(\frac{p_{\mathrm{O}_2}}{p^{ref}} \right) \right) \Bigg] \tag{2.97c}$$

with the choice of adsorption coefficient

$$\underset{\mathrm{s}}{D} = \underset{\mathrm{s}}{A_0} \frac{m_{\mathrm{Om}}^2}{k_{\mathrm{B}}}, \tag{2.98}$$

where $[\underset{\mathrm{s}}{A_0}] = \mathrm{m}^{-2}\mathrm{s}^{-1}$ denotes the rate of adsorption.

The two systems are coupled by the adsorption boundary condition

$$\boldsymbol{j}_{\mathrm{Om}}\nu|_S = \left(1 + m_{\mathrm{Om}} \frac{(1-\nu^{\#})m}{m^{\#}} y\right) \boldsymbol{J}_{\mathrm{Om}}\nu|_S \tag{2.99}$$

$$= \underset{\mathrm{s}}{A_0} m_{\mathrm{Om}} \left(-\frac{\Delta G_{\mathrm{A}}}{k_{\mathrm{B}}T} + \ln \frac{y|_S \ (1-\underset{\mathrm{s}}{y})}{(1-y|_S) \ \underset{\mathrm{s}}{y}} \right), \tag{2.100}$$

where ν denotes an outer normal of YSZ domain at S.

If not stated otherwise, the simulation parameters used are given in table 2.B.1.

2.C The finite volume method

In order to perform the spatial discretization, we introduce collocation points $x_1 = x_S, x_2, \ldots, x_{n-1}, \ x_n = x_B$ in the simulation domain $\Omega = (x_S, x_B)$. The density of these points ins increased in a geometric fashion towards the electrode surface at x_S. Around the collocation points, we define the control volumes $\omega_1 = [x_1, \frac{x_2+x_1}{2}]$ $\omega_i = [\frac{x_i+x_{i-1}}{2}, \frac{x_i+x_{i+1}}{2}]$ $(i = 2 \ldots n-1)$, $\omega_n = [\frac{x_n+x_{n-1}}{2}, x_n]$.

The finite volume discretization method used to perform the numerical simulation is based on the classical Scharfetter-Gummel scheme from semiconductor device simulation [72] which assumes constant species fluxes between neighboring control volumes, The fluxes are expressed via the unknowns in the corresponding collocation points based on an analytical solution of the flux equation. This approach automatically introduces an upwind stabilization of the discretization scheme which is necessary to handle the possibly steep electric potential gradients in the polarization boundary layer.

In order to handle the non-idealities occurring in generalized PNP models, the scheme needs to be adapted in a thermodynamically consistent manner. For an introductory discussion of the general ideas in the context of semiconductors, see [73], In the context of electrolyte simulation, a reformulation based on species activities as primary variables can be a starting point for a corresponding modification [74].

Here, we use an approach which starts from the reformulation of the species flux based on the introduction of a drift potential $g(y, \varphi)$ combined of the excess chemical potential describing the non-ideality and the electrostatic potential, an idea which goes back at least to [75],

$$\boldsymbol{j}_{\mathrm{Om}} = -\widetilde{D} \ \partial_x y + y \ \partial_x g(y, \varphi). \tag{2.101a}$$

On $[x_k, x_l]$, we set $\bar{y}_{kl} = \frac{1}{2}(y_k + y_l)$ and

$$\boldsymbol{j}_{\mathrm{Om}} = \left(1 + m_{\mathrm{Om}} \frac{(1-\nu^{\#})m}{m^{\#}} \bar{y}_{kl}\right) \boldsymbol{J}_{\mathrm{Om}} = -\widetilde{D} \ \partial_x y + y \ \underbrace{\widetilde{D} \partial_x f(y, \varphi)}_{\partial_x g(y,\varphi)}, \tag{2.102a}$$

temperature	T	$800\,°\mathrm{C}$
dielectric constant	χ	27
Zr cation charge number	z_{Zr}	$+4$
Y cation charge number	z_{Y}	$+3$
oxide ion charge number	$z_{\mathrm{Om}}, z_{\mathrm{Oi}}$	-2
Zr molar mass	M_{Zr}	$91.22\,\mathrm{g\,mol^{-1}}$
Zr atomic mass	m_{Zr}	$15.15 \times 10^{-26}\,\mathrm{kg}$
Y molar mass	M_{Y}	$88.91\,\mathrm{g\,mol^{-1}}$
Y atomic mass	m_{Y}	$14.76 \times 10^{-26}\,\mathrm{kg}$
O molar mass	M_{Om}	$16\,\mathrm{g\,mol^{-1}}$
Om atomic mass	$m_{\mathrm{Om}}, m_{\mathrm{Oi}}$	$2.66 \times 10^{-26}\,\mathrm{kg}$
ratio of C/A lattices	m	2
YSZ molar fraction	$x^{\#}$	0.08
ratio of immobiles	$\nu^{\#}$	$[0, \frac{1}{m}\frac{2+x^{\#}}{1+x^{\#}}]$
specific lattice volume of YSZ	$V^{\#}$	$3.35 \times 10^{-29}\,\mathrm{m^3}$
lattice cation number density	$n_{\mathrm{C}}^{\#}$	$(V^{\#})^{-1}$
reaction kin. coef.	$\underset{\mathrm{s}}{R_0}$	$1 \times 10^{10}\,/\mathrm{m^2/s}$
oxide ion adsorption coef.	$\underset{\mathrm{s}}{A_0}$	$1 \times 10^{17}\,/\mathrm{m^2/s}$
surface density of cations	$\underset{\mathrm{s}}{a^{\#}}$	$\sqrt[3]{V^{\#}} \approx 1.04 \times 10^{-19}\,\mathrm{m^2}$
surface ratio of imm. ox. ions	$\underset{\mathrm{s}}{\nu^{\#}}$	0.9
surface ratio of C/A latt.	$\underset{\mathrm{s}}{m}$	[0,4]
gibbs energy of adsorption	ΔG_{A}	$0.2\,\mathrm{eV}$
gibbs energy of reaction	ΔG_{R}	$0.2\,\mathrm{eV}$
partial pressure of O_2	$p_{\mathrm{O_2}}$	$21\,\mathrm{kPa}$
standard pressure	p^{ref}	$100\,\mathrm{kPa}$

Table 2.B.1: Summary of parameters for the bulk-surface model.

where

$$\widetilde{D} = D\; m_{\mathrm{Om}} \frac{(1-\nu^{\#})m}{V^{\#}} \left(1 + m_{\mathrm{Om}} \frac{(1-\nu^{\#})m}{m^{\#}} \bar{y}_{kl}\right), \tag{2.103a}$$

$$\begin{aligned} \partial_x f = &\left(1 + m_{\mathrm{Om}} \frac{(1-\nu^{\#})m}{m^{\#}}\right) \partial_x \left(\ln(1-y)\right) \\ &- z_{\mathrm{Om}} \frac{e_0}{k_{\mathrm{B}}T} \left(1 + m_{\mathrm{Om}} \frac{(1-\nu^{\#})m}{m^{\#}} \bar{y}_{kl}\right) \partial_x \varphi. \end{aligned} \tag{2.103b}$$

The numerical flux between neighboring control volumes ω_k and ω_l is then computed as

$$\begin{aligned} \boldsymbol{j}_{\mathrm{Om},kl}^{\mathrm{NUM}} = \frac{\widetilde{D}}{|x_k - x_l|} \Bigg[&y_k B \left(-\frac{g(y_k,\varphi_k) - g(y_l,\varphi_l)}{\widetilde{D}}\right) - \\ &y_l B \left(\frac{g(y_k,\varphi_k) - g(y_l,\varphi_l)}{\widetilde{D}}\right) \Bigg], \end{aligned} \tag{2.104a}$$

where $y_k, y_l, \varphi_k, \varphi_l$ are values in computational nodes and $B(x) := \frac{x}{\exp(x)-1}$ is Bernoulli function. Under the assumption of $\boldsymbol{j}_{\mathrm{Om}}$ and $\partial_x g(y,\varphi) = g'$ being constant, as in [72], the direct calculation of the numerical flux can be done using the integration factor $\exp(-\frac{g'}{\approx D})$ and integrating over $[x_k, x_l]$.

3. Thermodynamic optimization of solid oxide cells

3.1 Introduction

In 1889 Gouy published paper [76], where he showed how to calculate useful power of a device by thermodynamic means. The calculation was based on two assumptions: (i) The environment surrounding the device is isothermal (ambient temperature) and (ii) the mechanical power should be maximized. Similar result was obtained by Stodola in [77]. Over more than a century of development was comprehensively reviewed in [78], where also the method of entropy production minimization (EPM) was elucidated. An advantage of thermodynamic optimization based on EPM is that one can plot a continuous map of losses (given by entropy production within EPM) revealing how much efficiency is lost at each place of the device, see e.g. [79].

To obtain the continuous map of losses, which is often proportional to entropy production density, one has to solve the continuum non-equilibrium thermodynamic equations governing the system under consideration. Usually the system is in a steady-state (not evolving in time), and classical irreversible thermodynamics (CIT), developed in [80, 17], in the form presented by Bedeaux and Kjelstrup, [81, 82], provides a systematic approach for developing thermodynamic descriptions of the systems.

An alternative to continuum non-equilibrium thermodynamics is the endoreversible thermodynamics [83, 84, 85] or finite-time thermodynamics [86, 87], where some parts of the system are studied in detail (as in the continuum approach) while some are described only on the macroscopic level of equilibrium thermodynamics as in the theory behind the Gouy-Stodola theorem. Such approach is advantageous in engineering applications because it reduces the amount of detail required in the full continuum calculations.

However, before trying to plot a map of losses, it is necessary to define what the losses mean in terms of the state variables chosen for description of the system, e.g. fields of concentrations, temperature and electric potential. Such task inevitably leads to the choice of an objective function that is to be maximized and constraints that are to be kept constant during the maximization. Regarding the Gouy-Stodola theorem, it might seem natural to identify the losses with entropy production, but it has been shown for example in [88, 89, 1] that it is not so quite often. Firstly, one can choose a different objective function than electric power, in which case entropy production clearly does not need to describe the losses. Secondly, which is more important, even if one chooses useful work as the function that should be maximized, entropy production is often inadequate measure of losses for example when boundary of the system is not isothermal.

Indeed, it was shown in [89] and [1] that when considering a non-isothermal fuel cell in steady state, entropy production is inadequate to address the map of losses of electric power, since electric power is given by the flux of Gibbs energy into the fuel cell diminished by a functional different from entropy production. In other words, consider a steady state non-isothermal fuel cell with some flux

Gibbs energy into the fuel cell. What is the maximum electric power one can produce? The maximum work coincides with minimum of a functional that is definitely different from entropy production.

So, maximum work at steady state does not necessarily correspond to minimum entropy production, which is zero entropy production by the second law of thermodynamics. Consider now the difference in exergy of the fuel and exhausts coming into and out of the fuel cell. This loss of exergy is often used as a measure of losses in the device, see for example review article [6], [90] for diffuser optimization, [91] for humidification-dehumidification system optimization, [92] for methane decomposition optimization, [93] for combustion optimization, or [94] for thermal storage optimization. But exergy destruction is proportional to entropy production as shown in [6], and since entropy production is often inadequate to measure losses in the device, analysis of exergy must be also often inapplicable, if power maximization is the optimization goal.

One could argue that exergy represents the maximum work one can obtain from the device when the device relaxes to equilibrium with its surroundings. This is of course true as shown for example in [95], §20. But is it always the goal of exergy analysis to find how much work the device could deliver when relaxing to equilibrium, for example when shutting down a power plant?

In summary, before one decides to measure efficiency of a device or a component of the device by evaluating exergy destruction, one should either declare that the goal is to find the maximum power the device can deliver when relaxing to thermodynamic equilibrium, which means also shutting down the device, or one should verify that zero entropy production corresponds to the most efficient steady state of the device. The former is relatively simple, but restrictive, since the device often works in a steady state. The latter needs a clear definition of efficiency (or an objective function, e.g. electrical power) and constraints, and usually relies on using continuum non-equilibrium thermodynamics.

Let us illustrate the latter approach on a fuel cell in a steady state, as in [1]. The objective function is the electrical power. The constraints contain flux of Gibbs energy into the fuel cell. It follows from non-equilibrium thermodynamics that if boundary of the fuel cell is isothermal, maximization of power is equivalent to minimization of entropy production inside the fuel cell. If the boundary is not isothermal, the equivalence is lost, and one should minimize a different functional than entropy production, which means that exergy destruction (which is proportional to entropy production) is inadequate to measure efficiency of the fuel cell.

It is the purpose of this paper to shed more light on such pitfalls one can meet when performing thermodynamic optimization. A one-dimensional steady state fuel cell is considered and described within non-quilibrium thermodynamics in the form of [81]. The model is chosen so that it can be solved analytically. The objective function is the electrical power and several examples of constraints are then considered. It is demonstrated that entropy production minimization does not coincide with power maximization. Finally, several examples are identified where exergy analysis and entropy production minimization are appropriate tools of power maximization. We hope that readers will be discouraged from blind using of exergy analysis.

3.2 Global balance laws

Consider a one-dimensional thermodynamic system, for example a fuel cell, in nonequilibrium steady-state. Although the total energy of the system is constant in time (steady state), there is non-zero flux of energy through boundary of the system, as well as non-zero fluxes of particular species (fuel, exhausts, and electrons). These transport processes are accompanied by transport of entropy. There is no source of total energy in the system, which means that energy fluxes through the boundary have to sum up to zero. On the other hand, entropy is being produced inside the fuel cell, which means that fluxes through the boundary sum up to the total entropy production inside the fuel cell.

Boundary of the system is characterized by two points, 0 and L. Difference of any quantity between the two points will be denoted by $\Delta(\bullet) = \bullet^L - \bullet^0$. It is assumed that electrochemical reactions take place at the boundary, i.e. within the two points, and so the two points themselves are also equipped with balance equations.

3.2.1 Total energy balance

Balance of total energy of the system reads

$$\frac{\partial}{\partial t} E_{\text{total}} = 0 = \Delta j_{\text{q}} + \sum_{\text{neutral}} \Delta(j_\alpha h_\alpha) + \Delta\Big(j_{\text{e}}(h_{\text{e}} + F\varphi_{\text{e}})\Big). \tag{3.1}$$

Subscript α denotes association to species α, in particular subscript e is reserved to denote electrons. Symbols j_α and h_α stand for molar flux of species α and partial molar enthalpy of the species, respectively. Symbol φ_{e} stands for energy of electrons due to electrostatic field φ, i.e., $\varphi_{\text{e}} = -\varphi$, and symbol j_{q} denotes heat flux.

From the practical point of view we cannot distinguish between chemical potential of charged species, μ_α, and the electrostatic potential energy of the species, $z_\alpha F\varphi$. Therefore, we prefer working with electrochemical potential, $\tilde{\mu}_\alpha = \mu_\alpha + z_\alpha F\varphi$, and define electric potential of charged species α as

$$z_\alpha F\phi_\alpha := \mu_\alpha + z_\alpha F\varphi, \tag{3.2}$$

which was proposed for example in [81], where the electrostatic potential, φ, is referred to as Maxwell potential. In particular, electric potential is defined as the electric potential of electrons,

$$-F\phi_{\text{e}} = \mu_{\text{e}} - F\varphi. \tag{3.3}$$

This is indeed the quantity measured by a voltmeter, since voltmeter in fact measures the tiny current passing through it, which deflects the arrow of the voltmeter by electromagnetic induction, and the current is proportional to difference in electrochemical potential of the electrons across the voltmeter. See [96] for more discussion.

Electrical work produced by the system can be expressed as the energy flux due to electrons passing boundary of the system,

$$\dot{W}_{\text{el}} = \Delta(i_{\text{e}}\phi_{\text{e}}), \tag{3.4}$$

where i_e is electric current density due flux of electrons. Similarly, i_α is electric current density due to a charged species α. Using the relation between enthalpy, chemical potential and entropy

$$h_\alpha = \mu_\alpha + T s_\alpha, \tag{3.5}$$

we obtain from (3.1) that

$$\dot{W}_\mathrm{el} = -\Delta(\underbrace{j_\mathrm{q} + T j_\mathrm{e} s_\mathrm{e}}_{j'_\mathrm{q}}) - \sum_\mathrm{neutral} \Delta(j_\alpha h_\alpha). \tag{3.6}$$

which is an another form of total energy balance (3.1). Note the usage of measurable heat flux j'_q, introduced in [81]. The measurable heat flux helps to keep the energy balance free of the electron entropy flux, which we cannot measure experimentally anyway. Equation (3.6) contains the usual meaning of balance of energy, that electrical work is equal to heat and enthalpy flux into the system.

3.2.2 Entropy balance

As in the case of total energy, entropy cannot accumulate inside the system due to steadiness of the state. Unlike energy, entropy is produced inside the considered system due to nonequilibrium nature of the state.

Flux of entropy and entropy production can be expressed as

$$j_\mathrm{s} = \frac{j'_\mathrm{q}}{T} + \sum_\mathrm{neutral} j_\alpha s_\alpha, \tag{3.7a}$$

$$\sigma_\mathrm{s} = j'_\mathrm{q} \cdot \frac{\partial}{\partial x}\frac{1}{T} - \frac{1}{T}\sum_\mathrm{charged} i_\alpha \cdot \frac{\partial \phi_\alpha}{\partial x} - \frac{1}{T}\sum_\mathrm{neutral} j_\alpha \cdot \left(\frac{\partial \mu_\alpha}{\partial x}\right)_T + \frac{1}{T}\sum_r \widetilde{A}_r \dot{\xi}_r. \tag{3.7b}$$

Gradient of chemical potential at constant temperature,

$$\left(\frac{\partial \mu_\alpha}{\partial x}\right)_T = \frac{\partial \mu_\alpha}{\partial x} - \underbrace{\frac{\partial \mu_\alpha}{\partial T}}_{=-s_\alpha}\frac{\partial}{\partial x}T, \tag{3.8}$$

serves as a driving force for uncharged species. We considered that electrochemical reactions are taking place among the species. Electrochemical affinity of reaction r is defined as

$$\widetilde{A}_r = -\sum_\alpha \nu_\alpha^r \tilde{\mu}_\alpha \tag{3.9}$$

where ν_α^r is the stoichiometric coefficient of species α in reaction r. Rate of the reaction (in $\mathrm{mol/m^3/s}$) is denoted by $\dot{\xi}_r$. See [1] or [81] for derivation of these formulas.

Finally, flux of entropy out of the system is equal to the total entropy production inside the system, which means that

$$\Delta\left(\frac{j'_\mathrm{q}}{T} + \sum_\mathrm{neutral} j_\alpha s_\alpha\right) = \int \sigma_\mathrm{s} \mathrm{d}x \overset{\mathrm{def}}{=} \Pi. \tag{3.10}$$

Total entropy production inside the system is denoted by Π. Note that the electron entropy flux is integrated into the measurable heat flux. Second law of thermodynamics asserts general positiveness of entropy production, which implies that

$$\Pi \geq 0. \tag{3.11}$$

3.2.3 Efficiency of a device producing electricity

Consider a device producing electrical work by converting heat or chemical energy into electric energy, e.g., a hydrogen fuel cell. Plugging $j_{\mathrm{q}}^{\prime 0}$ from the entropy balance (3.10) into energy balance (3.6) yields

$$\dot{W}_{\mathrm{el}} = -j_{\mathrm{q}}^{\prime L}\left(1 - \frac{T^0}{T^L}\right) + \sum_{\text{neutral}} \Delta\left(j_\alpha(T^0 s_\alpha - h_\alpha)\right) - T^0\Pi. \tag{3.12}$$

This last equation connects electric power and entropy production. There is only one term on the right hand side which is always non-positive, $-T^0\Pi$. Let us assume that the objective function we wish to maximize is the electrical work. Then it seems natural to design the device so that the entropy production is minimal while keeping the resources, the first two terms on the right hand side of Eq. (3.12), constant, which leads to the method of Entropy Production Minimization (EPM), reviewed in [6]. The resources are equal to exergy flux into the device and the non-positive term is negative of the exergy destruction. It is clearly true that when keeping exergy flux constant, the useful work is maximal when exergy destruction (or entropy production) is minimal.

Consider non-isothermal boundary of the system. Exergy flux into the system then contains heat fluxes through all parts of the boundary except for the part with temperature T_0, temperature reservoir T_0. This temperature reservoir is often referred to as the surroundings. What if we do not wish to keep all those heat fluxes constant when performing the maximization? That is often the case for example in fuel cells, where efficiency is expressed as the ratio of electrical work and flux of Gibbs energy into the system. No heat fluxes appear in the definition of efficiency, and thus one could seek for maximum work when fixing only flux of Gibbs energy into the fuel cell.

Such choice of optimization constraints has the important implication that, since exergy flux is no longer constant, entropy production is no longer the functional that should be minimized. See [1] for quantitative results. This idea is further explored in the rest of this paper.

3.2.4 Physical model, constraints and optimization

Let us assume that we have chosen a physical model of the device. Hence, we have a collection of governing parameters of the model uniquely determining the state of the device. Such governing parameters are for example boundary conditions, material parameters or geometrical features. If we assign a value to each parameter, the values of all terms from Equation (3.12) are accessible, in principle, by means of computation. Hence the electric power, entropy production and all energy fluxes through the boundary are determined by the governing parameters through the chosen physical model.

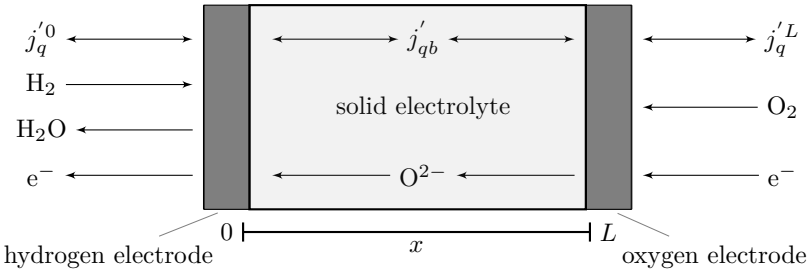

Figure 3.3.1: Scheme of the one-dimensional solid oxide fuel cell model. The cell consists of 3 parts - the HOR surface at $x = 0$, the electrolyte inbetween $(0, L)$, and the ORR surface at $x = L$. The surfaces are considered as points in the one-dimensional model, they are assumed infinitely thin. Quantities in the electrolyte are often denoted by subscript b as bulk. Current density is constant thorough the cell and is denoted by j. Temperature is considered continuous in $[0, L]$.

Fixing the boundary energy flux value is easy when the energy flux is considered as one of the governing parameters. Otherwise, the boundary energy flux value depends on the governing parameters and is determined by the chosen model. In such case fixing the flux value generally means that not all values of the governing parameters are suitable. Respecting such constraint requires to distinguish some parameters as dependent and adjust their value in order to satisfy the constraint. These parameters, values of which are being changed during the optimization, are referred to as optimization parameters while the fixed parameters will be called governing.

Optimization means adjusting an optimization parameter in such a way that a cost or profit functional is minimized or maximized, respectively. Let us restrict us to case of maximizing the electric power. The electric power is, in principle, unbounded, so that we need to assume a constraint on energy resources flowing through the boundary. Assumption of constrained power sources is in this case inevitable, which means that at least one optimization parameter is needed.

3.3 Simple solid oxide fuel cell model

A concrete example of fuel cell optimization is shown in this section, and validity of EPM hypothesis is examined. The model is chosen and simplified so that it is analytically tractable. The purpose of the model is not to describe a real device, but to elucidate the relations between optimization and EPM. A variety of optimization constraints is tried out in order to expose the limits of EPM.

3.3.1 Solid oxide fuel cell

Considered a solid oxide fuel cell composed of three parts as it is illustrated in figure 3.3.1. The ionic conductive solid is enclosed by two reaction surfaces, where oxygen reduction and hydrogen oxidation, respectively, take place. The fuel cell model works as follows. Oxygen molecules on the right reaction surface enter the reaction while decomposing and accepting electrons. Then, the ions formed on the reaction surface are transported through the solid. Finally, the ions are

stripped of the electrons and form water vapor in reaction with hydrogen on the left reaction surface. The electrochemical reactions read

$$\frac{1}{2}\mathrm{O_2} + 2\,\mathrm{e^-} \longrightarrow \mathrm{O^{2-}} \qquad \text{at} \quad x = L, \tag{3.13}$$

$$\mathrm{H_2} + \mathrm{O^{2-}} \longrightarrow \mathrm{H_2O} + 2\mathrm{e^-} \qquad \text{at} \quad x = 0, \tag{3.14}$$

Electrons produced in hydrogen oxidation reaction (HOR) flow through an outer circuit, where load – for example a resistor – is connected, to the surface where oxygen reduction reaction takes place (ORR). Both reactions, HOR and ORR, can be added to the overall reaction

$$\mathrm{H_2} + \frac{1}{2}\mathrm{O_2} \longrightarrow \mathrm{H_2O}, \tag{3.15}$$

chemical (Gibbs) energy of which is being converted to electrical work.

Solid electrolyte

This article is restricted to a steady state in one-dimensional approximation for the sake of simplicity. The considered electrolyte consists of a segment $(0, L)$ of a conductive solid subject to boundary conditions. Because there are no electrochemical reactions taking place in the electrolyte, the oxide ions are neither consumed nor created therein, and flux of the ions is thus constant in space (due to the 1D approximation),

$$\frac{\mathrm{d}j}{\mathrm{d}x} = 0. \tag{3.16}$$

Total electric current in the electrolyte is given by electric current of the ions, i.e. $j = i_\mathrm{i} = z_\mathrm{i} F j_\mathrm{i}$. The electric potential of oxide ions is defined analogously to electric potential of electrons in equation (3.3), and entropy flux due to the ions is included into the bulk measurable heat flux,

$$j_\mathrm{qb} = j_\mathrm{q} + T\frac{j}{z_\mathrm{i}F}s_\mathrm{i}, \tag{3.17}$$

which expresses heat transport within the bulk solid electrolyte. The total energy density balance (3.1) then becomes

$$0 = \frac{\mathrm{d}j_\mathrm{en}}{\mathrm{d}x} = \frac{\mathrm{d}}{\mathrm{d}x}(j'_\mathrm{qb} + \phi_\mathrm{i} j) \implies -\frac{\mathrm{d}j'_\mathrm{qb}}{\mathrm{d}x} = j\frac{\mathrm{d}\phi_\mathrm{i}}{\mathrm{d}x}. \tag{3.18}$$

$$\tag{3.19}$$

In general, the stationary entropy density balance reads

$$\frac{\mathrm{d}j_\mathrm{s}}{\mathrm{d}x} = \sigma_\mathrm{s}, \tag{3.20}$$

where σ_s and j_s stands for entropy production density and total entropy flux, respectively. Inside the solid electrolyte the stationary entropy **density** balance is as follows

$$\frac{\mathrm{d}}{\mathrm{d}x}\frac{j'_\mathrm{qb}}{T} = -\frac{j'_\mathrm{qb}}{T^2}\frac{\mathrm{d}T}{\mathrm{d}x} - \frac{j}{T}\frac{\mathrm{d}\phi_\mathrm{i}}{\mathrm{d}x}, \tag{3.21}$$

where the left hand side is derivative of entropy density flux and the right hand side is the entropy production due to transport of heat and ions. The force flux relations read

$$\lambda \frac{\mathrm{d}T}{\mathrm{d}x} = -j'_{\mathrm{qb}} + \frac{TS^*}{F} j, \tag{3.22a}$$

$$\frac{\mathrm{d}\phi_{\mathrm{i}}}{\mathrm{d}x} = -\frac{S^*}{F}\frac{\mathrm{d}T}{\mathrm{d}x} - rj, \tag{3.22b}$$

where j'_{qb}, j, T and ϕ_{i} stand for measurable heat flux, electric current, temperature and electric potential of the ions, respectively, see [81, Eqs. (9.8)]. The r is an electric resistivity, λ is thermal conductivity at zero current, and S^* stands for the transported entropy, which is, in accordance with [81, Eqn. (9.6)], defined as

$$\pi = TS^* = \left(\frac{j'_{\mathrm{qb}}}{j/F}\right)_{T=\mathrm{const.}}, \tag{3.23}$$

where π is Peltier's coefficient. These equations describe interaction between charged species and temperature gradient.

Straightforward integration of equation (3.22b) gives that

$$\Delta\phi_{\mathrm{i}} = -\frac{S^*}{F}\Delta T - rjL. \tag{3.24}$$

Differentiating equation (3.22a) with respect to x, consequently introducing the total energy balance (3.18) in order to get rid of the $\frac{\mathrm{d}}{\mathrm{d}x}j'_{\mathrm{qb}}$ term and comparing the results with equation (3.22b) multiplied by the j yields

$$\lambda \frac{\mathrm{d}^2}{\mathrm{d}x^2} T = -rj^2. \tag{3.25}$$

This last equation is a linear differential second-order one, and equipped with the boundary temperatures it gives

$$T(x) = -\frac{rj^2}{2\lambda}x^2 + \left(\frac{\Delta T}{L} + \frac{rj^2 L}{2\lambda}\right)x + T^0, \quad x \in [0, L]. \tag{3.26}$$

Consequently, from equation (3.22a) the measurable heat flux becomes

$$j'_{\mathrm{qb}}(x) = rj^2 x - \lambda\frac{\Delta T}{L} - \frac{rj^2 L}{2} + \frac{S^* j}{F}T(x), \quad x \in [0, L]. \tag{3.27}$$

Integrating the local entropy production density in the solid electrolyte, (3.21), expressed in the terms of temperature gradient and current along the the bulk of the electrolyte yields

$$\Pi_{\mathrm{b}} = \int_0^L \sigma_{\mathrm{s}} = \int_0^L \frac{\lambda}{T^2}\left(\frac{\mathrm{d}T}{\mathrm{d}x}\right)^2 + \frac{rj^2}{T^2}\,\mathrm{d}x. \tag{3.28}$$

It is possible to evaluate this integral analytically due to the quadratic behavior of temperature. Thus, using explicit temperature formula (3.26), total entropy production inside the electrolyte becomes

$$\Pi_{\mathrm{b}} = j^2\frac{(T^L + T^0)}{2T^0T^L}rL + (\Delta T)^2\frac{\lambda}{T^0T^LL}. \tag{3.29}$$

The entropy balance for the electrolyte reads

$$\frac{j'^L_{\mathrm{qb}}}{T^L} - \frac{j^0_{\mathrm{qb}}}{T^0} = \Pi_{\mathrm{b}}, \tag{3.30}$$

where the boundary heat fluxes are evaluated at $0+$ and $L-$.

Surface balances

The one-dimensional fuel cell model consists of three parts - two one-point surfaces, where reactions take place, and a bulk electrolyte. The model was solved analytically within the electrolyte in the preceding section. Let us now consider balance laws on the surfaces.

Oxygen electrode $x = L$

Total energy balance on the surface is simply a comparison of the energy fluxes flowing into and out of the surface. Due to the definition of measurable heat flux on the boundary, (3.6), and measurable heat flux in the electrolyte, (3.17), we observe a measurable heat flux discontinuity. This is displayed in the total energy balance of the oxygen reaction surface as follows

$$j_{\mathrm{q}}'^{L} - j_{\mathrm{qb}}'^{L} - j\phi_i^L + j_{\mathrm{e}}^L \phi \mathrm{e}^L + j_{\mathrm{o}}^L h_{\mathrm{o}}^L = 0, \quad x = L. \tag{3.31}$$

Unlike the measurable heat flux, the other energy fluxes do not have their counterparts because they do not appear on the respective sides of the surface.

Entropy flux through the surface from the side of the electrolyte (at $L-$) is given only by the respective measurable heat flux divided by temperature at L, T^L. Entropy flux from the outer part of the surface consists of a measurable heat flux contribution and flux of entropy due to oxygen. Entropy production within the surface is given by entropy production due to the electrochemical reaction taking place therein. Entropy balance of the surface then reads

$$\frac{j_{\mathrm{q}}'^{L}}{T^L} - \frac{j_{\mathrm{qb}}'^{L}}{T^L} + j_{\mathrm{o}}^L s_{\mathrm{o}}^L = \frac{1}{T^L} \widetilde{\mathcal{A}}^L \dot{\xi}^L, \quad x = L, \tag{3.32}$$

where s_{o}, $\widetilde{\mathcal{A}}^L$ and $\dot{\xi}^L$ denote partial oxygen entropy, reaction electrochemical affinity and surface reaction rate, respectively. The right hand side of equation (3.32) is entropy production due to the surface reaction, which is the only source of entropy production on the surface. The electrochemical affinity of oxygen reduction reaction (3.13) reads

$$\widetilde{\mathcal{A}}^L = 2F(\phi_{\mathrm{i}}^L - \phi_{\mathrm{e}}^L) + \frac{\mu_o^L}{2}, \quad x = L, \tag{3.33}$$

in accordance with Eq. (3.9).

From the steady-state assumption and charge conservation it follows that

$$2F\dot{\xi}^L = j, \tag{3.34}$$

where j is the electric current due to transport of the ions, also equal to $-4Fj_{\mathrm{o}}$ with j_{o} being molar flux of oxygen.

For simplicity we assume linear relation between electrochemical affinity $\widetilde{\mathcal{A}}^L$ and reaction rate $\dot{\xi}^L$,

$$j = \frac{K_{\mathrm{o}}}{2RT^L} \widetilde{\mathcal{A}}^L \quad x = L. \tag{3.35}$$

The oxygen reduction reaction current exchange density K_{o} is assumed to be a temperature-independent constant characterizing kinetics of the reaction. R is the universal gas constant.

Finally, combining equation (3.34) with equation (3.35) leads us to formula for the surface entropy production due to ORR,

$$\frac{1}{T^L}\widetilde{\mathcal{A}}^L\,\dot{\xi}^L = \frac{R}{FK_\mathrm{o}}j^2. \tag{3.36}$$

Hydrogen electrode $x = 0$

Description of situation at the HOR surface is analogous to the ORR surface. The energy balance reads

$$-j_\mathrm{q}'^0 + j_\mathrm{qb}'^0 + j\phi_i^0 - j\phi\mathrm{e}^0 - j_\mathrm{h}^0 h_\mathrm{h}^0 - j_\mathrm{w}^0 h_\mathrm{w}^0 = 0 \quad \text{at} \quad x = 0, \tag{3.37}$$

where we experience a similar discontinuity of the measurable heat flux as in the previous case. The steady state condition implies $j = 2Fj_\mathrm{h}$ and $j = -2Fj_\mathrm{w}$.

The entropy balance is also analogous to the previous case,

$$-\frac{j_\mathrm{q}'^0}{T^0} + \frac{j_\mathrm{qb}'^0}{T^0} - j_\mathrm{h}^0 s_\mathrm{h}^0 - j_\mathrm{w}^0 s_\mathrm{w}^0 = \frac{1}{T^0}\widetilde{\mathcal{A}}^0\,\dot{\xi}^0 \quad \text{at} \quad x = 0, \tag{3.38}$$

The electrochemical affinity of the HOR reads

$$\widetilde{\mathcal{A}}^0 = 2F(\phi_\mathrm{i}^0 - \phi_\mathrm{e}^0) + \mu_\mathrm{h}^0 - \mu_\mathrm{w}^0, \tag{3.39}$$

and charge conservation implies

$$2F\dot{\xi}^0 = j. \tag{3.40}$$

As in the case of the ORR surface we assume a linear dependence of reaction rate on the electrochemical affinity,

$$j = \frac{K_\mathrm{h}}{2RT^0}\widetilde{\mathcal{A}}^0 \quad \text{at} \quad x = 0. \tag{3.41}$$

where K_h is current exchange density characterizing the HOR kinetics.

Finally, the entropy production due the HOR at the surface is

$$\frac{1}{T^0}\widetilde{\mathcal{A}}^0\,\dot{\xi}^0 = \frac{R}{FK_\mathrm{h}}j^2. \tag{3.42}$$

3.3.2 Total entropy production

To obtain the total entropy production of whole fuel cell model we simply add the production in solid electrolyte, (3.29) and productions due to the electrochemical reactions, (3.36) and (3.42). We obtain

$$\begin{aligned}\Pi_\mathrm{tot} &= \Pi_\mathrm{b} + \frac{1}{T^0}\widetilde{\mathcal{A}}^0\,\dot{\xi}^0 + \frac{1}{T^L}\widetilde{\mathcal{A}}^L\,\dot{\xi}^L \\ &= j^2\Big(\frac{(T^L + T^0)}{2T^0T^L}rL + \frac{R(K_\mathrm{o} + K_\mathrm{h})}{FK_\mathrm{o}K_\mathrm{h}}\Big) + (\Delta T)^2\frac{\lambda}{T^0T^LL}.\end{aligned} \tag{3.43}$$

3.3.3 Current and voltage

Observing affinity of the total fuel cell reaction, (3.15),

$$\widetilde{\mathcal{A}}_{\mathrm{tot}} = \mu^0_{\mathrm{h}} + \frac{1}{2}\mu^L_{\mathrm{o}} - \mu^0_{\mathrm{w}}, \tag{3.44}$$

we see that it can be expressed in terms of ORR and HOR affinities from equations, (3.33) and (3.39), as

$$2Rj\Big(\frac{T^L}{K_{\mathrm{o}}} + \frac{T^0}{K_{\mathrm{h}}}\Big) = \widetilde{\mathcal{A}}^L + \widetilde{\mathcal{A}}^0 = 2F\Delta(\phi_{\mathrm{i}} - \phi_{\mathrm{e}}) + \widetilde{\mathcal{A}}_{\mathrm{tot}}. \tag{3.45}$$

Introducing the equation (3.24) instead of $\Delta\phi_{\mathrm{i}}$, expressing $\Delta\phi_{\mathrm{e}}$ yields

$$\Delta\phi_{\mathrm{e}} = \frac{\widetilde{\mathcal{A}}_{\mathrm{tot}}}{2F} - j\Big(rL + \frac{R}{F}\Big(\frac{T^L}{K_{\mathrm{o}}} + \frac{T^0}{K_{\mathrm{h}}}\Big)\Big) - \frac{S^*}{F}\Delta T. \tag{3.46}$$

3.4 Fuel cell model optimization

In the preceding section we have outlined a simplified one-dimensional steady-state model of a solid oxide fuel cell. The model was simple enough to admit analytical solution, which will be advantageous in the present section.

Before proceeding with the optimization of the solid oxide fuel cell model from section 3.3, we need to specify governing and optimized parameters, constraints and an objective, as we have discussed in general in the section 3.2.4. Those specifications have to respect the physical nature of problem as well as they must neither over- nor underdetermine the model equations.

Let us choose the electrical power $\dot{W}_{\mathrm{el}}$ to be the optimization objective, which we want to maximize with respect to optimized parameter.

3.4.1 Optimization without a priori constraints

Optimization can proceed so that all but one necessary boundary conditions are fixed and the remaining one is varied in order to attain maximum power.

Optimization of thickness L

Let us choose material parameters λ, r, S^*, K_{o} , K_{h}, boundary conditions T^L, T^0, p^L, p^0, $\Delta\phi_{\mathrm{e}}$ to be some given parameters (governing parameters) while thickness L will be the optimized parameter within $0 < a \leq L \leq b < \infty$. In other words, we seek the thickness L for which the electrical power is maximal.

Such choice of governing parameters reveals that the IV-formula (3.46) determines current j as a decreasing function of thickness. Therefore, by definition of electric power (3.6), it follows that the power is maximal for the smallest possible L, therefore

$$a = \arg\max_L \dot{W}_{\mathrm{el}}(L) = \arg\max_L j(L), \tag{3.47}$$

and that $\dot{W}_{\mathrm{el}}$ is monotone with respect to L, which also means that

$$\max_L \dot{W}_{\mathrm{el}} \leq \dot{W}_{\mathrm{el}}(0). \tag{3.48}$$

The power is thus bounded with respect to L, and it decreases as L increases.

Let us now inspect the entropy production dependence on L. The values of entropy production (3.43) tend to infinity for $L \to 0$. Moreover, entropy production is a smooth non-negative function, i.e.,

$$0 < \arg\min_L \Pi_{\mathrm{tot}}(L). \tag{3.49}$$

Therefore, for a sufficiently small we have

$$a < \arg\min_L \Pi_{\mathrm{tot}}(L) \quad \Longrightarrow \quad \arg\max_L \dot{W}_{\mathrm{el}}(L) < \arg\min_L \Pi_{\mathrm{tot}}(L), \tag{3.50}$$

which means that maximum power is not attained for the same L as minimum entropy production.

In summary, when thickness L is the parameter that is varied in order to find maximum power, the maximum power is attained for the smallest possible L. On the other hand, entropy production density tends to infinity as $L \to 0$, which means that EPM is not a valid optimization strategy in this case.

Optimization of heat conductivity λ

In this case we assume that L is a governing parameter, but thermal conductivity λ is the optimization parameter. The current (3.46) is constant with respect to λ and so is the electric power, see Eq. (3.6). On the contrary, entropy production (3.43) is increasing with λ increasing. Therefore, EPM does not coincide with electrical power maximization in this case.

3.4.2 Optimization with constrained resources

It was demonstrated in the a priori unconstrained optimization examples in the preceding section that EPM often does not correspond with maximization of useful power. The examples, however, are somewhat ill-posed because we maximize the power without paying attention to the amount of resources used. In practice, the energy resources are limited, therefore, we introduce constraints on "source" energy fluxes in this section.

Expressing the general formula for power (3.12) in the particular situation of the solid oxide fuel cell model yields

$$\dot{W}_{\mathrm{el}} = \underbrace{-j_{\mathrm{q}}'^{L}\Big(1 - \frac{T^0}{T^L}\Big) + \frac{j}{2F}\Big(\widetilde{\mathcal{A}} + \Delta T s_{\mathrm{o}}^{L}/2\Big)}_{\text{no a priori sign}} \underbrace{- T^0\Pi_{\mathrm{tot}}}_{\geq 0}, \tag{3.51}$$

which can be rewritten as

$$\dot{W}_{\mathrm{el}} = C - T^0\Pi_{\mathrm{tot}} \quad \text{with respect to the optimization parameters.} \tag{3.52}$$

The terms with no a priori sign are the exergy flux into the fuel cell, and if they are kept constant (denoted by C), maximization of useful power corresponds to minimization of entropy production. EPM is then a valid optimization method in that case.

What if we do not wish to fix all the terms with no a priori sign in equation (3.51)? Does then EPM still lead to the maximum power? The answer is negative in general, as we have shown in Sec. 3.4.1. Moreover, we show in the following that even if constraints on energy influx are chosen, EPM does not often lead to the maximum power anyway.

It is convenient to assume that the fuel cell model is connected to an external load with resistance[1]. Using the Ohm's law, $\Delta\phi_{\mathrm{e}} = Zj$, for the external load, Eq. (3.46) yields an useful formula electric current

$$j = \frac{\frac{\widetilde{\mathcal{A}}}{2F} - \frac{S^*}{F}\Delta T}{rL + Z + \frac{R}{F}\left(\frac{T_L}{K_{\mathrm{o}}} + \frac{T_0}{K_{\mathrm{o}}}\right)}. \tag{3.53}$$

The electric power of the fuel cell model can be also expressed as

$$\dot{W}_{\mathrm{el}} = Zj^2 \tag{3.54}$$

alternatively.

For all further optimization examples we assume that the set of governing parameters (that remain constant) consists of T^L, T^0, p_{w}, p_{o}, p_{h} , λ, r, K_{o}, and K_{h} while Z and L are the optimization parameters. It is necessary from the mathematical point of view to have two optimization parameters instead of one because otherwise we could not enforce any constraint.

Gibbs energy flux constraint

Optimization with Gibbs energy flux into the fuel cell as the constraint is a natural choice in fuel cells because efficiency is often expressed as

$$\eta = \frac{\dot{W}_{\mathrm{el}}}{\widetilde{\mathcal{A}}_{\frac{j}{2F}}}, \tag{3.55}$$

where the denominator is just the Gibbs energy flux. Hence, we consider

$$\frac{j}{2F}\widetilde{\mathcal{A}}(Z, L) = C, \quad C \text{ is constant.} \tag{3.56}$$

Total affinity, given by formula (3.44), is independent of Z and L, and constraint (3.56) in fact fixes the current j. Observing the formula for j, Eq. (3.53), we see that constraint (3.56) implies

$$Z = C_{\mathrm{ref}} - rL, \quad \text{where } C_{\mathrm{ref}} \text{ is a positive constant.} \tag{3.57}$$

Both optimization parameters, Z and L, have to be positive. Assuming that L has to be greater than some smallest possible positive thickness a, we see that maximum value of Z is

$$Z_{\max} = C_{\mathrm{ref}} - ra. \tag{3.58}$$

Because j is constant, the electric power is linear in Z, and maximum power is achieved when Z is maximal possible, hence,

$$\arg\max_{Z} \dot{W}_{\mathrm{el}} = C_{\mathrm{ref}} - ra. \tag{3.59}$$

[1]With a little abuse of notation, we can set Z negative, which corresponds to an external voltage source.

This last equation identifies the value of Z for which the power is maximal.

Let us now search for minimum of entropy production. Introducing relations (3.57) into entropy production (3.43) gives

$$\Pi_{\mathrm{tot}} = j^2 \left(\frac{(T^L + T^0)}{2T^0 T^L}(C_{\mathrm{ref}} - Z) + \frac{R(K_{\mathrm{o}} + K_{\mathrm{h}})}{F K_{\mathrm{o}} K_{\mathrm{h}}} \right) + \frac{(\Delta T)^2 \lambda r}{T^0 T^L (C_{\mathrm{ref}} - Z)}, \tag{3.60}$$

minimum of which is (given by solving a quadratic equation)

$$\arg\min_Z \Pi_{\mathrm{tot}} = C_{\mathrm{ref}} - \left| \frac{\Delta T}{j} \right| \left(\frac{2\lambda r}{T^L + T^0} \right)^{\frac{1}{2}}. \tag{3.61}$$

In general we have

$$\left[ra \neq \left| \frac{\Delta T}{j} \right| \left(\frac{2\lambda r}{T^L + T^0} \right)^{\frac{1}{2}} \right] \implies \left[\arg\min_Z \Pi_{\mathrm{tot}} \neq \arg\max_Z \dot{W}_{\mathrm{el}} \right] \tag{3.62}$$

Electric power thus gains maximum value for different Z than at which entropy production reaches minimum. Optimization with constrained Gibbs energy flux is demonstrated in figure 3.4.1a.

It was shown in [1] that maximum of electric power coincides with minimum of entropy production if $\Delta T = 0$, which can be seen also from Eq. (3.51) easily. How is this result reflected in Eq. (3.62)? Entropy production (3.43) becomes linear in L in the isothermal case and is thus minimal when Z is maximal, i.e. where $\dot{W}_{\mathrm{el}}$ is maximal. In formula (3.62) the left hand side becomes zero as well as the right hand side. This also agrees with Fig. 3.4.1a, where extremal values Π_{tot} and $\dot{W}_{\mathrm{el}}$ tend to each other as $\Delta T \to 0$.

In summary, when the flux of Gibbs energy is kept constant during the optimization, useful power and entropy production do not reach extrema (maximum and minimum, respectively) simultaneously if the fuel cell is not isothermal. If the fuel cell is isothermal, the extrema coincide.

Heat and Gibbs energy flux constraint

Another example of constraint is to fix both Gibbs energy flux and heat flux through the hot reservoir, assuming $T^L \geq T^0$,

$$-j_{\mathrm{q}}'^L(Z, L) + \frac{j(Z, L)}{2F}\widetilde{\mathcal{A}} = C, \quad C \text{ is constant.} \tag{3.63}$$

The implicit relation which binds Z and L is no longer as simple as in the case of Gibbs energy flux constraint, Sec. 3.4.2. Unlike as in the previous case, we cannot write an explicit formula relating Z and L. Nevertheless, plugging constraint (3.63) into equation (3.51), we obtain

$$\dot{W}_{\mathrm{el}} = \underbrace{-j_{\mathrm{q}}'^L + \frac{j}{2F}\widetilde{\mathcal{A}}}_{\text{constant}} + \frac{T^0}{T^L} j_{\mathrm{q}}'^L + \frac{j}{2F}\left(\widetilde{\mathcal{A}} + \Delta T s_{\mathrm{o}}^L/2\right) - \underbrace{T^0 \Pi_{\mathrm{tot}}}_{\geq 0}. \tag{3.64}$$

The non-constant terms in front of the entropy production in this formula make EPM invalid also in this case. The corresponding electric power and entropy production are plotted in figure 3.4.1b for different boundary temperatures.

3.4.3 Exergy flux as constraint

Finally, one can consider

$$-j_{\mathrm{q}}'^{L}\left(1-\frac{T^0}{T^L}\right)+\frac{j}{2F}\left(\widetilde{\mathcal{A}}+\Delta T s_{\mathrm{o}}^L/2\right)=C,\quad C \text{ is constant.} \tag{3.65}$$

Such constraint collapses equation (3.51) into the form of equation (3.52), and minimum of entropy production thus implies maximum of power for any couple of optimization parameters in this case. Constraint (3.65) however coincides with exergy flux into the fuel cell.

Instead of fixing the whole flux of exergy into the fuel cell, we can fix both its components separately, i.e.

$$j_{\mathrm{q}}'^{L}(Z,L,\lambda)=C_1,\quad \text{and } \frac{j(Z,L)}{2F}\widetilde{\mathcal{A}}=C_2,\quad C_1 \text{ and } C_2 \text{ are constant.} \tag{3.66}$$

Having two constraints, we have to work with three optimization parameters, for example Z, L, λ.

Note that by Eq. (3.53) current j does not depend on λ. Therefore, the second constraint in (3.66) implies that the Gibbs energy flux is also fixed. Treating L as a function of Z, the first constraint in (3.66) yields the following dependence of λ on Z:

$$\lambda=\frac{C_{\mathrm{ref}}-Z}{r\Delta T}\left[-C_1+j\frac{T^L}{F}\left(S^*+\frac{s_{\mathrm{o}}}{4}\right)+j^2\left(\frac{C_{\mathrm{ref}}-Z}{2}+\frac{RT^L}{FK_{\mathrm{o}}}\right)\right]. \tag{3.67}$$

Finally, we plug (3.67) into entropy production (3.43), and get

$$T^0\Pi(Z)=j^2\left(C_{\mathrm{ref}}-Z+\frac{R}{F}\left(\frac{T^L}{K_{\mathrm{o}}}+\frac{T^0}{K_{\mathrm{h}}}\right)\right)+j\frac{\Delta T}{F}\left(S^*+\frac{s_{\mathrm{o}}}{4}\right)-\left(1-\frac{T^0}{T^L}\right)C_1. \tag{3.68}$$

Bearing in mind that j is constant, we can see that the minimum of entropy production coincides with the highest possible value of Z, where Z is limited by the minimal thickness a as in equation (3.58). Maximum of electric power is also reached at the maximal possible value of Z, reasoning of which is the same as in section 3.4.2. This is, however, not surprising, since fixing constraints (3.66) inevitably leads to fixed flux of exergy into the fuel cell.

3.5 Conclusion

Efficiency of industrial devices producing electricity is often examined by means of exergy analysis, that means by evaluating exergy destruction within the devices. Since exergy destruction is proportional to entropy production, reducing exergy destruction in fact means reducing entropy production. But the final goal of such optimization is to raise the useful (electric) power delivered by the device. Is reduction of entropy production always accompanied by growth of the useful power? Not in general, as is demonstrated in this paper on several examples.

Before saying whether entropy production minimization (EPM) leads to useful power maximization in a particular case, it is necessary to state what are the

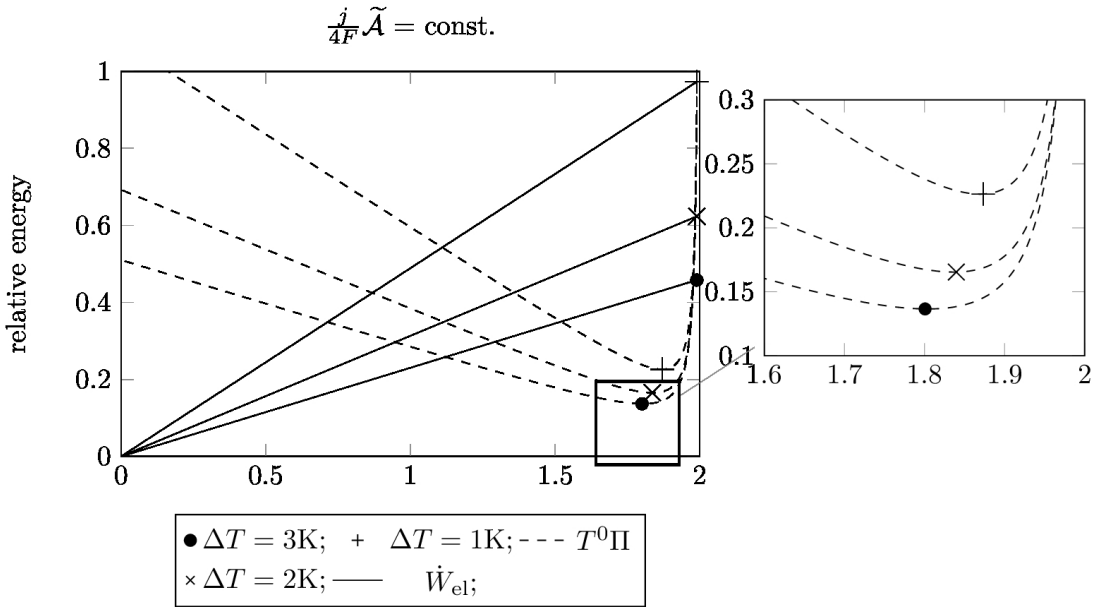

(a) Gibbs energy flux is kept constant. The maxima of power are attained on boundary for every temperature difference. The entropy minima tend to power maxima with decreasing temperature difference.

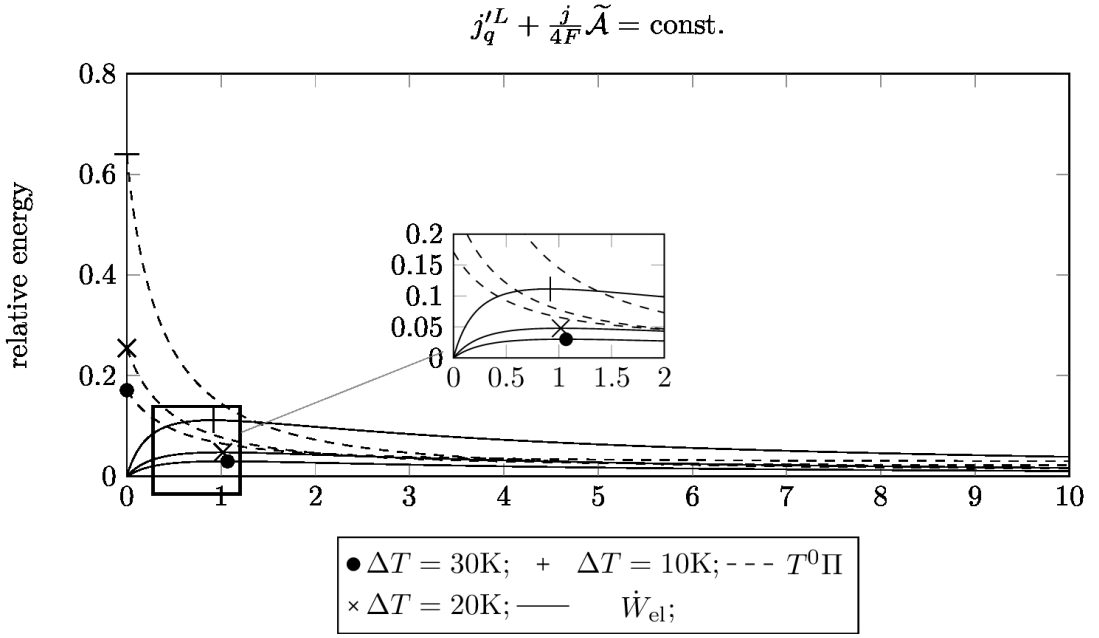

(b) Sum of Gibbs energy flux and heat from hot reservoir is constrained. Entropy production minima lie at boundary $Z = 10$. Work maxima tend move to $Z = 0$, with decreasing temperature difference.

Figure 3.4.1: The resistance Z is the optimization parameter. Marks denote extremes of power and entropy production, respectively. Both, entropy production and power values are relative to their value at $[Z, L] = [1, 1]$. Boundary temperature T^L is in every case set constant to 1073 K, T^0 is varied.

constraints of the optimization, i.e., which quantities are kept fixed. For example when exergy flux into the device is fixed (either as a whole or each part of it), EPM is equivalent to maximization of useful power. Similarly when the maximum work is sought that a device can deliver when relaxing to equilibrium (being shut down), the maximum is obtained when no entropy is produced.

Consider now a fuel cell, which can be seen as a prototype of device converting chemical energy into electricity. Therefore, it is reasonable to keep only flux of Gibbs energy into the fuel cell constant during the maximization. Indeed, Gibbs energy expresses the useful energy of the fuel while flux of exergy also contains heat fluxes from all but one temperature reservoirs. If flux of Gibbs energy into the fuel cell is fixed and boundary of the fuel cell is isothermal, then EPM again leads to useful power maximization. On the other hand, if the boundary is not isothermal, EPM fails to provide maximum useful power, see Fig. 3.4.1a. The situation is similar when flux of Gibbs energy and the heat flux from the hotter temperature reservoir are kept fixed as useful power and entropy production attain their respective extrema at different conditions, see Fig. 3.4.1b. Finally, not fixing any energy flux through the boundary makes EPM also inadequate for useful work maximization.

In summary, before assessing efficiency of a device by means of exergy analysis, one should first define the optimization procedure, which includes defining constraints fixed during the optimization, and then one should verify that entropy production minimization is equivalent to useful power maximization in the particular case given by the device and the optimization procedure. Skipping any of these steps, one may end up in a pitfall hidden behind the widely used theory of exergy analysis.

Summary and Discussion

The three topics were presented from the most abstract to the most applied, although, the actual order of formulation was opposite. Let us now summarize in this reverse order in order to document the questions that were solved during the formulation process.

Exergy Analysis is a useful tool for the optimization of a certain class of devices [6]. The limits of the entropy production minimization principle, which is the basis of the Exergy Analysis, were investigated in [1, 2]. In particular, the entropy production minimization does not lead to power maximization of devices with non-isothermal boundary [1]. This pitfall is documented on an analytically tractable one-dimensional example of a solid oxide hydrogen fuel cell [2]. The cell is described as a bulk yttria-stabilized zirconia where oxide ions and heat are transported, enclosed with two reaction surfaces where reactions (3.14) or (3.13), respectively, occur. The model is formulated within the framework of non-equilibrium thermodynamics [1] thus the entropy production density is explicitly described. The device converts the temperature gradient and the chemical energy of the fuel into electricity. The electric power is maximized with respect to selected model parameters. It is shown that the values of the parameters maximizing the electric power do not coincide with the values of the parameters minimizing the entropy production of the device.

Although the model successfully demonstrates the limits of the Exergy Analysis applicability, its overall predictive power is poor. First, the choice of the electron potential (3.3) permits only the description of ion oxide transport in a diffusional equilibrium, i.e., when the concentration of the oxide ions does not change. Generally, a partial mass density is subject to time derivative in the mass balance equation, cf. (2.24b), and the mass flux is proportional to the gradient of the respective electrochemical potential. A dependency of the electrochemical potential on the partial mass density is therefore necessary to solve the mass balance in time domain. Second, the linearized Butler-Volmer-type kinetics describing the electrochemical reaction (3.33) and (3.39) relies on the overpotential, which in this case is the difference of the electrostatic potential in the ionic phase and in the electric conductor in the vicinity of the triple phase boundary. The jump in the electrostatic potential across the boundary is due to the double layer, i.e., charge aggregation close to the interface. Hence, this type of ion transport and electrochemical reaction model is useful to describe the processes which permit the diffusional equilibrium of the double layer, although they can neither predict the structure of the double layer nor the dynamics of the oxide ions arising in the unsteady regimes, e.g., during electrochemical impedance spectroscopy or cyclic voltammetry measurement. This was the actual incentive for the investigation covered in the second chapter.

The results of the second chapter are contained in the paper [4]. The yttria-stabilized zirconia – also called the Nernst mass – is a solid crystalline material. The yttria doping stabilises the cubic face-centered structure of the cation lattice at lower temperatures and also creates vacations – vacant sites – in the anion lattice. A free energy density of YSZ bulk and surface is formulated in Section 2.2 of the second chapter, yielding an explicit formula for the chemical potential of

oxide ions (2.23a) and allowing for the description of time dependent electro-diffusive transport of oxide ions beyond the diffusional equilibrium regime. The oxide ions are allowed to occupy the admissible lattice sites, therefore, a non-vanishing free charge density may appear. In the bulk, the resulting system of equations consists of the Poisson equation for the electrostatic potential and the balance of oxide ions (2.35). Coupled to the bulk is a simplified model of YSZ|gas|metal surface describing the adsorption of oxide ions, adsorption of gases, and surface chemical reactions with electrons is presented in Section 2.4. The model predictions can fit experimentally measured capacitance of YSZ blocking electrode, see Fig. 2.5.3.

Despite the positive result, several questions regarding the validity of the modeling approach arise. First, the characteristic length of the double layer is around 1 nm whereas the YSZ lattice constant is approximately 0.5 nm. Therefore, the actual geometry of the interface, which cannot be handled in the 1D approximation, will come into play. In this context, the localization of the electron-transfer reaction is questionable, furthermore it ignores possible quantum behavior of the reacting electrons. Second, the chemistry of a real electrode material may also include intermediate reaction steps. Finally, equation (2.24c) is not valid in two and three spatial dimension, because the respective sides have different curl, cf. (1.4.7). This leads to questions concerning the consistency of the original thermodynamic framework [5] used for the formulation of the YSZ interface model. To this end, the alternative thermodynamic formulation of the equations describing the dynamics of charged mixture has been developed in the first chapter.

Multiscale continuum thermodynamic theory coupling fluid mechanics and electrodynamics, including fields of polarization and magnetization, has been developed in the first chapter [3]. The kinematics of the advected fields is accounted for by using the semidirect product of Lie algebras [18]. The developed Hamiltonian system (1.78) is eventually endowed with gradient dissipation (1.80). The principle of Dynamic Maxmization of Entropy is employed to find out dissipation-resulting reductions of the coupled description to less detailed levels recovering some well known models, e.g., the Landau-Lifshitz spin relaxation, the Single Time Relaxation model for polarized dielectric and the generalized Poisson-Nernst-Planck model. The Maxwell-Stefan Poisson-Nernst-Planck model (1.133) is a model of charged species experiencing a friction when moving relatively to the one fixed species, e.g., crystalline lattice. A derivation of simple boundary dynamics for this model is proposed in Appendix 1.5 together with chemical kinetics in Appendix 1.4, thus, reconstructing the structure of the model derived in the second chapter.

We will conclude with a critical discussion of the results of the first section. First, the exact form of the Lorentz force acting upon the macroscopic polarization charge remains unclear, see Section 1.5. To this end, we intend to further investigate dynamics of two-(oppositely charged)particle distribution function coupled with the electrodynamics and subsequent reductions of the description to a one-particle distribution function with polarization field. Second, the absence of consistently treated boundaries and boundary conditions in the GENERIC formalism impedes the systematic application of the theory, especially in the field of electrochemistry, where the role of boundaries is crucial. Third, the presented

theory is only valid for velocities that are small compared to the speed of light and it is not compatible with the special relativity theory. Finally, we pose a burning question: is it possible to derive Lorentz-invariant formulation of thermodynamics of charged continuum within GENERIC?

List of Figures

List of Tables

List of Abbreviations

Abbreviation	Word/Phrase
CIT	Classical Irreversible Thermodynamics
CV	Cyclic Voltammetry
EPM	Entropy Production Minimization
GENERIC	Generalized Equation for Reversible Irreversible Coupling
gPNP	generalized Poisson-Nernst-Planck
HOR	Hydrogen Oxidation Reaction
MS PNP	Maxwell-Stefan Poisson-Nernst-Planck
LSM	Lanthanum Strontium Manganite
ORR	Oxygen Reduction Reaction
PNP	Poisson-Nernst-Planck
SOEC	Solid Oxide Electrochemical Cell
SOEC	Solid Oxide Electrolysis Cell
SOFC	Solid Oxide Fuel Cell
SRT	Single Relaxation Time
TPB	Triple Phase Boundary
YSZ	Yttria-stabilised Zirconia

List of Publications

P1. VÁGNER, P.; PAVELKA, M.; MARŠÍK, F. Pitfalls of Exergy analysis. *Journal of Non-Equilibrium Thermodynamics*. 2017. ISSN 0340-0204. Available from DOI: 10.1515/jnet-2016-0043.

P2. VÁGNER, P.; PAVELKA, M. Multiscale thermodynamics of charged mixtures. *arXiv:1903.01274*. 2019. Available also from: http://arxiv.org/abs/1903.01274. Submitted to Continuum Mechanics and Thermodynamics 28/02/2019.

P3. VÁGNER, P.; GUHLKE, C.; MILOŠ, V.; MÜLLER, R.; FUHRMANN, J. A continuum model for yttria-stabilised zirconia incorporating triple phase boundary, lattice structure and immobile oxide ions. *WIAS Preprints*. 2019. Available from DOI: 10.20347/WIAS.PREPRINT.2584. Submitted to Physical Chemistry Chemical Physics on 02/04/2019.

P4. PAVELKA, M.; KLIKA, V.; VÁGNER, P.; MARŠÍK, F. Generalization of Exergy analysis. *Applied Energy*. 2015, vol. 137, pp. 158–172.

P5. POLONSKÝ, J.; KODÝM, R.; VÁGNER, P.; PAIDAR, M.; BENSMANN, B.; BOUZEK, K. Anodic microporous layer for polymer electrolyte membrane water electrolysers. *Journal of Applied Electrochemistry*. 2017, vol. 47, no. 10, pp. 1137–1146.

Bibliography

1. PAVELKA, M.; KLIKA, V.; VÁGNER, P.; MARŠÍK, F. Generalization of Exergy analysis. *Applied Energy*. 2015, vol. 137, pp. 158–172.
2. VÁGNER, P.; PAVELKA, M.; MARŠÍK, F. Pitfalls of Exergy analysis. *Journal of Non-Equilibrium Thermodynamics*. 2017. ISSN 0340-0204. Available from DOI: 10.1515/jnet-2016-0043.
3. VÁGNER, P.; PAVELKA, M. Multiscale thermodynamics of charged mixtures. *arXiv:1903.01274*. 2019. Available also from: http://arxiv.org/abs/1903.01274. Submitted to Continuum Mechanics and Thermodynamics 28/02/2019.
4. VÁGNER, P.; GUHLKE, C.; MILOŠ, V.; MÜLLER, R.; FUHRMANN, J. A continuum model for yttria-stabilised zirconia incorporating triple phase boundary, lattice structure and immobile oxide ions. *WIAS Preprints*. 2019. Available from DOI: 10.20347/WIAS.PREPRINT.2584. Submitted to Physical Chemistry Chemical Physics on 02/04/2019.
5. DREYER, W.; GUHLKE, C.; MÜLLER, R. Bulk-surface electrothermodynamics and applications to electrochemistry. *Entropy*. 2018, vol. 20, no. 12, pp. 939. ISSN 1099-4300. Available from DOI: 10.3390/e20120939.
6. BEJAN, Adrian. Entropy generation minimization: The new thermodynamics of finite size devices and finite time processes. *Journal of Applied Physics*. 1996, vol. 79, no. 3, pp. 1191–1218. Available from DOI: http://dx.doi.org/10.1063/1.362674.
7. GRMELA, M.; ÖTTINGER, H.C. Dynamics and thermodynamics of complex fluids. I. Development of a general formalism. *Phys. Rev. E*. 1997, vol. 56, pp. 6620–6632. Available from DOI: 10.1103/PhysRevE.56.6620.
8. ÖTTINGER, H C; GRMELA, M. Dynamics and thermodynamics of complex fluids. II. Illustrations of a general formalism. *Phys. Rev. E*. 1997, vol. 56, pp. 6633–6655. Available from DOI: 10.1103/PhysRevE.56.6633.
9. ÖTTINGER, H C. *Beyond Equilibrium Thermodynamics*. Wiley & Sons, 2005. ISBN 9780471727910. Available also from: http://books.google.cz/books?id=Prh9moT1WzMC.
10. PAVELKA, M; KLIKA, V; GRMELA, M. *Multiscale Thermo-Dynamics*. Berlin: de Gruyter, 2018. ISBN 9783110350951.
11. ARNOLD, V.I. Sur la géometrie différentielle des groupes de Lie de dimension infini et ses applications dans l'hydrodynamique des fluides parfaits. *Annales de l'institut Fourier*. 1966, vol. 16, no. 1, pp. 319–361.
12. DZYALOSHINSKII, I. E.; VOLOVICK, G. E. Poisson brackets in condense matter physics. *Annals of Physics*. 1980, vol. 125, no. 1, pp. 67–97.
13. GRMELA, M. Bracket formulation of diffusion-convection equations. *Physica D*. 1986, vol. 21, pp. 179–212.
14. GRMELA, M. Particle and bracket formulations of kinetic equations. *Contemp. Math.* 1984, vol. 28, pp. 125–132.

15. MORRISON, P.J. Bracket formulation for irreversible classical fields. *Phys. Lett. A*. 1984, vol. 100, pp. 423.

16. PAVELKA, M.; KLIKA, V.; ESEN, O.; GRMELA, M. A hierarchy of Poisson brackets in non-equilibrium thermodynamics. *Physica D: Nonlinear phenomena*. 2016, vol. 335, pp. 54–69.

17. GROOT, S. R. de; MAZUR, P. *Non-equilibrium Thermodynamics*. New York: Dover Publications, 1984.

18. ESEN, O; PAVELKA, M; GRMELA, M. Hamiltonian coupling of electromagnetic field and matter. *International Journal of Advances in Engineering Sciences and Applied Mathematics*. 2017, vol. 9, no. 1, pp. 3–20.

19. JACKSON, J D. *Classical electrodynamics*. John Wiley & Sons, 1998. ISBN 0-471-30932-X.

20. MARSDEN, J E; WEINSTEIN, A. The Hamiltonian structure of the Maxwell-Vlasov equations. *Physica D: nonlinear phenomena*. 1982, vol. 4, no. 3, pp. 394–406.

21. MARSDEN, J; RATIU, T; WEINSTEIN, A. Semidirect products and reduction in mechanics. *Transactions of the american mathematical society*. 1984, vol. 281, no. 1, pp. 147–177. ISSN 0002-9947. Available from DOI: 10.2307/1999527.

22. ESEN, O; SÜTLÜ, S. Hamiltonian dynamics on matched pairs. *International Journal of Geometric Methods in Modern Physics*. 2016, vol. 13, no. 10.

23. DUMBSER, M.; PESHKOV, I.; ROMENSKI, E.; ZANOTTI, O. High order ADER schemes for a unified first order hyperbolic formulation of continuum mechanics: Viscous heat-conducting fluids and elastic solids. *Journal of Computational Physics*. 2016, vol. 314, pp. 824–862.

24. PESHKOV, I; PAVELKA, M; ROMENSKI, E; GRMELA, M. Continuum Mechanics and Thermodynamics in the Hamilton and the Godunov-type Formulations. *Continuum Mechaanics and Thermodynamics*. 2018, vol. 30, no. 6, pp. 1343–1378.

25. HOLM, D D. Hamiltonian dynamics of a charged fluid, including electro- and magnetohydrodynamics. *Physics Letters A*. 1986, vol. 114, no. 3, pp. 137–141.

26. MARŠÍK, F; DVOŘÁK, I. *Biotermodynamika*. Academia, 1998.

27. PURCELL, E M. *Electricity and Magnetism*. Cambridge University Press, 2011. ISBN 978-1-107-01360-5.

28. RUSSAKOFF, G. A derivation of the macroscopic Maxwell equations. *Amer J of Phys*. 1970, vol. 38, no. 10, pp. 1188–1195.

29. LANDAU, L.; LIFSHITS, E. On The Theory of the Dispersion of Magnetic permeability in ferromagnetic bodies. *Phys. Zeitsch. der Sow.* 1935, vol. 8, pp. 153–169.

30. FECKO, M. *Differential Geometry and Lie Groups for Physicists*. Cambridge University Press, 2006. ISBN 9781139458030.

31. LAKSHMANAN, M. Fascinating World of Landau-Lifshitz-Gilbert Equation: An Overview. *Philosophical Transactions of the Royal Society A: Mathematical, Physical and Engineering Sciences*. 2011, vol. 369, no. 1939, pp. 1280–1300. ISSN 1364-503X, 1471-2962. ISSN 1364-503X, 1471-2962. Available from DOI: 10.1098/rsta.2010.0319. arXiv: 1101.1005.

32. GINZBURG, V.L.; LANDAU, L.D. On the theory of superconductivity. *Zhur. Eksp. Theor. Fiz.* 1950, vol. 20, pp. 1064–1082.

33. MIELKE, A.; PELETIER, M. A.; RENGER, D. R. M. On the Relation between Gradient Flows and the Large-Deviation Principle, with Applications to Markov Chains and Diffusion. *Potential Analysis*. 2014, vol. 41, no. 4, pp. 1293–1327. ISSN 1572-929X. Available from DOI: 10.1007/s11118-014-9418-5.

34. MIELKE, A.; RENGER, D. R. M.; PELETIER, M. A. A Generalization of Onsager's Reciprocity Relations to Gradient Flows with Nonlinear Mobility. *Journal of Non-equilibrium Thermodynamics*. 2016, vol. 41, no. 2.

35. MONTEFUSCO, A; PELETIER, M A; ÖTTINGER, H C. Coarse-graining via the fluctuation-dissipation theorem and large-deviation theory. *eprint arXiv:cond-mat.stat-mech/1809.07253v1*. 2018.

36. JANEČKA, A; PAVELKA, M. Non-convex dissipation potentials in multiscale non-equilibrium thermodynamics. *Continuum Mechanics and Thermodynamics*. 2018, vol. 30, no. 4, pp. 917–941.

37. JANEČKA, A; PAVELKA, M. Gradient dynamics and entropy production maximization. *Journal of Non-equilibrium Thermodynamics*. 2018, vol. 43, no. 1, pp. 1–19.

38. CALLEN, H.B. *Thermodynamics: an introduction to the physical theories of equilibrium thermostatics and irreversible thermodynamics*. Wiley, 1960. Available also from: http://books.google.cz/books?id=mf5QAAAAMAAJ.

39. JAYNES, E. T. Delaware Seminar in the Foundation of Physics, M. Bunge ed. In: Springer New York, 1967, chap. Foundations of probability theory and statistical mechanics.

40. GRMELA, M. Role of thermodynamics in multiscale physics. *Computers and Mathematics with Applications*. 2013, vol. 65, no. 10, pp. 1457–1470. ISSN 0898-1221. Available from DOI: http://dx.doi.org/10.1016/j.camwa.2012.11.019.

41. GRMELA, M. Contact Geometry of Mesoscopic Thermodynamics and Dynamics. *Entropy*. 2014, vol. 16, no. 3, pp. 1652–1686. ISSN 1099-4300. Available from DOI: 10.3390/e16031652.

42. GRMELA, M; PAVELKA, M; KLIKA, V; CAO, B Y; BENDIAN, N. Entropy and Entropy Production in Multiscale Dynamics. *Journal of Non-Equilibrium Thermodynamics*. 2019, vol. Submitted.

43. BÖTTCHER, CJF; BORDEWIJK, P. *Theory of electric polarization: Dielectrics in Time-Dependent Fields, Volume II*. Elsevier, 1979. ISBN 0-444-41579-3.

44. BROWN, W F. *Micromagnetics*. Interscience Publishers, 1963. No. 18.

45. DREYER, W.; GUHLKE, C.; MÜLLER, R. Modeling of electrochemical double layers in thermodynamic non-equilibrium. *Phys. Chem. Chem. Phys.* 2015, vol. 17, no. 40, pp. 27176–27194. Available from DOI: 10.1039/c5cp03836g.

46. GUHLKE, C. *Theorie der elektrochemischen Grenzfläche*. 2015. PhD thesis. Technische Universität Berlin.

47. FUHRMANN, J. A numerical strategy for Nernst–Planck systems with solvation effect. *Fuel cells*. 2016, vol. 16, no. 6, pp. 704–714.

48. DREYER, W; GUHLKE, C; MÜLLER, R. A new perspective on the electron transfer: recovering the Butler–Volmer equation in non-equilibrium thermodynamics. *Physical Chemistry Chemical Physics*. 2016, vol. 18, no. 36, pp. 24966–24983.

49. DREYER, W.; GUHLKE, C.; LANDSTORFER, M. A mixture theory of electrolytes containing solvation effects. *Electrochem. Commun.* 2014, vol. 43, pp. 75–78. ISSN 1388-2481.

50. GRMELA, M. Multiscale equilibrium and nonequilibrium thermodynamics in chemical engineering. In: *Advances in Chemical Engineering*. Elsevier, 2010, vol. 39, pp. 75–129.

51. WALDMANN, L. Non-Equilibrium Thermodynamics of Boundary Conditions. *Zeitschrift für Naturforschung A*. 1967, vol. 22, no. 8. ISSN 1865-7109, 0932-0784. ISSN 1865-7109, 0932-0784. Available from DOI: 10.1515/zna-1967-0820.

52. ÖTTINGER, H.C. Nonequilibrium thermodynamics for open systems. *Phys Rev E*. 2006, vol. 73, no. 3, pp. 036126.

53. BIEBERLE, A.; GAUCKLER, L. J. State-space modeling of the anodic SOFC system Ni, H_2–H_2O—YSZ. *Solid State Ionics*. 2002, vol. 146, no. 1–2, pp. 23–41. ISSN 0167-2738. Available from DOI: http://dx.doi.org/10.1016/S0167-2738(01)01004-9.

54. BESSLER, W. G.; GEWIES, S.; VOGLER, M. A new framework for physically based modeling of solid oxide fuel cells. *Electrochim. Acta*. 2007, vol. 53, no. 4, pp. 1782–1800. Available from DOI: 10.1016/j.electacta.2007.08.030.

55. ZHU, H.; KEE, R. J.; JANARDHANAN, V. M.; DEUTSCHMANN, O.; GOODWIN, D. G. Modeling elementary heterogeneous chemistry and electrochemistry in solid-oxide fuel cells. *Journal of the electrochemical society*. 2005, vol. 152, no. 12, pp. A2427–A2440.

56. VOGLER, M.; BIEBERLE-HÜTTER, A.; GAUCKLER, L.; WARNATZ, J.; BESSLER, W. G. Modelling study of surface reactions, diffusion, and spillover at a Ni/YSZ patterned anode. *Journal of The Electrochemical Society*. 2009, vol. 156, no. 5, pp. B663–B672.

57. BAZANT, M. Z.; THORNTON, K.; AJDARI, A. Diffuse-charge dynamics in electrochemical systems. *Phys rev E*. 2004, vol. 70, no. 2, pp. 021506.

58. LANDSTORFER, M.; GUHLKE, C.; DREYER, W. Theory and structure of the metal-electrolyte interface incorporating adsorption and solvation effects. *Electrochim. Acta*. 2016, vol. 201, pp. 187–219. ISSN 0013-4686. Available from DOI: 10.1016/j.electacta.2016.03.013.

59. LANDSTORFER, M.; FUNKEN, S.; JACOB, T. Advanced model framework for solid electrolyte intercalation batteries. *Phys. Chem. Chem. Phys.* 2011, vol. 13, pp. 12817–12825. Available from DOI: 10.1039/C0CP02473B.

60. BRAUN, S.; YADA, C.; LATZ, A. Thermodynamically Consistent Model for Space-Charge-Layer Formation in a Solid Electrolyte. *J. Phys. Chem. C*. 2015, vol. 119, pp. 22281–22288. Available from DOI: 10.1021/acs.jpcc.5b02679.

61. KLERK, N.J. de; WAGEMAKER, M. Space-Charge Layers in All-Solid-State Batteries; Important or Negligible? *ACS Appl. Energy Mater*. 2018, vol. 1, pp. 5609–5618. Available from DOI: 10.1021/acsaem.8b01141.

62. ZHU, H.; KEE, R.J. Membrane polarization in mixed-conducting ceramic fuel cells and electrolyzers. *Int. J. Hydrogen Energ.* 2016, vol. 41, no. 4, pp. 2931–2943. ISSN 0360-3199. Available from DOI: 10.1016/j.ijhydene.2015.10.100.

63. SCOTT, H. G. Phase relationships in the zirconia-yttria system. *Journal of Materials Science*. 1975, vol. 10, no. 9, pp. 1527–1535. ISSN 0022-2461, 1573-4803. ISSN 0022-2461, 1573-4803. Available from DOI: 10.1007/BF01031853.

64. HUND, F. Anomale Mischkristalle im System ZrO_2-Y_2O_3 Kristallbau der Nernst Stifte. *Zeitschrift für Elektrochemie und angewandte physikalische Chemie*. 1951, vol. 55, no. 5, pp. 4.

65. LANDAU, L. D.; PITAEVSKII, L. P.; LIFSHITZ, E. M. *Electrodynamics of continuous media*. Butterworth, 1984.

66. HAYASHI, H.; SAITOU, T.; MARUYAMA, N.; INABA, H.; KAWAMURA, K.; MORI, M. Thermal expansion coefficient of yttria stabilized zirconia for various yttria contents. *Solid state ionics*. 2005, vol. 176, no. 5-6, pp. 613–619.

67. MAIER, J. *Physical chemistry of ionic materials: ions and electrons in solids*. John Wiley & Sons, 2004.

68. SOMMERFELD, A. Zur Elektronentheorie der Metalle auf Grund der Fermischen Statistik. *Z. Physik*. 1928, vol. 47, no. 1-2, pp. 1–32.

69. GUHLKE, C.; GAJEWSKI, P.; MAURELLI, M.; FRIZ, P.K.; DREYER, W. Stochastic many-particle model for LFP electrodes. *Continuum Mech. Thermodyn.* 2018, vol. 30, no. 3, pp. 593–628.

70. ELSHOF, J. E. ten; HENDRIKS, M. G. H. M.; BOUWMEESTER, H. J. M.; VERWEIJ, H. The near-surface defect structure of yttria-stabilised zirconia determined by measurement of the differential capacity. *J Mater Chem*. 2001, vol. 11, no. 10, pp. 2564–2571. ISSN 09599428, 13645501. ISSN 09599428, 13645501. Available from DOI: 10.1039/b100923k.

71. BEZANSON, J.; EDELMAN, A.; KARPINSKI, S.; SHAH, V. B. Julia: A fresh approach to numerical computing. *SIAM Review*. 2017, vol. 59, no. 1, pp. 65–98.

72. SCHARFETTER, D. L.; GUMMEL, H. K. Large-signal analysis of a silicon read diode oscillator. *IEEE Trans Electron dev*. 1969, vol. 16, no. 1, pp. 64–77.

73. FARRELL, P.; ROTUNDO, N.; DOAN, D.H.; KANTNER, M.; FUHRMANN, J.; KOPRUCKI, Th. Numerical methods for drift-diffusion models. In: PIPREK, J. (ed.). *Handbook of Optoelectronic Device Modeling and Simulation: Lasers, Modulators, Photodetectors, Solar Cells, and Numerical Methods*. Boca Raton: CRC Press, 2017, vol. 2, chap. 50, pp. 733–771. Available also from: `https://www.crcpress.com/Handbook-of-Optoelectronic-Device-Modeling-and-Simulation-Two-Volume-Set/Piprek/p/book/9781498749381`.

74. FUHRMANN, J. Comparison and numerical treatment of generalised Nernst–Planck models. *Comp Phys Comm*. 2015, vol. 196, pp. 166–178. Available from DOI: `10.1016/j.cpc.2015.06.004`.

75. YU, Z.; DUTTON, R. *SEDAN III, A Generalized Electronic Material Device Analysis Program* [Stanford Electronics Laboratory Technical Report]. 1985. While the report seems to be unavailable by now, the source code can be accessed via `http://www-tcad.stanford.edu/oldftp_sw/Sedan-III/relB.8830.tar.Z`.

76. GOUY, G. Sur l'énergie utilizable. *Journal de Physique*. 1889, vol. 8, pp. 501–518.

77. STODOLA, A. Die Kreisprozesse der Gasmaschine. *Zeitschrift d. Ver. d. Ingenieure*. 1898.

78. BEJAN, A. *Advanced Engineering Thermodynamics*. Wiley, 2006. ISBN 9780471677635. Available also from: `https://books.google.ca/books?id=LWyqQgAACAAJ`.

79. SCIACOVELLI, Adriano. Entropy generation analysis in a monolithic-type solid oxide fuel cell (SOFC). *Energy*. 2009, vol. 34, no. 7, pp. 850–865. ISSN 0360-5442. Available from DOI: `10.1016/j.energy.2009.03.007`.

80. MEIXNER, J.; REIK, H.G. *Thermodynamik der Irreversible Prozesse, in Handbuch der Physik*. Springer, Berlin Heidelberg New York, 1959.

81. KJELSTRUP, S.; BEDEAUX, D. *Non-Equilibrium Thermodynamics of Heterogeneous Systems*. World Scientific, 2008. Series on Advances in Statistical Mechanics. ISBN 9789812779137.

82. KJELSTRUP, S.; BEDEAUX, D.; JOHANNESSEN, E. *Non-Equilibrium Thermodynamics for Engineers*. World Scientific, 2010. Science and culture series (Singapore).: Physics. ISBN 9789814322157.

83. HOFFMANN, KH; BURZLER, JM; SCHUBERT, S. Endoreversible thermodynamics. *Journal of Non-Equilibrium Thermodynamics*. 1997, vol. 22, no. 4, pp. 311–355. ISSN 0340-0204.

84. SIENIUTYCZ, Stanislaw; SPAKOVSKY, Michael R. von. Finite time generalization of thermal exergy. *Energy Conversion and Management*. 1998, vol. 39, no. 14, pp. 1423–1447. ISSN 0196-8904. Available from DOI: http://dx.doi.org/10.1016/S0196-8904(98)00023-5.

85. HOFFMANN, KH; BURZLER, J; FISCHER, A; SCHALLER, M; SCHUBERT, S. Optimal process paths for endoreversible systems. *Journal of Non-Equilibrium Thermodynamics*. 2003, vol. 28, no. 3, pp. 233–268. ISSN 0340-0204. Available from DOI: 10.1515/JNETDY.2003.015.

86. CURZON, F. L.; AHLBORN, B. Efficiency of a Carnot engine at maximum power output. *American Journal of Physics*. 1975, vol. 43, pp. 22–24. Available from DOI: 10.1119/1.10023.

87. NOVIKOV, I. I. The Efficiency of Atomic Power Stations. *J. Nucl. Energy*. 1958, vol. II 7, no. 125. [Atomnaya Energiya 3, 409 (1957)].

88. SALAMON, P; HOFFMANN, K H; SCHUBERT, S; BERRY, R S; ANDRESEN, B. What conditions make minimum entropy production equivalent to maximum power production? *J. Non-Equilib. Thermodyn*. 2001, vol. 26, pp. 73–83.

89. PAVELKA, M; MARŠÍK, F. Detailed thermodynamic analysis of polymer electrolyte membrane fuel cell efficiency. *International Journal of Hydrogen Energy*. 2013, vol. 38, no. 17, pp. 7102–7113. ISSN 0360-3199. Available from DOI: http://dx.doi.org/10.1016/j.ijhydene.2013.03.149.

90. ARSHAD, M H; KAHRAMAN, R; SAHIN, A Z; BEN-MANSOUR, R. Second law analysis of compressible flow through a diffuser subjected to constant heat flux at wall. *Energy Conversion and Management*. 2010, vol. 51, pp. 2808–2815.

91. AL-SULAIMAN, F A; NARAYAN, G P; V, J H Lienhard. Exergy analysis of a high-temperature-steam-driven, varied-pressure, humidification-dehumidification system coupled with reverse osmosis. *Appl Energy*. 2013, vol. 103, no. 0, pp. 552–561. ISSN 0306-2619. Available from DOI: http://dx.doi.org/10.1016/j.apenergy.2012.10.020.

92. GUTIÉRREZ, F.; MÉNDEZ, F. Entropy generation minimization for the thermal decomposition of methane gas in hydrogen using genetic algorithms. *Energy Conversion and Management*. 2012, vol. 55, pp. 1–13.

93. ISHIDA, M; ZHENG, D; AKEHATA, T. Evaluation of a chemical-looping-combustion power-generation system by graphic exergy analysis. *ENERGY*. 1987, vol. 12, no. 2, pp. 147–154. ISSN 0360-5442. Available from DOI: 10.1016/0360-5442(87)90119-8.

94. SCIACOVELLI, A.; VERDA, V. Second-law design of a latent heat thermal energy storage with branched fins. *International Journal of Numerical Methods for Heat and Fluid Flow*. 2016, vol. 26, no. 2, pp. 489–503.

95. LANDAU, L.D.; LIFSCHITZ, E.M. *Statistical physics*. Pergamon Press, 1969. Course of theoretical physics, no. pt. 1.

96. PAVELKA, M; WANDSCHNEIDER, F; MAZUR, P. Thermodynamic derivation of open circuit voltage in vanadium redox flow batteries. *Journal of Power Sources*. 2015, vol. 293, pp. 400–408.